An Ab Initio Investigation of Lead (II) Complexes as Possible Corrosion Products in a CANDU Supercritical Water-Cooled Reactor (SCWR)

By

Dijana Anzelj

A Thesis Submitted to
Saint Mary's University, Halifax, Nova Scotia,
in Partial Fulfillment of the Requirements for
the Degree of Master of Science in Applied Science

April, 2016, Halifax, Nova Scotia

Approved: Dr. Cory Pye
Supervisor
Department of Chemistry

Approved: Dr. Colleen Barber
Supervisory committee member
Department of Biology

Approved: Dr. Cherif Matta
Supervisory committee member
Department of Chemistry and Physics
Mount Saint Vincent University

Approved: Dr. Jamie Martell
External Examiner
Department of Chemistry
Cape Breton University

Date: April 15, 2016

Table of Contents

An Ab Initio Investigation of Lead (II) Complexes as Possible Corrosion Products in a CANDU Supercritical Water-Cooled Reactor (SCWR)

By Dijana Anzelj

Abstract

Supercritical Water Cooled Reactor (SCWR), direct-cycle pressure tube reactor, is the Generation IV conceptual design. SCWR operates at 25 MPa and 650 ºC and offers significant advances of sustainable energy production, safety, and proliferation resistance. Under extreme conditions, traces of heavy metals could dissolve from the construction material and form complexes with surrounding anions and deposit within reactor, causing corrosion. Lead is the metal of interest because it exists as an impurity within construction material and causes embrittlement. It is essential to predict and control water chemistry to ensure the sustainability of SCWR. Pressurized and heated solutions are challenging for experimental research; computational method becomes a key research tool. Comprehensive *ab initio* calculations were performed on lead (II) complexes containing water, chloride, hydroxide and ammonia ligands. Results compare favourably to literature data, where available. The best candidates for corrosion products are: $[Pb(H_2O)_8]^{2+}$; $[Pb(OH)_2]$ and $[PbCl_2]$ and their hydration products.

April 15, 2016

Acknowledgments

Above all, I would like to express my great gratitude to my Master's thesis supervisor, Dr. Cory Pye, who encouraged me and guided me with patience and compassion throughout this educational journey. Dr. Pye sparked my interest and enthusiasm for Quantum Mechanics through his lectures and was instrumental in me pursuing and completing my graduate research. Dr. Pye's exceptional understanding always kept me motivated towards the final goal. This truly amazing educational experience would not have been possible without Dr. Pye, who understood my challenges and navigated me through the process. This great opportunity will have a positive impact on my future direction. Appreciation is also extended to my Master's thesis committee members, Dr. Colleen Barber and Dr. Cherif Matta. Their valuable time and guidance in completing this scientific research is greatly appreciated.

Also, I would also like to express my great appreciation to Dr. Katherine Robertson. Her valuable advice, understanding and support kept me moving forward.

I would like to thank the Natural Sciences and Engineering Research Council (NSERC), Natural Resources Canada (NRCan) and Atomic Energy of Canada Limited (AECL) for funding the research project that I am so honored and appreciative to have been part of. Also, many thanks to the Atlantic Computational Excellence network (ACEnet) for the valuable computer time that they provided.

Special thanks to Dr. Kathy Singfield who sparked my interest in thermodynamics. Gratitude is extended to Dr. Adam Piorko, who was always supportive and encouraging. Many thanks to the Dean of Science, Dr. Steven Smith, as well as to the graduate studies advisor, Mr. Keith Bain, both of who were supportive and understanding of the challenges I encountered along the way. My gratitude extends to Dr. Christa Brosseau, secretary Mrs. Mary Jane MacNeil and technician Elizabeth McLeod, who were truly inspiring, and whose enthusiasm and positivity were greatly appreciated.

Heartfelt thanks goes to my parents Ivka and Slobodan Lekić, whose exceptional work ethics, integrity, honesty and commitment inspired me to pursue my dreams and to devote myself to my research work with pride and joy.

My special thanks goes to my children, Marko and Anabella Anželj, who at only three and six, kept me inspired and entertained with their pure hearts, offering me comfort and unconditional love.

I would also like to thank the amazing group of friends I made in the Chemistry Department. Graeme Soper, Ismat Sumar and Amit Kumar made this exceptional educational journey that much more fun and exciting.

List of Tables

List of Figures

List of Abbreviations

Atlantic Computational Excellence Network	ACEnet
Atomic Energy of Canada Limited	AECL
Becke 3-Parameter Lee-Yang-Parr Hybrid Functional	B3LYP
Canadian Deuterium Uranium	CANDU
Density Functional Theory	DFT
Effective Core Potential	ECP
Generation IV International Forum	GIF
Hartree-Fock	HF
High Performance Computing	HPC
Linear Combination Of Atomic Orbitals	LCAO
Light Water Reactor	LWR
Molecular Orbital	MO
Second-order Møller-Plesset Perturbation Theory	MP2
Potential Energy Surface	PES
Self- Consistent Field	SCF
Supercritical Water-cooled Reactor	SCWR
Slater-Type Orbital	STO

Chapter 1: Introduction

1.1 Importance of Nuclear Reactors

Nuclear reactors are an important source of electricity, whose efficiency and sustainability affects billions of lives on our planet.[1, 2, 3, 4, 5, 6, 7, 8.] Nuclear reactors in Canada are used only for peaceful purposes. Nuclear reactors generate neutrons for neutron scattering and produce Cobalt-60 and thus play important roles in electricity generation, medical diagnosis and treatment, agriculture, as well as research and manufacturing. Cancer cells are more sensitive to radiation than healthy cells; γ-rays from Cobalt-60 are used to treat different forms of cancer. In agriculture, γ-rays from Cobalt-60 increase the yield and pest resistance of staple foods, which have saved hundreds of millions of lives in third world countries. Furthermore, neutron scattering is used to test the structural integrity of critical components of airplanes, which ensures safe flights by reducing chances of in-flight failures.[9]

Nuclear power is the largest non-hydro source of low carbon energy and it is considered to be a clean energy source. Nuclear energy offers environmental benefits by avoiding ~ 2.5 billion tons of CO_2 emission annually. Replacing current major sources of electricity (burning coal, natural gas or oil) with nuclear energy would greatly benefit the environment by reducing global CO_2 emissions by 30 % (back to 1996 levels). Hence, nuclear energy is considered to be part of "green solution' to global warming and climate change.[9.]

1.2 Supercritical Water-Cooled Reactor (SCWR)

Atomic Energy of Canada Limited (AECL) is the original developer of the CANDU (Canadian Deuterium Uranium) nuclear reactor. For over 60 years, AECL has been responsible for evolution of CANDU based nuclear reactors, starting with the very first 1950s and 1960s CANDU prototypes through current world-wide used nuclear reactors (Generation II concept of nuclear reactors), and Generation III reactors, such as Advanced Light Water Reactor (ALWR), that are currently starting to be employed. Both Generation II and III nuclear reactors are said to be safe and reliable, but the ever growing world population has higher needs for electricity.[10]

Due to the increased world energy demands coupled with alarming increase in global CO_2 emission, US Department of Energy in 2001 started a new program called Generation IV Initiative, where 10 different countries including Canada (The Generation IV International Forum (GIF)) have proposed six innovative, efficient and economically sustainable concepts of Generation IV nuclear reactors.[1, 2, 3, 4, 5, 6, 7, 8, 10, 11, 12, 13, 14.]

The evolution of CANDU nuclear reactor concepts allows for the extension of current pressure tube reactor concept to a novel and improved nuclear reactor concept based on strategic and environmental considerations, climate change mitigation and sustainable energy production. The idea is to maintain the original underlying proven CANDU concept, originally developed by Atomic Energy of Canada Limited (AECL), but to enhance both design and application aiming for: better performance (increased thermal efficiency), increased sustainability (to be achieved by optimizing fuel usage and minimization of waste production), higher safety, improved economics, longer design life (up to 60 years) and proliferation resistance. [1, 2, 3, 4, 5, 6, 7, 8, 10, 11, 12, 13, 14.]

Torgerson[10] et al. illustrate nuclear reactor evolution from the current CANDU design towards the novel concept of Generation IV nuclear reactors (Figure 1).

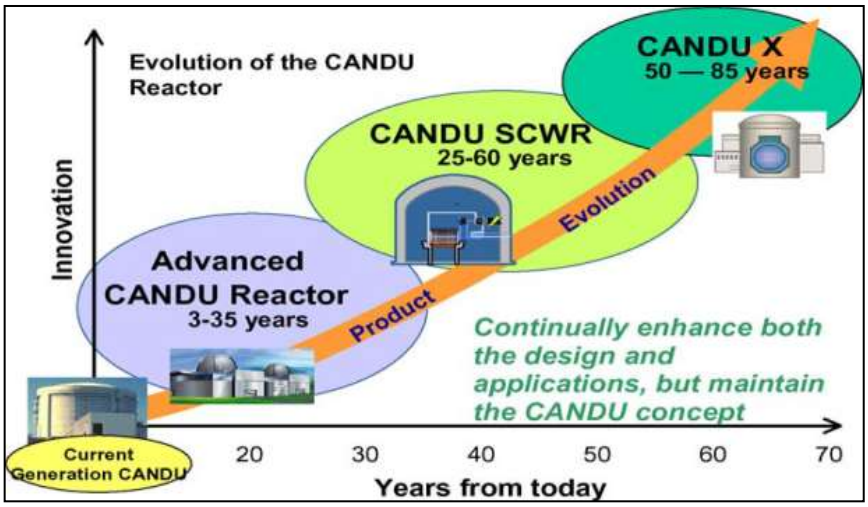

Figure 1: Evolution of CANDU nuclear reactors.[10]

One of the most promising Generation IV nuclear reactor concepts is the Super Critical Water Cooled Reactor (SCWR), which is at an advanced stage of its development. The development time frame is 2025-2060, the length of which depends on the quality of research and development. SCWR operates at very high temperature (inlet temperature of 350 °C and an outlet temperature up to 650 °C) and pressure (up to 25 MPa), which offers many advantages over current Light Water Reactor (LWR): the utilization of a single phase coolant with high enthalpy; heat transfer system is simplified (due to elimination of components such as pressurizer, steam generation, steam separation and recycle pump); direct cycle with no phase separation resulting in overall smaller volume system, allowing for expansion in turbines which in turn offers higher thermal efficiency (~45% vs. 33% of current LWR), improved economics and longer design life (up to 60 years, offering lower financial risk for investment).[1,2,3,4,5,6,7,8,10,11,12,13.] SCWR is intended for different applications such as

process heat, hydrogen production, and steam applications including extraction of oil from oil sands, desalination with primary purpose of economic energy production. The SCWR is considered to be a hybrid between current LWR and a fossil fuel SCW power plant. [1,2,3,4,5,6,7,8,10,11,12,13,14,15,16, 17, 18, 19, 20, 21, 22,23, 24, 25, 26, 27, 28, 29, 30,31 ,32, 33.]

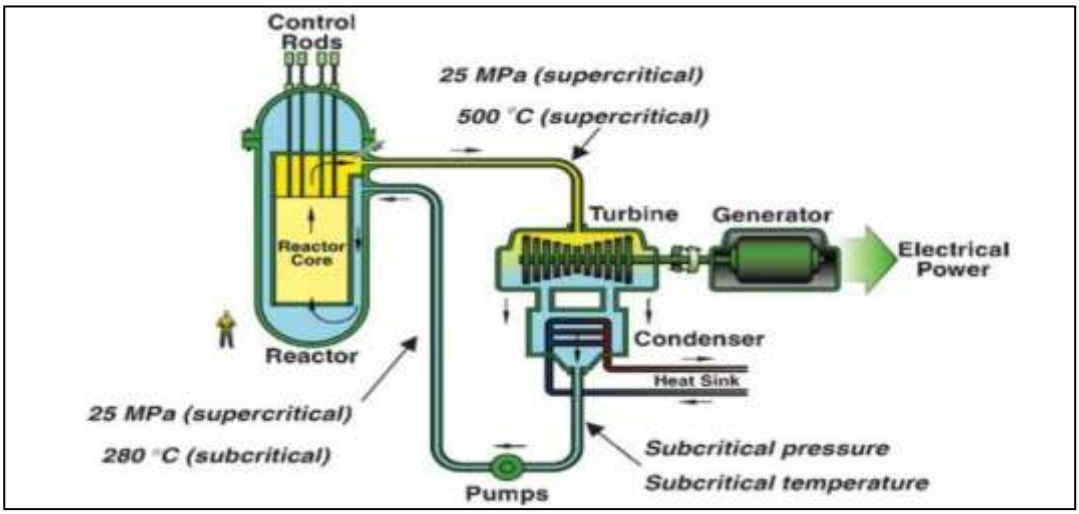

Figure 2: Schematic representation of Super Critical Water-Cooled Reactor[11]

1.3 Challenges with SCWR Development

Super-critical water cooled reactor (SCWR) as the name implies utilizes Super Critical Water (SCW) as a working fluid. Super Critical Water (SCW) refers to water above the thermodynamic critical point, specifically above 374 ºC and 22.1 MPa (Figure 3).[34] SCW coolant is responsible for increased thermal efficiency within SCWR, because SCW is a single phase fluid with characteristics of both gas and liquid. SCW behaves as a dense gas, implying that any small temperature and pressure changes in super critical region may induce significant water property changes (density, heat capacity, dielectric constant, hydrogen bonding, and transport properties). At the critical point, the specific enthalpy of water increases significantly (20 %), dielectric constant decreases 10 fold (8

vs. 80 for the subcritical region) and supercritical water becomes a non-polar solvent with reduced ability to dissolve ions.[16.]

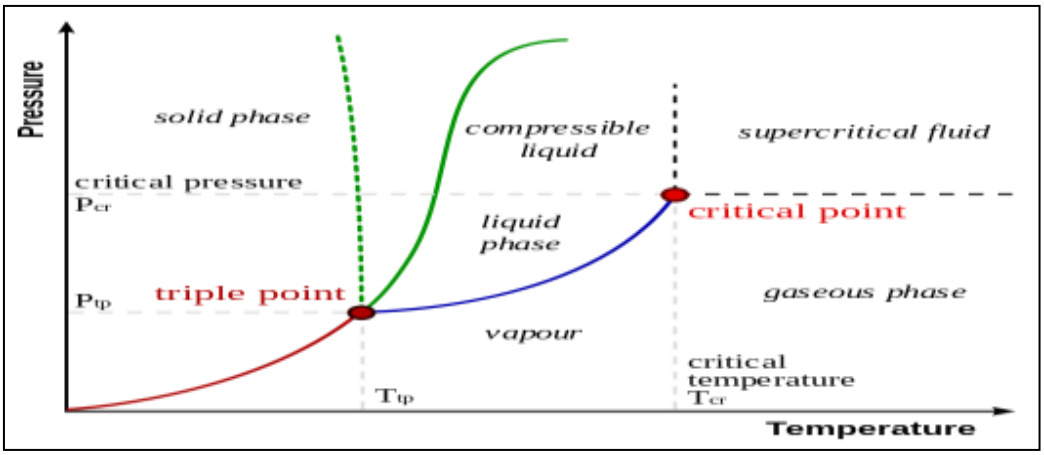

Figure 3: Water Phase Diagram.[34]

Even though there are many advantages of SCWRs, because of the increased temperatures and pressures at which they operate, these conditions can also become a liability. SCW coolant can very quickly become an aggressive oxidative environment which may result in general corrosion of the construction material within the nuclear reactor. SCW is beyond the operating conditions of the current nuclear reactors and introduces significant challenges with respect to development of Generation IV SCWR - the possibility of corrosion occurring on pipes and valves of the nuclear reactor, which may even cause nuclear reactor leakage.[16, 20, 21.] The long term sustainability and viability of the Generation IV CANDU-SCWR concept largely depends on the ability to predict and control water chemistry inside the reactor in order to minimize corrosion associated with new design.[1, 16.] This is ultimately the goal of my research.

1.4 Lead

Lead is one of the very first metals known to humans. It is believed, that the oldest lead artifact is a figure made about 3000 BC. Lead was utilized for many ornaments and building structures through many civilisations, starting with ancient Egyptians.[35, 36, 37.]

Lead is a chemical element that belongs to group 14 of the periodic table. Lead has atomic number 82 and atomic mass equal to 207.2 $gmol^{-1}$.[36.] Under normal conditions, lead is in 2+ oxidation state and has following electron configuration [Xe] $4f^{14}5d^{10}6s^{2}6p^{0}$.[21] Under certain conditions lead can be found in +4 oxidation state, but +2 oxidation state is the more common one. The +2 oxidation state is the most important in aqueous chemistry, hence it was utilized in my research investigation. Lead's chemical and physical properties include: bluish white color, solid, very soft, highly malleable, ductile, poor conductor of electricity, density of 11.34 g/cm^3, melting point of 328 °C, boiling point 1755 °C. There are 4 stable isotopes of lead: ^{204}Pb (1.48%), ^{206}Pb (23.6%), ^{207}Pb (22.6), ^{208}Pb (52.3%).[37.]

Lead is referred to as both a heavy metal and a poor metal (having melting and boiling point lower than those of transition metals).[37] Lead dioxide is used in lead-acid storage batteries, while lead nitrate is used for production of fireworks and other pyrotechnics. Lead, due to its high density, is effectively used for shielding against x-rays and gamma radiation.[35.] High density coupled with high limpness and high damping capacity gives lead advantages over other materials to be successfully used for deadening sound and for isolating equipment from mechanical vibrations. Additional uses of lead include structural material for building purposes, bullets, etc.[35.]

The main limitations of lead's use as a structural material are due to its susceptibility to creep. Lead deforms at very low stresses, subsequently resulting in stresses far below the ultimate tensile strength. However this does not completely limit lead from being used in construction material. Lead's strength is increased by alloying lead with metals such as calcium and antimony and thus allowing it to be used for construction building purposes.[35.]

Lead has been manufactured for more than 600 years and it is a well-established toxin, however its underlying aqueous chemistry is not well researched.[21, 22.] Heavy metals such as lead can easily damage the central nervous system, lungs, kidneys, liver and other vital organs, while long-term exposure may cause degenerative disorders such as Alzheimer's disease, Parkinson's disease and even cancer.[21] Lead unfortunately affects mostly children and can cause irreversible cerebral damage in children whose mothers were chronically exposed to lead during pregnancy. Lead is a well-established toxin, but its chemistry is very poorly researched on molecular level and thus requires extensive research. Understanding of the mechanism of lead poisoning at the molecular level is said to require in-depth understanding of the binding properties of lead (II) complexes.[21, 22.] Hence, my research will not only contribute to sustainable development of SCW nuclear reactor, but it will also contribute to world's research of lead chemistry on molecular level.

1.5 The Importance of Studying Lead with Respect to SCWR Development

The proposed structural materials for Generation IV SCWR are Fe-Ni-Cr and zirconium alloys. Corrosion could produce the following metal species of interest: Mn^{3+},

Fe^{3+}, Fe^{2+}, Co^{2+}, Ni^{2+}, Cu^{+}, Zn^{2+}, Pb^{2+}, ZrO^{2+}, Cr^{3+}, CrO_4^{2-} and their hydrolysis products.[3, 4, 17, 18, 20, 23] Iron, nickel, chromium and zirconium are major alloy materials since their composition has a large influence on corrosion resistance.

The importance of studying lead (Pb^{2+}) with respect to SCWR development is the fact that lead is found as an impurity within the above proposed construction material of SCWR. Trace amount of lead (Pb^{2+}) are found to be major cause of the embrittlement and crack propagation via stress corrosion cracking.[35] Hence, lead is a very important metal species to investigate with respect to development of SCWR.

At extreme temperatures and pressures (650 ºC and 25 MPa), traces of heavy metals such as Pb^{2+} tend to dissolve from the construction material into the Super Critical Water (SCW). SCW has a low density with dielectric constant 10 times lower than at room temperature (8 vs. 80) and acts as a non-polar solvent. Hence, SCW cannot successfully dissolve ions as it would otherwise in a subcritical region.[16] Instead, lead forms neutral complexes with surrounding anions (hydroxide (OH^-) and chloride (Cl^-)), and water (H_2O), and/or ammonia (NH_3). Ammonia may be added to the reactor for pH adjustment, chloride from the river water via leakage of the cooling system and hydroxide from the feed water. The power cycle of SCWR is direct cycle with no phase separation; any species formed in the reactor core will be carried out of the core along with supercritical coolant and may deposit on the fuel or turbines resulting in corrosion of construction material, ultimately leading into nuclear reactor leakage.[16, 18, 22]Experimental studies under extreme SCW conditions (650 ºC and 25 MPa) are challenging; computational methods are an excellent starting point.[16] In Chapter 3, it will be shown that results regarding the coordination number of Pb (II) water complexes are

contradictory and call for in-depth investigation. Formation of lead-ligand complexes is poorly understood both experimentally and theoretically, thus require extensive research.[17] Therefore, to obtain full control over corrosion due to lead (II) complex formation and their transport through SCWR requires understanding and prediction of the most plausible lead (II) complexes.

1.6 Research Objectives

A major challenge affecting development of SCWR is the possibility of corrosion of construction material due to the extreme operating conditions (650 ºC and 25 MPa), which are beyond experience of current nuclear reactor.[15, 16, 17, 18, 19, 20] The long term sustainability and viability of the Generation IV CANDU-SCWR concept largely depends on the ability of the operators to control its water chemistry.[1, 16.] Hence, it is essential to predict and understand formation of metal-ligand complexes within supercritical water (SCW) before appropriate chemistry water control strategy can be designed, so that corrosion associated with new design can be minimized.

The primary objective of this research is to perform a comprehensive *ab initio* calculations of lead (II) complexes including 4 different ligands: water (H_2O), ammonia (NH_3), hydroxide (OH^-) and chloride (Cl^-). The studies will include optimized molecular geometries, bond lengths, energetics, vibrational frequencies and Raman intensities of lead (II) complexes up to and including enneacoordinate species (species with nine binding ligands). Hence, the very first catalogue of systematically predicted lead (II) speciation, was obtained. The molecular geometries will be fully optimized at HF, MP2 and B3LYP levels of theory coupled with basis sets (CEP-121G, LANL2DZ, SDD for

lead and 6-31G*, 6-31+G*, 6-311+G* for smaller atoms (hydrogen, oxygen, nitrogen and chloride)).

Raman intensities are standard for HF calculations and therefore simulated Raman spectra are obtained from vibrational frequency data at HF/SDD/6-311+G*. Even though computational calculations are performed at zero Kelvin and gas phase, it is an excellent starting point since experimental research under extreme temperatures and pressures is currently formidable.

Results obtained within my research will be subsequently forwarded to Dr. Peter Tremaine at University of Guelph, who will experimentally probe lead (II) complexes utilizing Raman Spectra at higher temperatures (250º - 350 ºC). Simulated Raman spectra obtained for a series of *ab initio* calculations will be utilized to assist in interpreting experimental Raman Spectra. Zero Kelvin, gas phase simulated Raman spectra will be very similar to the one obtained at very high temperatures and pressures owing to the anharmonicity and weaker molecular bonds at extreme temperatures and pressures.

Ultimately, results will be forwarded to the engineers involved with the design of the SCWR, which will decide on an appropriate chemistry water control strategy for SCWR concept, including suitable chemical additives, optimum concentrations, and the maximum concentration of impurities that can be tolerated in the feed water at the core inlet.

The short term expected outcome of this research is:

(i) to predict the most plausible lead (II) complexes with H_2O, NH_3, OH^- and Cl^-; ultimately gaining the systematic understanding and control of SCWR chemistry.

(ii) to design experiments for basic research on SCW systems.

The long term expected outcome of this research is:

(i) the leadership in manufacturing technology if SCWR is developed in Canada;

(ii) world energy savings associated with 45 % thermal efficiency, longer design life (up to 60 years; lower financial risk for investment); and co-generation of hydrogen as an industrial feedstock and fuel to reduce greenhouse gas emission.[1, 2, 3, 4, 5, 6, 7, 8, 10, 11, 12, 13]

Chapter 2: Computational Methods

2.1 Theoretical Background

2.1.1 Classical Mechanics vs. Quantum Mechanics

Classical mechanics was discovered by Isaac Newton in the late seventeenth century, who postulated the equation of motion of the particle called Newton's second law:

Equation 1: $F = ma = m\left(\frac{d^2x}{dt^2}\right)$ [38],

where *F* is the force acting on the particle, *m* is the mass of the particle and *a* is the acceleration, the second derivative of position of particle *(x)* with respect to time *(t)*.

Classical mechanics appeared to be very successful in describing motions of macroscopic objects (large visible objects). However, towards the end of the nineteenth century, a series of experiments showed that classical mechanics failed when applied to microscopic particles (atomic and subatomic particles).[38] The experimental evidence that influenced scientists to search for brand new set of laws that will successfully describe behavior of small particles include black body radiation, low-temperature heat capacities and atomic and molecular spectra.[38] In the late 1800s, scientists were probing the intensity of light emitted by a heated blackbody as function of frequency (ν) at constant temperature (T). Blackbody refers to an object that absorbs all the light that falls on it. Scientist found that classical mechanics failed to describe behavior of black body radiation.[38.] It is the German physicist Max Planck, who in 1900 developed a theory that accounted for experimental observations of blackbody radiation by proposing that the energy of each electromagnetic oscillator is limited to discrete values and is not

continuous as initially believed by classical mechanics. That is, blackbody can emit energy only in discrete amounts (hν), meaning the emission is quantized, where, h is Planck's constant (h= 6.6 $x10^{-34}$ Js) and ν is a frequency of radiation. Hence, Planck's hypothesis of quantized energy emission was the beginning of the quantum mechanics.[38, 39.]

The photoelectric effect was the second application of energy quantization. Emission of electrons from the metal surface due to radiation is called photoelectric effect. By classical mechanics, it was expected that the kinetic energy of the emitted photoelectron would increase with increased intensity of the light and be independent of its frequency. However, results showed complete opposite, the kinetic energy of the emitted photoelectron increased proportionally with frequency of the light while being independent of the light's intensity.[38.] In 1905, Albert Einstein supported Planck's hypothesis by regarding light as composed of particle like entities called photons, where each photon has energy equal to hν.[38.]

Equation 2: $E_{photon}=h\nu$.[38]

Einstein's explanation of the photoelectric effect showed that light can be treated as both a wave and a particle, which was definitely a major breakthrough in physics for that time.[38.] Albert Einstein was awarded The Nobel Prize in Physics in 1921 for his contribution to Quantum Mechanics, more specifically for his discovery of the law of the photoelectric effect.[40]

In 1892, the French physicists Pierre-Louis Dulong and Alexis Thérèse Petit proposed a thermodynamic rule called Dulong- Petit Law. This thermodynamic law states that the molar heat capacities of all monoatomic metals are close to 25 J K^{-1} mol^{-1}.

However, the Dulong- Petit Law was based on relatively limited experimental evidence of heat capacities for monoatomic solids. Heat Capacity (C) is the quantity of the heat (q) used to change the temperature (T) of a substance by a given amount. According to Classical Mechanics, this constant volume molar heat capacity (C_v) of a monoatomic metal is equal to 3R. This was definitely true for high temperature experiments. Once technology advanced enough for experiments to be carried at low temperature, the classical mechanical approach failed, resulting in heat capacities lower than 3R, furthermore as temperature approached zero heat capacities approached zero.[39.] In order to account for the decrease of heat capacity at low temperatures, Einstein back in 1905 has assumed that each atom oscillates about its equilibrium position with single frequency (ν) with energy with discrete values (nhν), thus deriving the Einstein formula[39]:

Equation 3: $C_{v,m} = 3Rf^2 \qquad f = \frac{\theta_E}{T}\left(\frac{e^{\theta_E/2T}}{e^{\theta_E/2T}-1}\right)$,

where the Einstein temperature,$\theta_E = h\nu/k$ which describes a high frequency corresponding to a high Einstein temperature. At higher temperatures (when T» θ_E), the exponentials in f can be expanded so that:

Equation 4: $= \frac{\theta_E}{T}\left\{\frac{1+\theta_E/2T+\cdots}{(1+\theta_E/T+\cdots)-1}\right\} \approx 1$. As a result, at high temperatures the classical result for heat capacity was obtained ($C_{V,m}$= 3R). However, at low temperatures (when T « θ_E), the following equation was obtained:

Equation 5: $f = \frac{\theta_E}{T}\, e^{-\theta_E/2T}$. Hence, f approaches zero as temperature (T) approaches zero, consequently accounting for heat capacity decreasing in value at lower temperature. At physical level, at low temperatures only few oscillators contain sufficient energy to oscillate, while at high temperatures all oscillators oscillate sufficiently due to the higher

level of energy and thus approach classical result of 3R. Furthermore, the temperature dependence of heat capacity based on Einstein's theory was plotted. The plot was satisfactory, but the numerical agreement was poor, which was is turn attributed to the fact that Einstein assumed that all the atoms oscillate with the same frequency, whereas in reality they oscillate over the wide range of frequencies (from zero to a maximum value, ν_D). Debye improved on Einstein's theory by averaging over all frequencies present. This final correction of heat capacity at low temperature is also known as the Debye formula[39]:

Equation 6: $C_{V,m} = 3Rf \qquad f = 3\left(\frac{T}{\theta_D}\right)^3 \int_0^{\theta_D/T} \frac{x^4 e^x}{(e^x-1)^2}\, dx,$

where $\theta_D = h\nu_D/k$ is the Debye temperature. Equation 6 gives better agreement with experimental values of heat capacities of solids at lower temperatures and underlines the fact that the quantization must be taken into account in order to sufficiently describe the thermal properties of metals.[39]

In 1913, Neils Bohr[38] applied the concept of quantization of energy to the hydrogen atom, assuming that energy of the electron is quantized and that an electron moves strictly on one out of many circular paths around the nucleus. When an electron undergoes transition from one energy level to another, then a photon of light is absorbed or emitted. Frequency of the photon of light is described with following equation:

Equation 7: $E_{upper} - E_{lower} = h\nu$.[38]

Bohr derived a formula for the hydrogen-atom energy levels and using above formula obtained agreement with hydrogen spectrum, but failed when applied to helium spectrum. The major difficulty arose from the fact that Bohr used classical mechanical approach to describe motion of electrons within the atom.[38.]

In 1923, Louis de Broglie[38] proposed that electron motion may have wavelength aspect to it. That is, electron of the mass m and velocity v would be related to the wavelength (λ) so that:

Equation 8: $\lambda=h/(mv)=h/p$,

where h is Planck's constant and p is linear momentum.[38.] Therefore, De Broglie's breakthrough in quantum mechanics was that not only the light (electromagnetic radiation), but also electrons and all other particles can have both particle like and wave like properties. Matter's ability to behave as both wave and a particle is defined as wave-particle duality. This quantum mechanics breakthrough was an important stepping stone in evolution of physics.[38.]

The fundamental difference between classical mechanics and quantum mechanics is that in classical mechanics the state of the dynamic system is fully specified by the position (x) and velocity (v), meaning that position and velocity of a particle can be exactly determined at each instant of time (t). Based on knowledge of the initial state of classical mechanical system, the final state can be fully determined. This leads to a conclusion that classical mechanics is deterministic in nature.[41]

In quantum mechanics, the Heisenberg uncertainty principle states that we cannot determine position and momentum of the microscopic particle at the same time. That is, if the position of the particle is known, then the momentum of the same particle is uncertain. According to quantum mechanics, the state of the system on microscopic scale is not characterized by specific position (x) and velocities (v) like it was case in classical mechanics. Instead, in quantum mechanics, state of dynamic system (for microscopic particles) is completely specified by state function. This state function is also known as a

wavefunction of the particle, denoted by Greek letter Ψ, because even though it is supposed to describe state of the particle it also has wavelike properties.[41.] According to quantum mechanics, measurements of the position of the particle will not yield particular value of x. Instead, based on initial knowledge that the particle is in the state Ψ, the most precise calculation of the position of the particle is the probability of finding the particle in the range from x and x+dx in any measurement of the position of the particle. The physical interpretation of probability wavefunction is denoted by $|\Psi(x)|^2\,dx$.[41.] That is, if it is certain that there is one single particle in the spatial range between x=0 and x=L, then the probability distribution function $|\Psi(x)|^2$ must be equal to 1, which in turn means that the wavefunction has been normalized:

Equation 9: $\int_0^L \Psi(x) * \Psi(x)dx = \int_0^L |\Psi(x)|^2 dx = 1.$[41]

In quantum mechanics, results can be obtained in terms of an average values also known as an expectation value. For example $\langle x \rangle_\Psi$ is expectation value of the position (x) of the particle in the state Ψ and it is given by:

Equation 10: $\langle x \rangle_\Psi = \int_0^L \Psi^*(x)\, x\Psi(x)\, dx = \int_0^L x\, |\Psi(x)|^2\, dx.$[41]

In conclusion, the major distinction between classical mechanics (CM) and Quantum Mechanics (QM) is that Classical Mechanics is "deterministic" (meaning it gives precise results to the equation of motion of macroscopic particles), while Quantum Mechanics is "statistical" or "probabilistic" in nature (gives no precise results, instead gives probability of finding the microscopic particles in the space).[41.]

The fundamental equation in quantum mechanics used for finding the wavefunction for any system was proposed in 1926 by Austrian physicist Erwin

Schrödinger.[39.] In general, the time-independent Schrödinger equation can be written in condensed form:

Equation 11: $\hat{H}\Psi=E\Psi$ [39.]

$\hat{H}$ is Hamiltonian operator, Ψ is an eigenfunction (wavefunction corresponding to the energy E) and E is the eigenvalue of the Hamiltonian.[39.]

The time-independent Schrödinger equation for a single particle moving in 1-D with no external potential (extended version):

Equation 12: $[-\frac{\hbar^2}{2m}\frac{\partial^2}{\partial x^2}]\ \Psi= E\Psi$.[39.]

The time-independent equation as the name implies is only used when there is no time dependence and describes stationary states. The time-independent Schrödinger equation predicts that wavefunctions can form stationary states or standing waves, also known as atomic and molecular orbitals (MO). [38, 39, 41]

In general, Hamiltonian operator is the total energy of the system. It is the sum of the kinetic energy operator and the potential energy operator, just as it was the case in Classical Mechanics.

Equation 13: $\hat{H}= -\frac{\hbar^2}{2m}\frac{\partial^2}{\partial x^2} + \hat{V}(x)$ [39];

where $-\frac{\hbar^2}{2m}\frac{\partial^2}{\partial x^2}$ is equal to kinetic energy operator of the system and $\hat{V}(x)$ is the potential energy operator of the system.[39.]

In case of time-independent Schrödinger equation, Hamiltonian is the operator, which "operates" on certain wavefunction (Ψ, where Ψ is a stationary state) resulting in the same wavefunction and constant Energy (E). That is:

Equation 14: (operator) (function) = (constant factor) (same function).[39.]

Hamiltonian operator ($\hat{H}$) or total energy (E_{tot}) of the system is said to play important role in the Schrödinger equation which deals with dynamics of quantum system. The state of the dynamic system in quantum mechanics is fully specified by the wavefunction (Ψ), therefore in order to predict how Ψ changes with time only first derivative of wavefunction with respect to time ($\frac{\partial \Psi}{\partial t}$) is necessary.[41]

Therefore, the time-dependent Schrödinger equation describes how a state function (wavefunction) change with time and it is proportional to the Hamiltonian "operating" on the state function (wavefunction):

Equation 15: $i\hbar\frac{\partial \Psi(x,t)}{\partial t} = \hat{H}\,\Psi(x, t)$ [41],

where *i* is the imaginary unit, the symbol ($\partial/\partial t$) is partial derivative with respect to time, ħ is h/2π (where h is a Planck's constant), and $\hat{H}$ is Hamiltonian operator (giving total energy of any given wavefunction).[41.]

Hence, for the one-particle, 1-D system, time dependent Schrödinger equation can be written in terms of the partial differential equation:

Equation 16: $i\hbar\frac{\partial \Psi(x,t)}{\partial t} = [-\frac{\hbar^2}{2m}\frac{\partial^2}{\partial x^2} + \hat{V}(x)]\,\Psi(x,t)$.[41]

For the 3- D systems involving x, y and z coordinates above time-dependent equation is written as:

Equation 17: $i\hbar\frac{\partial\Psi(x,y,z,t)}{\partial t} = [-\frac{\hbar^2}{2m}(\frac{\partial^2}{\partial x^2}+\frac{\partial^2}{\partial y2}+\frac{\partial^2}{\partial z^2})+\hat{V}(x,y,z)]\,\Psi(x,y,z,t)$.[41]

This equation can be compressed into following equation:

Equation 18: $i\hbar\frac{\partial\Psi(x,y,zt)}{\partial t} = [-\frac{\hbar^2}{2m}\nabla^2+\hat{V}(x,y,z)]\,\Psi(x,y,z,t)$.[41.]

The symbol ∇^2 is called the Laplacian and is the sum of three second derivatives $\left(\frac{\partial^2}{\partial x^2}+\frac{\partial^2}{\partial y2}+\frac{\partial^2}{\partial z^2}\right)$.[38, 39, 41.]

Hence, the solution to the Schrödinger equation is a wavefunction (Ψ), which fully describes the dynamics of the system.[38, 39, 41.]

The Schrödinger equation and its solutions presented a breakthrough in physics because it was the very first equation describing dynamic system in quantum mechanics.[38, 39, 41] The Schrödinger equation predicts that if certain properties of a system are measured then only discrete values can be obtained, meaning that results are quantized. [38, 39, 41.] This is very important breakthrough in quantum mechanics and signifies important distinction between classical mechanics and quantum mechanics.[39.]

A significant difference between classical mechanics and quantum mechanics is the fact that quantum mechanics involves only 1st time derivative ($\partial\Psi/\partial t$), while classical mechanics uses second derivative with respect to time (d^2x/dt^2).[41.] This in turn directly influences how the state of dynamic system is specified in classical mechanics and quantum mechanics. This also leads to a significant distinction between classical mechanics (CM) and quantum mechanics (QM), where in CM action on the system within the equation of the motion (Newton's 2nd. law) is Force (F), while in QM action on the system is Hamiltonian operator ($\hat{H}$) also known as the total energy of the system.[41.]

Schrödinger equation in quantum mechanics is said to be analogous to the classical Newton's 2nd law equation and it is a key postulate in quantum mechanics that opened doors to a totally new way of dealing with problems in mechanics on atomic and subatomic level.[41.] Since in quantum mechanics, wavefunction fully describes the state of the system, therefore the time dependent wavefunction Ψ (x, t) contains all the information on the dynamics of the system (which could be also experimentally determined).[41.]

2.1.2 Computational Chemistry: Born-Oppenheimer Approximation

Computational chemistry is based on quantum mechanics and it is utilized to complement experimental studies, as well to calculate molecular properties of the systems that are too expensive to purchase or difficult to find. Obtained calculations give valuable information regarding: geometry optimizations, frequency calculations, transition structures, electron and charge distribution and similar.[42].

An exact solution of the Schrödinger equation for hydrogen atom (consisting of one electron) can be obtained. However, the Schrödinger equation for atoms with more than one electron and/or for molecules cannot be exactly solved, because of the interelectronic repulsions involved. That is, interelectronic repulsion term within the Schrödinger equation for many electron systems and molecules is not separable and therefore exact solution is not possible.[38, 43.]

The Schrödinger equation for molecules containing several atomic nuclei is overwhelming and requires alternative method to simplify such complicated equation. Hence, the Born-Oppenheimer approximation was introduced to simplify multi-electron Schrödinger equation problem.[38.]

The Born-Oppenheimer approximation was proposed in 1927 by J. Robert Oppenheimer and his graduate supervisor Max Born at that time. The key element that made the Born-Oppenheimer approximation successful is the fact that nuclei are much heavier in mass than electrons ($m_n >> m_e$) and therefore nuclei move much slower than electrons, hence nuclei motion can be ignored.[38.] Consequently, nuclei are treated as being fixed while motions of electrons are evaluated through the electron Schrödinger equation.[39.] According to Born-Oppenheimer approximation, the molecular Schrödinger

equation can be decoupled into two equations: the Schrödinger equation for electronic motion (where nuclear kinetic term is omitted) and Schrödinger equation for nuclear motion (rotational and vibrational motions).[38, 39, 41] Therefore the wavefunction for the molecule becomes:

Equation 19: $\Psi_{molecule} = \Psi_{electron} \times \Psi_{nuclei}$.[43.]

Hence, molecular Schrödinger equation:

Equation 20: $(\frac{-\hbar^2}{2}\sum_\alpha \frac{1}{m_\alpha}\nabla_\alpha^2 - \frac{\hbar^2}{2m_e}\sum_i \nabla_i^2 + \sum_\alpha \sum_{\beta>\alpha} \frac{Z_\alpha Z_\beta e'^2}{r_{\alpha\beta}} - \sum_\alpha \sum_i \frac{Z_\alpha e'^2}{r_{i\alpha}} + \sum_j \sum_{j>i} \frac{e'^2}{r_{ij}})$

$\Psi = E\Psi$.[43, 44.]

, where α and β refer to nuclei, while i and j refer to two separate electrons.

The very first term $(\frac{-\hbar^2}{2}\sum_\alpha \frac{1}{m_\alpha}\nabla_\alpha^2)$ is operator for the kinetic energy of the nuclei.

The second term $(-\frac{\hbar^2}{2m_e}\sum_i \nabla_i^2)$ is the operator for the kinetic energy of the electrons.

The third term $(\sum_\alpha \sum_{\beta>\alpha} \frac{Z_\alpha Z_\beta e'^2}{r_{\alpha\beta}})$ is the potential energy for the repulsion between α and β nuclei.

The fourth term $(-\sum_\alpha \sum_i \frac{Z_\alpha e'^2}{r_{i\alpha}})$ is the potential energy of the attraction between i electron and α nucleus.

The very last term $(\sum_j \sum_{j>i} \frac{e'^2}{r_{ij}})$ is the potential energy of the repulsion between i and j electrons.

Hence, the sum of above 5 terms is equal to the molecular Hamiltonian operator ($\hat{H}$).[38, 45.]

Furthermore, electronic wave equation can be extracted and calculated by assuming that nuclei are being fixed. In this case, the very first term, kinetic energy of the nuclei is

equal to zero, since nuclei are fixed ($(\frac{-\hbar^2}{2}\sum_\alpha \frac{1}{m_\alpha}\nabla_\alpha^2) = 0$). Hence, Resulting electronic Schrödinger equation is expressed as:

Equation 21: $(-\frac{\hbar^2}{2m_e}\sum_i \nabla_i^2 + \sum_\alpha \sum_{\beta>\alpha} \frac{Z_\alpha Z_\beta e'^2}{r_{\alpha\beta}} - \sum_\alpha \sum_i \frac{Z_\alpha Z_\beta e'^2}{r_{i\alpha}} + \sum_j \sum_{j>i} \frac{e'^2}{r_{ij}})\ \Psi_e = E_e \Psi_e$.[38,45.]

Here, the energy E_e refers to the electronic energy which includes internuclear repulsion, where internuclear distances $r_{\alpha\beta}$ are fixed at constant value.[38.]

The electronic wave equation describes properties of electrons such as motion, position and corresponding energies (while nuclei are held fixed).[38, 39, 51] Once the electronic Schrödinger equation is solved, then nuclear motion is considered. As mentioned earlier, nuclei move much slower than electrons and therefore slight change in nuclei configuration (from $q'_\alpha\ to\ q''_\alpha$) causes electrons to instantly adjust to the change, so that electronic wavefunction changes (from $\Psi\ (q_i\ q'_\alpha\ )\ to\ \Psi\ (q_i\ q''_\alpha\ )\ )$ as well electronic energy will change according to a new configuration (from U (q'_α) to U (q''_α)).[45.] Here, q_i and q_α symbolize the electronic and nuclear coordinates, respectively.[43.] Furthermore, the nuclear Schrödinger equation is given by:

Equation 22: $(\frac{-\hbar^2}{2}\sum_\alpha \frac{1}{m_\alpha}\nabla_\alpha^2 + U\ (q_\alpha))\ \Psi_N = E\Psi_N$.[38, 45.]

The nuclear coordinates q_α are variable in the nuclear Schrödinger equation, although E is a constant. Therefore, the nuclear Schrödinger equation describes the motion, position and energies associated with translational, rotational and vibrational motions of the nuclei.[45.]

The principle of Born-Oppenheimer can be utilized to obtain bond distances between atoms. By selecting specific internuclear distance in diatomic molecule, the Schrödinger equation for the electrons can be solved, thus energy of the molecule with

respect to bond distance can be determined. Then different separation distance between two nuclei can be chosen thus repeating calculations, which in turn allows for determination how the energy of the molecule changes with bond distances.[39.]

The Born-Oppenheimer approximation is very successful for ground state molecules, implying that it introduces only a small error for the ground electronic state of diatomic molecules. However, approximation introduces large errors for excited state polyatomic molecules.[38, 39.]

The potential energy of the surface (PES) describes the relationship between the energy (E) of the molecule and its geometry. It is considered to be an important concept in computational chemistry. Born-Oppenheimer is considered as a cornerstone of a computational chemistry, because it includes concept of the potential energy surface (PES) and makes concept of molecular geometry meaningful.[38, 39, 40.]

In conclusion, Born-Oppenheimer approximation simplifies rather formidable molecular Schrödinger equation by allowing for solving both electronic Schrödinger equation (which gives electronic wavefunction and electronic energy) and the nuclear Schrödinger equation (which gives the nuclear wavefunction and nuclear energy).[46]

2.1.3 Theory and Importance of *Ab Initio* Calculations

Computational methods, such as *ab initio* (Latin for "from the beginning") is based on quantum mechanics and utilizes Schrödinger equation to obtain detailed information about molecular structures (optimized molecular geometries and energetics associated of the system, vibrational frequencies). [47.]

The wavefunction (Ψ) describes the behavior of the electrons, atoms and molecules. The exact solutions are available for simple cases, such as particle in the box, rigid rotor, hydrogen atom, while for many-electron atoms only approximation can be given. *Ab Initio* Computational method, also known as non-empirical method, uses well defined approximations such as Born-Oppenheimer approximation to solve complex molecular Schrodinger equation. This means that electronic and nuclear Schrodinger equations are separated and solved accordingly making calculations much simpler. Also, using the same approximation, electronic energies can be calculated at different internuclear distances.[47, 48.] Hence, the *ab initio* method does not necessarily infer accuracy, instead it refers to approximation that can be gradually brought to approach the accurate limit.[47.]

The main goal of the quantum chemistry *ab initio* calculations is to solve the Schrödinger equation which will in turn give information regarding optimized molecular geometries, bond angles, bond lengths and vibrational frequencies.[47.]

Quantum mechanics was in the past, a subject for experts only, while today's advanced computer software and hardware allows anyone to be able to perform sophisticated calculations using *ab initio* calculations.[48.] Researchers utilize electronic structure method to predict molecular structure as well as physiochemical properties of

the system. Modern quantum chemistry software is user friendly and no longer depends on detailed knowledge of the quantum mechanics.[48.]Quantum mechanical calculations, *ab initio* methods, were in the past only possible for very small molecules, but with beginning of 21st century, computational calculations are made possible for molecules involved in biological processes (systems involving 50-100 molecules).[48.] Hence, the availability of advanced computers has allowed Schrodinger equation of many-electron systems to be solved to high levels of approximation and to be in excellent agreement with results obtained through experimental studies. Hence, computational chemistry nicely complements experimental studies such as (NMR, IR, X-ray crystallography).[48.] For example, X-ray crystallography reveals molecular crystal structures, which is in fact difficult for computational calculations since it requires interaction potentials. However, computational methods such as ab initio calculations add valuable information regarding the molecular system such as molecular geometries, bond lengths and bond angles.[48.]

Sauer et al.[46] introduces experimental methods of solid investigation such as NMR spectroscopy and STM (scanning tunneling microscopy). Even though these experimental studies were useful investigation tools, they were unable to answer questions regarding the geometry of the molecular structure or what is nature of the bond between given atoms. Quantum mechanical *ab initio* method was found to be important research tool since it gives answers to questions regarding molecular geometry and energetics of the given molecular system.[46.] Hence, *ab initio* calculations as well as supercomputers are expected to become essential research tool for biological systems in the near future, implying that even computational methods can provide realistic experimental settings

involving liquid systems at room temperatures (since liquid environment is naturally occurring for biological systems.)[48.]

2.1.4 Hartree-Fock Method (HF)

The Hartree-Fock (HF) method is the simplest *ab initio* method of calculations, zero-order approximation wavefunction, which was first introduced by Hartree in 1928.[49] It provides a very well defined stepping stone to more sophisticated levels of theories, which come close to the solution of the Schrödinger equation.[41, 46, 48.]

The optimized electronic molecular geometries and its corresponding energies are obtained by solving electronic Schrödinger equation (Equation 17). However, due to the electron-electron interaction term within the Hamiltonian operator, this equation can be solved only by introducing large approximation.[45] The goal of computational chemistry is to find appropriate approximation methods and to test their validity. HF method is considered to be the most basic approximation method, because it views motion of the electron around the static nucleus as an averaged potential of all electrons within the given molecular system. That is, it replaces repulsion between individual electrons by interaction of each electron with the average charge distribution due to the rest of the electrons. Hartree-Fock calculations (HF) calculations are successful for determining molecular geometries, bonds and angles, which takes into account Coulombic electron-electron repulsion by integrating repulsion term. [49] HF method decouples the many-electron Schrödinger equation into many single-electron equations. Hence, each one electron equation is much simpler to be solved and results in single-electron wavefunction (also known as orbital) and corresponding orbital energy.[50]

When solving Schrödinger equation, electrons must be indistinguishable and must obey the Pauli Exclusion Principle, where all electronic wavefunctions must be antisymmteric with respect to interchange of two electrons. The Pauli Exclusion Principle states that no two electrons with the atom can have the same four electronic quantum numbers (n, l, m_l and m_s quantum number). Also, each orbital can contain maximum of two electrons with two different spins. For example if one electron has spin up (α= +1/2), then 2nd electron must have opposite spin or spin down where (β=-1/2). [50.]

The HF approximation assumes that an N particle wavefunction (Ψ (r)) is a product of single-electron wavefunctions (ψ (r)), which are antisymmetric with respect to each other. This HF approximation is presented in following Slater determinant for n electron system (Equation 19), which is described as an antisymmeterized linear combination of products of N one-electron wave functions.[50.]

Equation 23: $\Psi(1, 2, \ldots, 2N) = \frac{1}{\sqrt{2N!}} \begin{vmatrix} \psi_1\alpha(1) & \psi_1\beta(1) & \cdots & \psi_N\alpha(1) & \psi_N\beta(1) \\ \psi_1\alpha(2) & \psi_1\beta(2) & \cdots & \psi_N\alpha(2) & \psi_N\beta(2) \\ \vdots & \vdots & \ddots & \vdots & \vdots \\ \psi_1\alpha(2N) & \psi_1\beta(2N) & \cdots & \psi_N\alpha(2N) & \psi_N\beta(2N) \end{vmatrix}$

Here, 2N is number of electrons in the closed shell system, in which wavefunction are represented by N doubly occupied spatial orbitals. Each of 2N electrons can have α (+1/2) or β (-1/2) spin orbitals. Molecular orbital is linear combination of atomic orbitals, where electrons are placed in each orbital, but these electrons are indistinguishable, because there is no way of knowing which electron is which. When two electrons are interchanged it is equivalent to switching two columns or rows of determinant, which in turn changes the sign of the determinant. This in turn satisfies antisymmetric property of the determinant. Also, if two electrons occupy the same orbital with same spin orbital, there

will be two identical columns or rows and subsequently determinant will be equal to zero.[50]

The Born-Oppenheimer approximation, ignores the nucleus-nucleus repulsion potential energy term (otherwise present in the Hamiltonian operator for a 2N electron molecule) can be ignored since they are constant for given molecular geometry. The energy term presented using Dirac notation is given in

Equation 24: $E = \langle \Psi(1,2,\dots,2N) | \hat{H} | \Psi(1,2,\dots,2N) \rangle$,

Which can also be written as following:

Equation 25: $E = 2 \sum_{i=1}^{N} I_j + \sum_{i=1}^{N} \sum_{j=1}^{N} (2J_{ij} - K_{ij})$,

Where,

Equation 26: $I_j = \int dr_j \, \psi_j^* (r_j) \left(-\frac{1}{2} \nabla_j^2 - \sum_A^M \frac{Z_A}{r_{jA}} \right) \psi_j (r_j)$

Equation 27: $J_{ij} = \iint dr_1 \, dr_2 \, \psi_i^* (r_1) \, \psi_j^* (r_2) \frac{1}{r_{12}} \psi_i (r_1) \, \psi_j (r_2)$

Equation 28: $K_{ij} = \iint dr_1 \, dr_2 \, \psi_i^* (r_1) \, \psi_j^* (r_2) \frac{1}{r_{12}} \psi_i (r_2) \, \psi_j (r_1)$

Here, I_j is the electronic energy of single electron moving under attraction of the nucleus. On the other hand, J_{ij} term represents Coulomb integral that represents electrostatic repulsion between an electron in orbital Ψ_i and electron in orbital Ψ_j. The very last term, K_{ij} represents exchange integrals, which differs in exchange of electrons.[50.]

The variational principle[51] states that using any trial wavefunction other than ground-state wavefunction will result in an energy that is greater than the ground state energy. Hence, if the trial wavefunction depends on the variational parameters, it implies that corresponding energy will also depend on the very same variational parameters. Hence, the variational principle allows the energy for trial wavefunctions to be minimized

with respect to each of the variational parameters and ultimately approach the ground-state energy. When the variational principle is applied to the Slater determinant, the resulting equation is:

Equation 29: $\hat{F}(r_1)\,\psi(r_1) = \varepsilon_i\,\Psi_i(r_1)$

Here, $\hat{F}$ (r) is the Fock operator that operates on the wavefunction $\psi(r_1)$, which in turn gives the same wavefunction and eigenvalue (ε_i) called Hartree-Fock orbital energy.

The Fock operator is represented in following equation:

Equation 30: $\hat{F}(r_1) = -\frac{1}{2}\nabla_1^2 - \frac{Z}{r_1} + \sum_j^N [2\hat{J}_j(r_1) - \hat{K}_j(r_1)$

Where $\hat{J}_j$ (r_1) and $\hat{K}_j$ are the Coulombic and exchange operators given by following equation:

Equation 31: $\hat{J}_j(r_1)\,\psi(r_1) = \psi_i(r_1) \int dr_2\, \psi_j^*(r_2)\frac{1}{r_{12}}\psi_j(r_2)$

Equation 32: $\hat{K}_j(r_1)\,\psi(r_1) = \psi_i(r_1) \int dr_2\, \psi_j^*(r_2)\frac{1}{r_{12}}\psi_j(r_2)$

The HF wavefunction does not solve exactly Schrödinger time independent equation, instead it approximates many electron problem to effective one electron quantum mechanical problem by utilization of Fock equation (Equation 30).

Hence, the HF method's major deficiency is the fact that it treats each electron as moving under influence of average effect of all other electrons, meaning that probability of finding one electron is independent of the position of the other electron. The HF method is known as the *model of the independent particle* due to its lack of correlation function.[53.] Therefore limitation of the given HF calculation method is the lack of the electron correlation between electrons of opposite spins, which induces systematic error in HF calculation (the calculated energies are too high). Correlation energy, denoted by

E_{corr}, is the energy difference between the exact energy and Hartree-Fock energy.[52] Hence, when the HF limit is achieved, then the error associated with the HF approximation for the given system is determined by the difference between HF limit energy (E_{HF}) and exact energy (E). This energy difference is called correlation energy (E_{corr}) and it is given in the following equation:

Equation 33: $E_{corr}=E- E_{HF}$,

where E is the actual energy of the system and E_{HF} is the energy of the system in the HF limit.[42,52.] Even though energies obtained utilizing HF method are systematically high, predicted optimum molecular geometries, energy trends, orbital shapes are reasonably accurate.[52.]

Neglect of electron correlation has profound effects with regards of determining accurate wavefunctions and molecular properties that are determined from them such as: metal-ligand and the hydrogen bonds are not balanced correctly, there is a preference for the higher coordination number, and too long bond distances might be obtained for in complexes with low oxidation numbers.[42, 53.]

2.1.5 Self-Consistent Field (SCF)

The Hartree-Fock method is also known as the self-consistent field (SCF) approximation, because it utilizes a self-consistent procedure to obtain HF orbital energy and optimized geometries based on information within the wavefunction (Equation 29). An initial guess is made with aim to evaluate the Coulomb operator ($\widehat{J_J}$ given in Equation 31) as well as the exchange operator ($\widehat{K_J}$ given in Equation 32), which are subsequently used to evaluate the Fock operator ($\hat{F}$ given in Equation 30). Once Fock operator is

obtained, the HF equation (equation 29) is evaluated in order to obtain new set of wavefunctions (orbitals), which are further more used to obtain new Coulomb and the exchange operator. This process is repeated until the values of energies and orbitals (wavefunctions) have converged, meaning resulting parameters are self consistent (constant) values from each iteration process to another. This iterative process of searching for converged energies and wavefunctions is called self-consistent field method (SCF).[53.]

2.1.6 Møller-Plesset Perturbation Theory (MP2)

The second order Møller-Plesset perturbation theory (MP2) is usually the very first correlation method applied when calculating energies for the new system. As the name implies, MP2 performs perturbation on molecular system initially treated with HF method, which was first introduced by Møller and Plesset in 1934.[54] It was not until 1975, when Binkley and Pople have put MP2 into practice as a computational method of investigating molecular geometries and their corresponding energies.[55]

MP2 method accounts more effectively for interelectronic repulsion than HF method does, by making minor corrections to HF method in terms of molecular geometries, molecular properties, and ionization energies.[47.] Hence, since HF method is also known as self-consistent field (SCF) approximation, the MP2 method is consequently called a post- SCF approximation. The MP2 method of approximation, unlike the HF method, accounts for electron correlation. The wave functions within MP2 method are “correlated”, which means that motion of electrons depends on the electron

repulsion between each electron, hence Columbic repulsions between each electron is taken into the account during calculations.[47, 50.]

The electron correlation problem within MP2 method of approximation is treated as an perturbation theory in Schrödinger equation and it is represented as follows:

Equation 34: $\hat{H} = \hat{H}^0 + \lambda \hat{H}^1$,

where $\hat{H}^0$ is the unperturbed Hamiltonian operator and $\hat{H}^1$ is the perturbation performed on the molecular system (perturbed Hamiltonian operator) and λ is order of perturbation.

Furthermore, the wavefunction is corrected as well and it consists of the eigenfuncntion (Ψ) of the unperturbed Hamiltonian operator ($\hat{H}^0$) plus series of correction terms (Equation 35).

Equation 35: $\Psi_n = \psi_n^{(0)} + \lambda\psi_n^{(1)} + \lambda\psi_n^{(2)} + \ldots$

Similarly,

Equation 36: $E_n = E_n^{(0)} + \lambda E_n^{(1)} + \lambda E_n^{(2)} + \ldots$

The first order perturbation to the one- electron Hamiltonian is Hartree-Fock (HF) approach. However, higher order of correction increases electron correlation. These higher corrections are labeled by MP abbreviations followed by the numbers 1, 2, 3, 4 which in turn indicates where perturbation-theory expansion is stopped.[47] Hence, the MP2 Energy term can be expressed as indicated in following equation.

Equation 37: $E_{MP2} = E_{HF} + E^{(2)}$

The energy correction ($E^{(2)}$) is given by following equation:

Equation 38: $E^{(2)}=\sum_{S\neq 0}\frac{|\langle\psi_S^0|\hat{H}^{(1)}|\phi_0\rangle|^2}{E_0-E_S^{(0)}}$,

Here: ψ_s^0 is the unperturbed wavefunction, ϕ_0 is the HF wavefunction, E_0 is the zero-order MP2 energy and $E_S^{(0)}$ is the correlated energy. On the other hand, $\hat{H}^{(1)}$ is the difference between true potential energy term (interelectronic repulsion) and the HF interelectronic potential.[45.]

The advantage of post SCF computational methods over HF method is that they improve the accurate description of the molecular system (more accurate representation of molecular geometry and energetics) as well as reliable thermodynamics associated with particular molecular system.[56] This higher accuracy of MP2 method is attributed to correlation function. When compared to experimental results, MP2 has very close results to experimentally obtained data, while HF method gives larger errors.[45, 50.]

A disadvantage regarding MP2 method of approximation is the fact that this method is more expensive than HF method. However, computer technology is evolving rapidly, which will in turn make MP2 method cheaper. Another disadvantage regarding MP2 method is the fact that it does not involve variational perturbation as it was case in HF method. Hence, MP2 method may give resulting energy that may be even lower than the exact total energy. [50.]

2.1.6 Density Functional Theory (DFT)

Density functional theory (DFT) was created by Hohenberg and Kohn in the 1964.[57] Hohenberg and Kohn were the first one to show that the ground state electronic energy (E_0) of the many-electron system is functional of electron density ($E_0[\rho]$), and that minimal energy is obtained by solving single-particle equation with an effective "exchange-correlation" potential.[47,49.] Authors regard Thomas-Fermi method and Hartree-Fock method to be a predecessor of Density Functional Theory. DFT method takes into account that the ground-state electronic energy is completely determined by electron density (ρ). Hence, the energy of the molecular system depend on the electron density and not many-particle wave function as it is the case with HF and MP2 methods of calculations.[47, 49, 53.]

Equation 39: $E_0 = E_0[\rho_0]$

Here, square brackets indicate a functional relationship between the energy and density. In mathematics, functional denotes the function of a function. Hence, in DFT method of calculations, functional is the function of electron density (ρ), which is in turn the function of coordinates in real space (ρ (x, y, z)). This electron density (ρ) can be measured by electron diffraction or X-ray diffraction.[45.]

Hohenberg and Kohn have shown that electronic energy (E) of the many-electron system is variational for any trial electron density (ρ), so that E_0 and q_0 are exact quantities (as indicated in following equation).

Equation 40: $E_0 = E_0[\rho_0] \leq E[\rho]$,

Since 1960's, DFT methods have been utilized in research that involves probing electronic structures of solids, while since 1990's have become progressively used in

molecular calculations.[52.] It is said that DFT method started evolving within the computational chemistry since 1980's. It is presented as a method that complements results obtained from experimental studies such as NMR, ESR and UV spectra. DFT method of calculation is specifically used to determine optimized geometrical structures, force fields, frequencies, activation barriers, dipole moments and one electron properties. DFT computational method is used to calculate molecular structures and thermochemical data that was once limited to HF method and post-HF method of calculations.[58.] The main advantage of DFT method is that obtains greater accuracy results than HF method at only slighter higher cost than HF method, while still cheaper than MP2 method for medium and larger molecular systems. Also, it can be utilized for large biological systems and is much faster calculation than it would be otherwise done with HF and MP2 calculations.[50] These advantages are attributed to the effects of electron correlation, which is computed via functional of electron density. DFT functional partitions the electronic energy into several components, which are in turn computed separately: the kinetic energy term, potential energy term involving electron-nuclear interactions, potential energy term and involving electron-electron potential (as presented in following equation).

Equation 41: $E= \langle T[\rho_0]\rangle + \langle V_{Ne}[\rho_0]\rangle + \langle V_{ee}[\rho_0]\rangle$

Here, angle brackets denote quantum-mechanical average value. The kinetic energy term, arising from the motion of electrons, is presented in terms of one-electron orbitals (ϕ). Hence, electron density can be expressed as following:

Equation 42: $\rho_s = \sum_i^n |\phi_i|^2$

The electron-electron repulsion term can be further decoupled into Coulomb self-interaction of the electron density (J [ρ]) and exchange-correlational term (E_{XC} [ρ]) which

contains remaining part of the electron-electron interaction. Therefore, DFT energy term can be written as presented in following equation:

Equation 43: $E_{DFT}= T_s [\rho]+ V_{Ne} [\rho] + J [\rho] + E_{XC} [\rho]$

The traditional functional of DFT method are BLYP which stand for Becke, Lee, Yang and Parr. Becke (B) refers to exchange functional, while LYP refers to correlation functional. The hybrid density functional available in Gaussian program is B3LYP, where B3 refers to Becke's three parameter exchange functional.[48, 50.] B3LYP is exactly the hybrid density functional that will be used within my research study. DFT method is said to be much more accurate than both HF and MP2 methods. [47, 48.]

Computational ab initio studies performed on water utilizing different levels of theory (HF, MP2 and DFT) at with different basis sets, concluded that electron correlation methods such as B3LYP and MP2 give closer result to experimental results than HF did. Closeness to experimental results was attributed to the electron correlation in MP2 and DFT computational methods. [47, 48.]

The weakness of DFT is that it depends on adequate knowledge of the exchange correlation energy functional and currently there is no known systematic way to achieve an arbitrarily high level of accuracy. The exchange-correlation potentials can be confidently determined when an accurate electron density is known.[38.] Hence, Kohn et al. [59] suggest that further research is necessary regarding the various unknown-exchange–correlation functionals. Improving functionals would eventually improve DFT calculations.[54.]

2.1.7 Geometry Optimization

Geometry optimization involves a mathematical procedure called nonlinear optimization involving different algorithms. An initial guess of molecular structure is given within the input, in terms of internal coordinates called z-matrix, where all atoms involved in bonding are specified, bond distances, alpha (inter-bond angle) and beta angles (dihedral angle). The wavefunction and energy are computed for the initial guess of the geometry. Here, bond lengths and angles are varied until the energy is decreased sufficiently reaching energy minima. The optimized geometry is obtained by an iterative process, where integrals are recalculated, repeating energy calculations and looping through SCF calculations of energy until an energy minimum has been identified and where forces within the molecule are sufficiently close to zero. Once geometry is optimized fully, output contains such as bond lengths, bond angles, vibrational spectrum (IR, Raman, NMR spectrum, etc.).

2.1.8 Importance of Choosing Appropriate *Ab Initio* Method

Rotzinger[53] emphasizes the importance of choosing appropriate computational methods as well as appropriate basis sets in order to obtain the most accurate molecular geometries, energies, bond lengths. The author further implies that treatment of electron correlation with appropriate techniques is essential in order to obtain reliable properties. The author also implies that different computational techniques may give different coordination number which in fact largely depends on the energy and molecular geometry of the given complex. In order to demonstrate high importance of choosing appropriate computational method and basis set, the author performs different computational

calculations using different computational methods as well as basis sets on various complexes.[53]

In this study, limitations of each computational method were summarized. For example, HF method prefers higher oxidation number complexes, because lower oxidation number complexes may result in longer bond distances. On the other hand, DFT calculations such as BLYP and B3LYP methods prefer lower coordination numbers. Also, DFT calculations indicate that hydrogen bonds are not being described correctly in highly charged metal complexes (2+ and higher).[53]

All this information is very valuable towards my research project since appropriate selection of appropriate computational method and basis set will be essential for successful and the most optimized molecular geometries and the most reliable computational results.[53]

2.1.9 Basis Sets

Basis sets are essential component of computational chemistry utilized to perform *ab initio* calculations. All theoretical calculations performed on molecular electronic structures are achieved by utilization of basis sets. Basis sets are mathematical descriptions of atomic orbitals (AO), which combine together into linear combination of atomic orbitals (LCAO) to approximate the molecular wavefunction (molecular orbital (MO)).[47.] It is of great importance to identify the most suitable mathematical function that will successfully describe the wavefunction. These mathematical functions are not necessarily only the traditional atomic orbitals, instead these functions can be any functions suitable for a complete description of molecular wavefunctions.[45.] The most

commonly used basis functions are Gaussian functions and Slater functions. These functions describe the electron distribution around an atom, while linear combination of atomic basis functions yields the electron distribution in the molecule as a whole. *Ab initio* calculations utilize Gaussian functions, while semiempirical methods use Slater functions.[45,60]

Furthermore, Gaussian functions are combined into linear combinations of Gaussian-type orbitals (GTO). A single Gaussian-type function, also known as primitive Gaussian, is combined with other primitive Gaussians into linear combination of them. Linear combination of primitive Gaussians is referred to as contracted Gaussian. This contracted Gaussian is a basis function, which are used in theoretical calculations. Linear combinations of basis functions define atomic orbitals (AO), while LCAO gives MO, as mentioned earlier. Basis sets used in *ab initio* calculations are based on idea of linear combination of GTOs.

Gaussian-type orbitals (GTO) are given by following equation:

Equation 44: $G_{lml}(r,\theta,\phi) = N_l r^l \exp(-\alpha r^2)\ Y_l^{ml}(\theta, \phi)$.

Here, N_l is the normalization constant, r is the distance between the nucleus and the electron, α is a shielding constant and $Y_l^{ml}(\theta, \phi)$ are spherical harmonics (which defines angular part of each wavefunction).

Slater-type orbitals (STO) were first introduced by John Slater[61] in 1930 and are expressed as:

Equation 45: $S_{lml}(r,\theta,\phi) = N_{nl} r^{n-1} \exp(-\zeta r)\ Y_l^{ml}(\theta, \phi)$.

Here, ζ (Greek symbol zeta) is the effective charge at the nucleus, the meaning of other symbols are the same as in Equation 41.

Hence, Slater-type atomic orbitals and Gaussian-type orbitals mainly differ in the exponential term as it is evident from their equations. STO are better suited for description of atomic orbitals, owing to the cusp at the nucleus (r=0), as well as more accurate description of decay at the extremities. The main advantage of Gaussian-type orbital is that it takes much less computer time to evaluate integrals. However, GTO suffers from the loss of the accuracy of the presentation. In order to make up for this disadvantage, a linear combination of different GTOs can be taken in order to accurately represent a single atomic orbital. Even though, GTO requires multiple functions for accurate descriptions of atomic orbitals, its speed makes it more desirable tool in theoretical calculations.

There are different basis sets: minimal, split valence, polarized and diffuse function basis sets, electron core potential (ECP) basis sets. [62.]

Minimal basis sets, as the name implies contains minimum number of basis functions (single ζ basis set) for theoretical calculations of each atom and uses fixed size atomic orbitals. An example of the minimal basis set is STO-3G, developed by Nobel prize winner Pople[63], and according to the name it uses 3 Gaussian functions/primitives per basis function (3G from the name), while STO means "slater type orbitals". Therefore STO-3G approximates Slater type orbital with Gaussian functions. Also, STOs decay exponentially with distance from the nuclei. STO-3G is used for the smallest systems, it is the fastest but the least accurate basis set. STO-3G is small basis set, but very efficient in determining molecular geometries. Few examples of experimental studies when

compared with STO-3G based *ab initio* calculation indicated deviation of 0.02 Å for given bond lengths. On the other hand, weakness of the minimal basis set STO-3G was said to be calculated energetics which had much greater deviation from the experimentally obtained values.[62.]

The more commonly used basis sets are Split-valence basis sets. These type of basis sets require more functions to more accurately describe orbitals, however they take advantage of the fact that outer shell electrons are more important for calculations than inner shell electrons. This in turn minimizes number of functions required for calculation using split-valence basis sets. Here, inner shell orbitals are described by single STO, while the outer valence electrons, as the name implies, split into inner and outer valence, with each outer orbital being described by an STO.[47.] The split valence basis sets include 3-21G and 6-31G and are combination of speed obtained from smaller basis set (STO-3G) and accuracy of larger basis set. Split valence basis sets allow valence orbitals to change size but not the shape. The double zeta valence basis sets, like 3-21G use two sizes of constructed functions for each valence atomic orbital. Similarly, triple zeta valence basis sets, like 6-311G, utilize three sizes of constructed functions for each valence atomic orbital[47.]

There are additional adjustment that can be when mathematically describing molecular orbitals, such as adding polarization function and/ diffuse function, subsequently forming polarized basis sets, as well as diffuse basis set.[47]

Polarized basis set contains * sign, which indicates that d function is added to the first row atoms and it is denoted as 6-31G (d) or 6-31G*. Further addition of p functions to hydrogen results in basis set called 6-31G** which equals to 6-31G (d, p). Polarized

basis set is most commonly used for medium sized systems. Unlike the split valence basis set, the polarized basis function allows orbitals to change the shape as well. This is possible since polarized basis set adds orbitals with angular momentum beyond what is required for the ground state for the atom.[47.]

Diffuse functions basis sets are presented as 6-31+G (d) or 6-31+G*, where diffuse function is added to heavy atoms meaning that orbitals are allowed to occupy a larger region of the space. If there is nomenclature such as 6-31++G (d) or 6-31++G* meaning diffuse function is added to the hydrogen atom as well. However, diffuse function on hydrogen very rarely makes significant improvement regarding the accuracy of calculations. Diffuse function are used for systems such as anions, molecules with lone pairs, systems in their excited states (allows orbitals to occupy more space). It is very important to carefully choose basis sets in order to obtain appropriate molecular geometries.[47.]

The basis sets chosen for small atoms (hydrogen, oxygen, nitrogen and chloride) with respect to my research are: 6-31G*, 6-31+G* and 6-311+G* basis sets.

Rotzinger[60] et al. showed that heavy metals exhibit large basis set superposition error (BSSE) when utilizing basis sets such as 6-31G*, 6-31+G*. This large error was attributed to the fact that, the basis sets for heavier atoms are complicated due to high number of electrons and therefore larger atoms require much larger basis sets in order to obtain accurate energetics as well as optimized geometries. Solution to such problem is given by introduction of Effective Core Potentials (ECP).

Larger atoms require much larger basis sets in order to obtain accurate energetics as well as optimized geometries. Large set of Gaussians are required to accurately

describe chemically inert core electrons. Solution to such problem is given by introduction of Effective Core Potentials (ECP). Within ECP calculations, the *"frozen core approximation"* is used. This means that core orbitals are inert to changes in chemical bonding. This approximate function is called the pseudopotential (PP) or effective core potential (ECP). Hence, ECPs solve the large atom problem by dealing with valence electrons only. Avoiding explicit treatments of core atomic orbitals minimizes the cost and complexity of computational calculations. ECP approximation makes sense, since many chemical properties of elements are described by valence electrons, which actively participate in chemical bonding. These chemical properties include: bond strengths, electron affinities, ionization potentials, excitation energies, as well as molecular geometries. Also, past research has indicated that ECP approximation obtains almost as accurate results as the more costly and time consuming all-electron (AE) calculations. Therefore, it is only natural that ECP basis sets are preferred over AE basis sets for treatment of all large atoms.

When constructing ECP basis sets, it is very important to choose appropriate size of the core. Size of the core can affect the accuracy of calculations (small cores being more accurate), as well as efficiency and large computational savings of calculations (large cores give more efficient results). However, when relativistic contributions are implicitly taken into account, then too small cores may lead to errors. This is attributed to the fact that nonrelativistic kinetic energy within the relativistically parameterized ECP approximation may not give the most accurate description of relativistic kinematics.

Dolg[64] et. al investigated errors associated with specific size of the core. For larger atom such as lead (Pb), two frozen cores are considered: [Xe] $4f^{14}$ $5d^{10}$ and [Xe] $4f^{14}$.

Here, when four valence electron system is considered for lead, frozen core (FC) errors can be as large as 1 eV. This was attributed to the fact that there is larger radial overlap of the Pb 6s and 6p valence orbitals with the Pb (78 electron) core shells. However, including 5d electrons into the valence shell, brings number of lead valence electrons to 14 valence electron system, which in turn reduces FC error to 0.07 eV. Very small errors, such as 0.01 eV are found when 5s and 5p electrons are also included in valence space making it 22 valence electron system.

The effective core potential (ECP) basis sets utilized within this research are: CEP-121G, LANL2DZ and SDD. The CEP-121G basis sets uses Stevens-Basch-Krauss pseudopotentials. LANL2DZ basis set utilizes Los Alamos pseudopotentials (also known as Hay and Wadt) plus Double Zeta (DZ). Furthermore, SDD uses Stuttgart/Dresden electron core potentials, also known as Stoll-Preuss (SP).[64.]

2.2 Methodology

Ab initio calculations, are performed using the Gaussian03 Software[65]. ACEnet (Atlantic Computational Excellence Network)[66], a High Performance Computing Cluster (HPC) was used, specifically *"Placentia",* located at Memorial University of Newfoundland, Canada.

The very 1st step was to learn with Gaussian 03 software commands, which are essential for conducting research. The 2nd step was to choose appropriate levels of theory, at which molecular geometries will be optimized. Hence, the molecular geometries were fully optimized using a stepping stone approach, where geometries were optimized sequentially at following levels of theory: HF (Hartree-Fock), MP2 (second-order Møller-Plesset perturbation theory) and B3LYP (Hybrid Density Functional Theory). The 3rd step

is to choose appropriate Basis sets for smaller and larger atoms respectively. Basis sets are essential component of computational chemistry utilized to perform ab initio calculations.

Small atoms such as oxygen, hydrogen, chloride and ammonia were studied using basis sets such as 6-31G*, 6-31+G* and 6-311+G*,[67.] while heavy metal such as Pb were investigated using effective core potential (ECP) basis sets such as CEP-121G, LANL2DZ and SDD. [68] The z-matrix was used to speed up the optimization process (to constrain complexes to an appropriate symmetry). The Z-matrix is utilized as a structural map, which specifies molecular structure in terms of internal coordinates including bond distances, interbond angles as well as dihedral angles.[53] Generally molecules are constrained to the highest possible symmetry and then funnelling down calculations toward the lowest symmetry molecular geometry. Optimized geometry should result in zero forces within the molecule, all principal force constants should be positive including vibrational frequencies.[47] Any problem with z-matrix coordinates was indicated with the appearance of imaginary frequencies (denoted as negative by the software). If imaginary vibrational frequencies occur it means that the geometry optimization did not end in energy minimum as intended, instead it has ended in transition state.[53] In these cases, symmetry was reduced based on movements of the ligands at these imaginary frequencies and optimizations were performed again for each level of theory. That is the eigenvectors of the imaginary frequencies point towards the new structural orientation where molecule is at the energy minimum.[47] Frequency calculations were performed at each level of theory and Hessian (FOpt=CalcFC) was evaluated at the beginning of each optimization. Optimized geometry (geom=allcheck) was used in the subsequent optimizations. When

geometry optimization ran out of steps before being fully converged the input was altered to Opt=CalcAll. Geometry optimizations were carried out to completion for all levels of theories in a sequence even when one or more levels did not converge to local minima. This ensured that no energy minima were missed. Frequency analysis and pictures of optimized molecular structures were obtained utilizing visualization program called MOLDEN.[69] The stability of energy minima were determined based on whether the structure was fully attached (stable) or was characterized by ligand dissociation (unstable). Also, the statement "skipped due to dissociation of ligands" implies that specific calculation was attempted, however the resulting structure was unstable, and/or coupled to an output error indicating a forbidden alpha angle of 0 and/or 180 degrees. Not all members of each series investigated could be found.

Simulated polarized Raman spectra are plotted utilizing computer code created by my research supervisor, Dr. Cory Pye. Raman intensity calculations are standard in HF level of theory frequency calculations, subsequently vibrational frequencies essential for Raman spectra are obtained from the HF/SDD/6-311+G* output file. Once *ab inito* calculations are completed on all molecules within a given system of complexes (water, hydroxide, chloride, and ammonia), the lead-ligand bond lengths, as well as vibrational frequency data will be plotted to determine any trends. Obtained results will be ultimately compared to existing literature data, both experimental and computational.

Chapter 3: Aqualead (II) Complexes

Successful development of a long lasting sustainable SCWR (Supercritical Water-Cooled Reactor) largely depends on being able to predict and control its water chemistry. In order to obtain the desired control over corrosion, associated with new design of a SCWR, it is essential to obtain an in-depth understanding of the formation of corrosion products such as metal-ligand complexes. The metal-ligand complexes chosen for study in this thesis are all lead (II) complexes including combinations with 4 different ligands: water (H_2O), chloride (Cl^-), hydroxide (OH^-) and ammonia (NH_3). These lead (II) complexes are important with respect to development of a SCWR nuclear reactor, because their formation and transport throughout the nuclear reactor pathway may result in the corrosion of construction material and may ultimately result in nuclear reactor leakage. Understanding of the underlying aqueous chemistry of lead (II) complexes is difficult since literature reports are scarce. This thesis will provide the very first catalogue of all possible lead (II) aqueous complexes, thus contributing to a deeper understanding of lead chemistry at the molecular level.

This chapter includes the computational results and a discussion/literature comparison of aqualead (II) complexes. These aqualead (II) complexes were investigated up to and including enneacoordinate species (species with nine binding ligands). All calculations were performed at zero Kelvin, under gas phase boundary conditions. All of the results presented in this chapter, including total energies, bond lengths, and stretching vibrational frequencies were calculated at the HF, MP2 and B3LYP levels of theory, coupled with SDD basis sets for Pb and 6-311+G* basis sets for the water atoms. Optimized molecular geometries are presented for the MP2/SDD/6-311+G* and

B3LYP/SDD/6-311+G* levels of theory. All of the simulated polarized Raman spectra come from vibrational frequency data calculated at the HF/SDD/6-311+G* level, since the Raman intensities are standard for HF calculations. The absolute energy minima structures are presented, unless other local minima were identified with different geometries.

3.1 Water, Chloride, Hydroxide and Ammonia Ligands

Ab initio investigations were performed on the ligands involved in the formation of the lead (II) complexes studied for the sake of a stability comparison. Table 3A.1 found in the Supplementary Material section, provides the total energies of these ligands at the HF, MP2 and B3LYP levels of theory. No basis sets are indicated, since only results utilizing 6-311+G* basis sets have been reported.

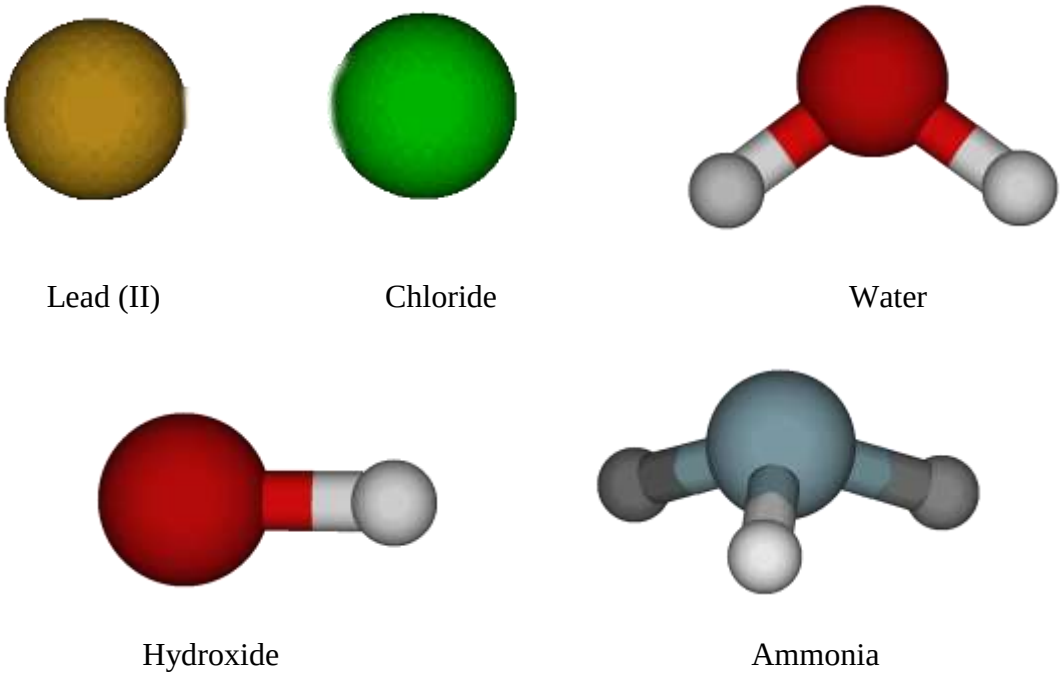

Figure 4: Optimized MP2 and B3LYP geometries for the lead (II) ion and all of the ligands utilized in the calculations of the lead (II) complexes.

3.2 Aqualead (II) Complexes, $[Pb(H_2O)_n]^{2+}$

The driving force behind research involving the hydration properties of Pb^{2+} is the fact that Pb^{2+} has been widely used in the production of everyday appliances including electronics, batteries and glass. Leaching of lead from these materials may result in lead poisoning of an individual or contamination of the surrounding environment, which can in turn be manifested in severe health problems and adverse environmental effects, respectively. Lead (II) is a well-known toxin, but its underlying aqueous chemistry (the binding properties of the Pb^{2+} ion) is surprisingly poorly understood and thus still requires extensive research.[21, 22.] The information provided in this thesis will contribute to the development of an appropriate water chemistry control strategy for the SCWR nuclear reactor. The optimized molecular geometries obtained herein (bond lengths, vibrational frequencies and energies) will complement previous theoretical studies, subsequently deepening the understanding of lead (II) solvation properties and may also contribute to an unraveling of the lead poisoning mechanism.

Experimental investigations of the hydration structure of Pb (II) have been surprisingly poorly documented in the literature. One of the challenges associated with the experimental investigation of the hydrated structure of the Pb (II) ion is the fact that X- rays are strongly absorbed by lead (Pb).[70] Hofer et al.[70] suggest that neutron diffraction would seem to be a more appropriate experimental technique to utilize, however no investigation of this kind has been documented so far.

Previous studies regarding the most stable coordination number (CN) for the $[Pb(H_2O)_n]^{2+}$ ion are contradictory and call for an in-depth investigation. The very first experimental study of the coordination number for solvated Pb (II) was published in

1966, where a value of 5.7 was extracted from a ^{1}H NMR experiment.[71] This coordination number was highly questioned, since the coordination numbers of Mg^{2+} and Ca^{2+} ions obtained using the same experimental technique were 3.8 and 4.3, respectively. More recent experimental and computational studies have given coordination number ranging between 6 and 10 respectively.[72, 73]

In addition to these specific experimental methodological problems, another property of the Pb (II) ion could introduce additional challenges. There are two valence electrons remaining in the electronic configuration ($6s^2 3d^{10}$), which makes the Pb (II) ion isoelectronic with Hg, but not with the noble gases. This may subsequently result in the formation of an asymmetric hydration structure, which has been reported in case of the Sn (II) ion.[74]

Hofer et al.[70] utilized *ab initio* quantum mechanical / molecular mechanical molecular dynamics (QM /MM MD) at the HF quantum mechanical level with an aim to probe the structural properties of the hydrated Pb(II) ion. Two well-defined hydration shells were identified, $[Pb(H_2O)_9{}^{I} (H_2O)_{24}{}^{II}]^{2+}$, with a capped, distorted square antiprism geometry in the 1st shell. The first hydration shell was characterized by 9 water ligands and was said to be flexible and continuously interchanging, with two dominant Pb (II)-O bond distances being 2.60 Å and 2.65 Å. The second hydration shell coordination number varied between 18 and 28 ligands, with an average coordination number of 24.6. Radial distribution functions identified the second shell as being mobile, suggesting that facile ligand exchange was occurring between the 2nd shell and the bulk. [70]

Furthermore, Hofer et al.[75] utilized *ab initio* HF methods in QM /MM MD simulations to investigate the dynamic properties of the hydrated Pb (II) complexes. This

study was performed subsequent to the previous study by Hofer et al.[70] confirming the previously reported ion-oxygen (Pb-O) distances.[70] The Pb-O bond distances were identified as 2.76 Å and 2.70 Å for ligands 1-4, and , and 2.68 Å and 2.66 Å for ligands 5 and 6. Ligands 7-9 were characterized as having lower ion-ligand distances (2.63 Å, 2.64 Å and 2.65 Å). It was concluded that the valence electrons were causing asymmetry of the ligand binding. The first hydration shell was identified as having coordination number of 9 and a high degree of internal flexibility, although the transition from the first to the second shell was limited. Hence, the mean ligand residence time of water molecules in the first hydration shell was estimated to be 0.23 ns, while in the second hydration shell the mean residence time was only 5.6 ps.[75]

Gourlaouen et. al.[22] investigated static and dynamic solvation properties of the aqueous Pb (II) ion utilizing *ab initio* computations for their static and Car-Parrinello Molecular Dynamics (CPMD) for their dynamic investigations. The structural investigation was carried out utilizing Gaussian03 software at the B3LYP level of theory coupled to a 6-31+G** basis set for water and an SDD (large core scalar relativistic pseudopotential (PP)) for lead. Density functional theory (DFT) was used, specifically B3LYP and BLYP functionals. The Pb-O radial distribution function indicated that the hydrated Pb^{2+} ion was hepta coordinate (coordination number 7). The radial distribution function obtained for the Pb-O bond was identified as very large and asymmetric, suggesting that short and long Pb-O distances coexist in the complex (short bond distances (< 2.6 Å), intermediate (2.6-3.0 Å) and long Pb-O bond lengths (>3.0 Å)). Averaging of the long and short Pb-O bond distances indicated that the aqueous Pb (II) complex is dynamically a holo-directed structure (a molecular conformation where

ligands are evenly spaced around the central atom), but statically a hemi-directed arrangement (where ligands preferably arrange in a sterically crowded conformation) corresponding overall to a distorted pentagonal bipyramid. The averaged bond distance was given as 2.7 Å with an associated root-mean-square deviation of 0.26 Å. The long Pb-O bond length was attributed to electrostatic repulsion between the Pb^{2+} lone pair ($6s^2$) and the lone pairs of the water molecules.[22]

Wander et al.[21] performed Hybrid DFT calculations using the Gaussian03 software package to investigate the geometric and electronic molecular structures of $[Pb(H_2O)_{1\text{-}9}]^{2+}$. Specifically, the B3LYP level of theory coupled to an aug-cc-pvdz basis set for water and an aug-cc-pvdz-PP basis set for Pb were used. Based on the optimized geometries, the authors identified the most stable complexes as $[Pb(H_2O)_{6\text{-}8}]^{2+}$, which were holo-directed in nature, while lower coordination number aqualead (II) species were dominated by hemi-directed structures. The unconstrained optimization of $[Pb(H_2O)_9]^{2+}$ resulted in the dissociation of one water ligand, while constraining $[Pb(H_2O)_9]^{2+}$ to C_3 symmetry gave a stable structure. However, it contained imaginary frequencies, an indication that the potential energy surface (PES) search did not find the lowest energy structure for the given complex. Hence, it was concluded that the highest reasonable coordination number for an aqualead (II) complex is 8. The authors also concluded that holo- vs. hemi- directed structural transitions are influenced by the coordination number and not by the hybridization number of the 6s lone pair orbital nor by the covalent bonding in Pb-O.[21]

Juan et al.[76] optimized the geometries of $[Pb(H_2O)_{1\text{-}9}]^{2+}$ using the Perdew-Burke-Ernzerhof generalized gradient approximation (PBE-GGA) of density functional theory (DFT) with CASTEP code under periodic boundary conditions. The results obtained

included bond distances, binding energies and Mulliken charge populations of the equilibrium geometries for $[Pb(H_2O)_{1\text{-}9}]^{2+}$. The primary stable hydration numbers were identified as 6, 7 and 8, while the $[Pb(H_2O)_6]^{2+}$ molecular geometry was identified as being the transition state between holo- and hemi-directed structures.

As already mentioned, lead has the unusual tendency to switch between holo- and hemi- directed conformations. Such behaviour is attributed to the sterically active lone pair of lead (II).[22] Looking for greater insight into the energetic origins of the hemi- and holo- directed behaviour of $[Pb(H_2O)_n]^{2+}$, Devereux et al.[77] utilized Reduced Variational Space (RVS) calculations, as well as well as *ab initio* calculations (HF and B3LYP levels of theory with 6-31+G** basis sets for the water atoms, and 4 different basis sets were tested for Pb). Three of the basis sets utilized for lead were large-core relativistic pseudopotential (PP): SDD, CRENBS and SBK, while one small-core relativistic PP (aug-cc-pvdz-PP) was also studied. Based on the obtained energetics, the most stable relativistic PP was aug-cc-pvdz-PP; its repulsion energy at short lead oxygen distances was much lower than those for the other basis sets. Bond distances for all 4 basis sets range from 2.283 to 2.388 Å and total energies for the hemi-conformations were found to be in the range of -197.6 to -254.8 kcal/mol. The study results suggested that hemi-directed structures were stable for both the $[Pb(H_2O)_4]^{2+}$ and $[Pb(H_2O)_5]^{2+}$ complexes, while $[Pb(H_2O)_6]^{2+}$ showed the holo- and the hemi- structures to be iso-energetic (separated by 1.5 kcal/mol).[77] It was concluded that the distribution of ligands around the central metal arises from a balance between the first-order Coulomb and exchange-repulsion energies that favours holo- conformation and second-order charge transfer plus polarization term that favours the hemi- conformation of lead (II) complexes.[77]

Shi et al.[78] investigated the stability and the optimized geometrical parameters of $[Pb(H_2O)_n]^{2+}$, for n=1, 2 and 3. An experimental study (hybrid quadruple/time-of-flight mass spectrometry) was performed, as well as a computational investigation (*ab initio* calculations) using Gaussian 98 software. Calculations were performed at the B3LYP level of theory and included SDD (a relativistic large core potential) for Pb and 6-31++G** basis sets for the water atoms (O and H). Shi et al.[78] were the first to show that doubly charged lead monohydrate, $[Pb(H_2O)]^{2+}$, does exist and can be synthesized via the ligand exchange reaction of $[Pb(CH_3CN)]^{2+}$ with H_2O, although $[Pb(H_2O)]^{2+}$ was obtained in only a low yield. Hence, Shi et al.[78] discarded the previous belief that the formation of the doubly charged monohydrate ion was impossible. The second ionization energy (IE) of lead is much larger than the first IE (12.6 eV) of water resulting in electron transfer from water to the doubly charged metal ion (M^{2+}), subsequently resulting in the formation of $M^{\cdot+}$ and H_2O^+.[79] DFT calculations suggested that $[Pb(H_2O)]^{2+}$ is stable in the gas phase, while $[Pb(H_2O)_2]^{2+}$ and $[Pb(H_2O)_3]^{2+}$ are metastable against the dissociative proton transfer. All three hydrated ions were found to be stable against dissociative charge transfer.

Furthermore, Shi et al.[80] documented the abundant formation of $[Pb(H_2O)]^{2+}$ in the gas phase, via a ligand-exchange reaction between $[Pb(N_2)_n]^{2+}$ and H_2O. This finding was in contrast to their previous study[78] where ligand-exchange reaction between $[Pb(CH_3CN)]^{2+}$ and H_2O produced only a low abundance of $[Pb(H_2O)]^{2+}$. The higher efficiency of the ligand exchange reaction for the $[Pb(N_2)_n]^{2+}$ complex was attributed to the weak binding of N_2 (the departing ligand) and was explained by binding enthalpy towards successful and stable formation of $[Pb(H_2O)]^{2+}$ complexes. The binding

enthalpies obtained for Pb^{2+} were 26.3, 60.4 and 91.9 kcal/mol for N_2, H_2O and CH_3CN, respectively. Based on the concept of relative binding enthalpy, $[Pb(N_2)(H_2O)]^{2+}$ is expected to lose nitrogen (N_2), while $[Pb(CH_3CN)(H_2O)]^{2+}$ should lose water, which, in turn explains why $[Pb(CH_3CN)]^{2+}$ and H_2O produced a low abundance of $[Pb(H_2O)]^{2+}$, while the ligand-exchange reaction between $[Pb(N_2)_n]^{2+}$ and H_2O produced $[Pb(H_2O)]^{2+}$ abundantly. [80]

Based on these previous studies, we decided to perform a comprehensive *ab initio* investigation of aqualead (II) complexes, up to and including coordination number 9, $[Pb(H_2O)_{1\text{-}9}]^{2+}$, with the aim of identifying the highest possible stable coordination numbers and the corresponding optimized geometries.

3.2.1 Results

Molecular geometry optimizations were performed for aqualead (II) complexes up to and including the coordination number nine, $[Pb(H_2O)_{1\text{-}9}]^{2+}$. The total energies for all of the aqualead (II) complexes studied are given in Tables 3A-2 to 3A-10 of the Supplementary Material section. Total energies are reported for 27 levels of calculations, including HF, MP2 and B3LYP levels of theory coupled to the chosen basis sets (CEP-121G, LANL2DZ and SDD) for Pb and (6-31G*, 6-31+G* and 6-311+G*) for H and O. However, for brevity, only the results involving the SDD/6-311+G* basis sets are discussed in this thesis. Stable structures were found for $[Pb(H_2O)_{1\text{-}6}]^{2+}$and $[Pb(H_2O)_8]^{2+}$ at all of the levels of theory studied. $[Pb(H_2O)_7]^{2+}$ was unstable and resulted in the dissociation of 3 water ligands. $[Pb(H_2O)_9]^{2+}$, when constrained to C_3 symmetry, was found to be unstable at the HF level of theory. It had all real frequency modes but

optimization still resulted in the dissociation of 3 water ligands (hydrogen bonded to neighboring water molecules). Furthermore, the unconstrained or C_1 symmetry structure of $[Pb(H_2O)_9]^{2+}$ was also unstable resulting in the dissociation of 1 or 3 water ligands depending on the level of theory. The MP2 and B3LYP optimized molecular geometries for the stable aqualead (II) complexes at their absolute energy minima are given in Figure 5 along with their respective symmetries.

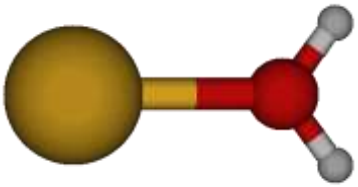

C_{2v}

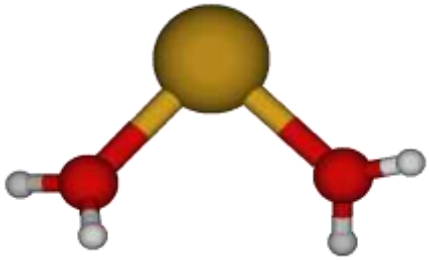

C_2

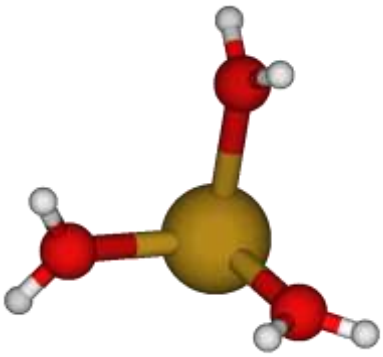

C_3

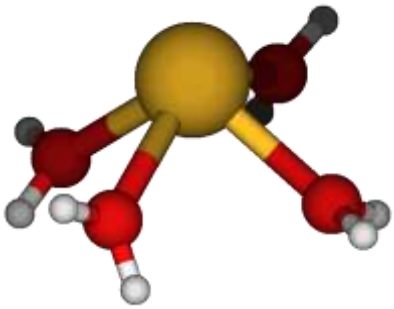

C_4

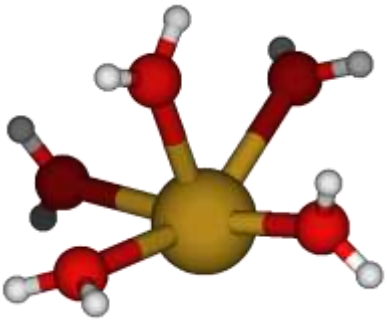

C_s

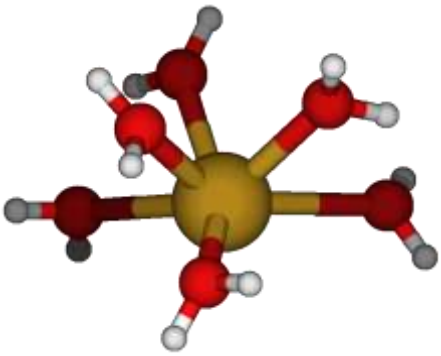

C_3

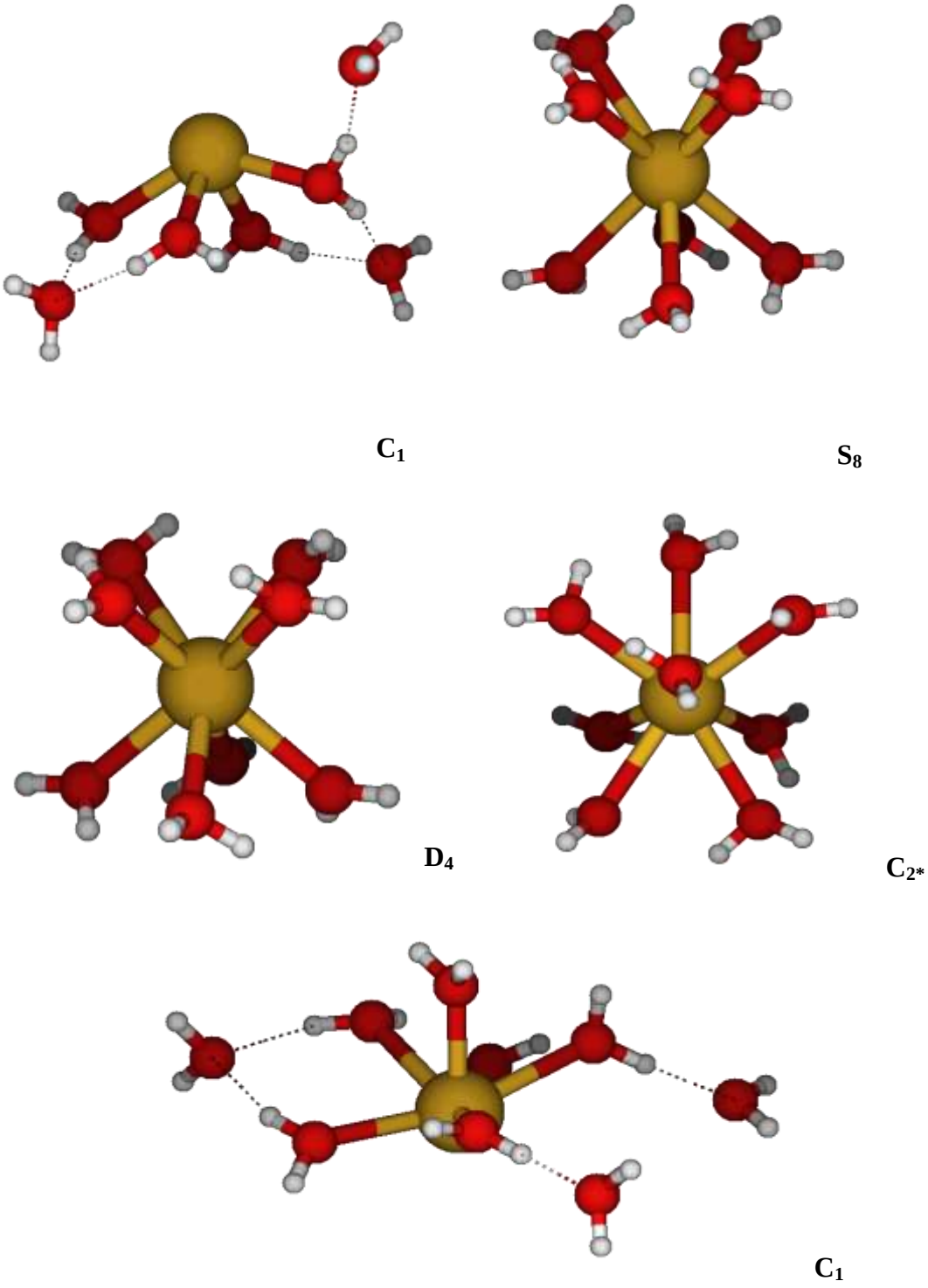

Figure 5: Optimized MP2 and B3LYP geometries for stable structures of $[Pb(H_2O)_{1\text{-}9}]^{2+}$. All structures are similar (yellow=lead, red=oxygen, white=hydrogen).* indicates structure only for the MP2 calculation.

The monohydrate, $[Pb(H_2O)_1]^{2+}$, did not cause any optimization problems as the highest possible C_{2v} symmetry was found to be stable at both the MP2 and B3LYP levels of theory.

The dihydrate, $[Pb(H_2O)_2]^{2+}$, was investigated under the constraints of D_{2h}. symmetry. Desymmetrization of the D_{2h} structure along A_u, a twisting mode, gave a D_{2d} structure. Further desymmetrization of the D_{2d} structure along E, a skeletal deformation mode, gave a structure of C_s symmetry, which contained an imaginary frequency mode. However, the D_{2h} structure was also desymmetrized along B_{2u}, a skeletal deformation mode. This gave a C_2 structure, which proved to be the most stable structure at all of the levels of theory studied (HF, MP2 and B3LYP).

The trihydrate, $[Pb(H_2O)_3]^{2+}$, was initially constrained to D_{3h} symmetry (two forms). Both of these forms have an A_1" imaginary mode, a twisting mode, which suggested that desymmetrization to the D_3 form would be appropriate. However, both D_3 forms were also found to contain imaginary frequency at all levels of theory. D_{3h} #1 was then desymmetrized along the A_2", skeletal deformation mode, to the C_{3v} #1, while D_{3h} #2 was desymmetrized to the C_{3v} #2 structure. D_{3h} #2 was also desymmetrized along E", a twisting mode, to a C_{2v} structure, which was found to contain imaginary frequencies. The D_3 structure was desymmetrized based on an A_2 mode, a skeletal deformation mode, to a structure of C_3 symmetry. This structure contained all positive frequencies, implying that potential energy surface (PES) had reached the absolute energy minima. Hence, C_3 symmetry was found to be the most stable for $[Pb(H_2O)_3]^{2+}$ at all of the levels of theory used.

The tetrahydrate complex, $[Pb(H_2O)_4]^{2+}$, was initially investigated under the constraint of D_{4h} symmetry (two forms). Numerous imaginary frequencies were found for the D_{4h} structures. Desymmetrization of the lower energy D_{4h} structure along the water twisting modes gave: for the largest modulus A_{1u} mode, a D_4 structure; along the E_g mode a D_{2h} structure; and along the B_{1u} mode the D_{2d} #1 structure. The desymmetrization of D_{4h} #2 along the B_{2u}, skeletal deformation mode, gave the D_{2d} #2 structure and along the A_{2u} skeletal deformation mode gave C_{4v} #1. The desymmetrization of D_{4h} #1 along the A_{2u} skeletal deformation mode gave the C_{4v} #2 structure. The C_{4v} #1 structure was slightly lower in energy than C_{4v} #2, hence it was desymmetrized along an A_2 mode to a structure of C_4 symmetry. The tetrahydrate C_4 structure, when desymmetrized along a B mode, reverted to a stable C_2 structure with no imaginary frequencies. There was thus ultimately an agreement among all levels of theory that the C_2 symmetry structure is the most stable geometry for $[Pb(H_2O)_4]^{2+}$.

The pentahydrate, $[Pb(H_2O)_5]^{2+}$, was initially investigated under the constraint of C_{2v} symmetry. The results showed imaginary B_1 frequency modes at all levels of theory, suggesting desymmetrization to the C_s structure was required. Subsequently, the C_s structure was found to be the most stable geometry at all of the levels of theory investigated.

The hexahydrate, $[Pb(H_2O)_6]^{2+}$, was initially constrained to have T_h symmetry, but was found to have imaginary modes of frequency. Desymmetrization along the imaginary T_u, twisting mode, gave a C_3 symmetry structure, which proved to be the most stable geometry at the HF and MP2 levels of theory. The optimized C_3 geometry of $[Pb(H_2O)_6]^{2+}$ was unstable at the B3LYP level and resulted in $[Pb(H_2O)_3]^{2+}$ plus 3

detached water molecules. These appeared to be hydrogen bonded to the hydrogens from the water ligands attached to the central lead atom.

The heptahydrate, $[Pb(H_2O)_7]^{2+}$, was initially optimized with C_{2v} symmetry, which proved to be unstable at all of the given levels of theory and resulted in a $[Pb(H_2O)_5]^{2+}$ structure with 2 dissociated water ligands. The two dissociated water ligands formed hydrogen bonds with adjacent water ligands. The oxygen of the detached water ligands accepts a hydrogen bond from one of the still bound water molecules. Further desymmetrization along the B_1 and B_2 imaginary frequency modes gave the structures C_s #1 and C_s #2 respectively. Both, C_s #1 and C_s #2 proved to be unstable, losing two water ligands at both the MP2 and B3LYP levels of theory. The heptahydrate was finally desymmetrized to a C_1 symmetry structure, which was unstable at all of the levels of theory. The ultimate product had 3 dissociated water ligands that were hydrogen bonded to neighbouring attached water ligands.

The octahydrate, $[Pb(H_2O)_8]^{2+}$, was initially investigated under the constraints of D_{4h} symmetry (two forms, with the D_{4h} #1 structure being slightly lower in energy) and D_{4d} symmetry (two forms with the D_{4d} #2 structure being slightly lower in energy). The D_{4d} #2 structure was desymmetrized along an A_2 mode to an S_8 structure, which was stable at all of the levels of theory using the SDD/ 6-311+G*. The D_{4h} #1 structure was desymmetrized along the largest-modulus A_{1u} mode, a water twisting mode, to a D_4 structure. Hence, $[Pb(H_2O)_8]^{2+}$, was found to be stable with S_8 and D_4 at all levels of theory when coupled to SDD/6-311+G* basis sets. However, the C_2 symmetry structure was at the lowest energy minimum at the HF and MP2/6-311+G*, while the B3LYP/6-311+G* C_2 symmetry structure converged back to a S_8 symmetry structure.

The enneahydrated species, $[Pb(H_2O)_9]^{2+}$, was initially constrained to have D_{3h} symmetry (4 forms, where #1 is the lowest in energy). The D_{3h} structures contained various imaginary frequencies and desymmetrization was carried out based on the observed imaginary frequencies. The D_{3h} #1 structure was desymmetrized along an A_1" mode to a D_3 structure, which contained imaginary frequencies, implying that the molecular geometry optimization did not reach the lowest energy minimum. In addition, the D_{3h} #1 structure was desymmetrized along an A_2' imaginary mode to a C_{3h} structure. Frequency analysis of the C_{3h} structure indicated that scanning of the potential energy surface did not reach the lowest energy structure. The C_{3h} structure was desymmetrized along the imaginary A_2 and E modes, to structures of C_3 and C_1 symmetry, respectively. The C_3 structure contained real (positive) frequency modes, but it was found to be unstable with the resulting dissociation of 3 water ligands. On the other hand, the unconstrained C_1 structure was unstable and resulted in dissociation of one water ligand at the MP2 level and two water ligands at the B3LYP level of theory.

The simulated polarized Raman spectra for monoaqualead (II) complex, $[Pb(H_2O)]^{2+}$, is plotted in Figure 6. Furthermore, plots were constructed of the Pb-O bond lengths and vibrational stretching frequencies and are shown in Figure 7, Figure 8 and Figure 9 for HF, MP2 and B3LYP respectively.

3.2.2 Discussion and Literature Comparison

The monohydrate complex, $[Pb(H_2O)]^{2+}$, is the most reported of the lead (II) aqua ion in the literature. The most stable optimized geometry for this ion has been found to be C_{2v} for all levels of theory studied with SDD/6-311+G* basis sets. The optimized

structure found for $[Pb(H_2O)]^{2+}$ is consistent with the computational study by Devereux et al.,[77] who utilized Gaussian03 to optimize the molecular geometry of $[Pb(H_2O)]^{2+}$ at the HF and B3LYP levels of theory, coupled to the large-core relativistic pseudo potential SDD for Pb and a 6-31+G** basis set for H_2O. Devereux et al.[77] found the optimized Pb-O bond distances to be 2.384 Å and 2.359 Å at the HF and B3LYP levels, respectively. These results are almost identical to the results reported here, 2.382 Å and 2.357 Å at the HF and B3LYP levels, respectively. The very slight difference in the results can be attributed to the fact that Devereux et al.[77] utilized a slightly smaller basis set for water (6-31+G**) compared to the 6-311+G* set utilized in this thesis.

The optimized geometries (stable conformations, bond lengths, energies and vibrational frequencies) reported in this thesis were compared to literature results where they are available. The Pb-O bond length data from this research was compared to previous computational studies. However, literature experimental data regarding Pb-O bond distances was not available, hence comparison was not possible. This is most likely due to challenges associated with the extensive absorption of X-ray induced by lead (Pb).[70]

Gourlaouen et al.[81] obtained a structure with C_{2v} symmetry for $[Pb(H_2O)]^{2+}$ at both the HF and B3LYP levels of theory. This is consistent with our finding that C_{2v} symmetry for $[Pb(H_2O)]^{2+}$ is the most stable at any level of calculation. The Pb-O bond lengths they found are 2.364 Å and 2.339 Å, at the HF and B3LYP levels, respectively. These bond lengths are slightly shorter than the HF and B3LYP results presented here (2.382 Å and 2.357 Å, respectively). The slightly shorter Pb-O bonds obtained by Gourlaouen et al.[81]

can be attributed to a choice of basis set for water (6-31+G**), which is slightly smaller than one utilized in this thesis.

Shi et al.[80] reported the Pb-O bond distance to be 2.330 Å in $[Pb(H_2O)]^{2+}$ at the B3LYP level of theory coupled with an SDD basis set for Pb and 6-31++G** doubly split-valence basis set for water. This B3LYP optimized Pb-O bond distance is slightly shorter than the one reported in this thesis at the B3LYP level of theory (2.357 Å). This slight difference can be attributed to the slightly lower quality basis set for water used by Shi et al.[80]

Wander et al.[21] reported the Pb-O bond distance to be 2.34Å for $[Pb(H_2O)]^{2+}$ at the B3LYP/ aug-cc-pvdz-PP level with a 60 electrons ECP (electron core potential) for Pb and an aug-cc-pvdz basis set for the water atoms. The slightly smaller Pb-O B3LYP bond distance reported by these authors is attributed to the fact that Wander et al.[21] utilized different pseudo potentials (aug-cc-pvd-PP) for Pb and slightly lower level basis sets for water (6-31+G*).

Juan et al.[76] have reported an average B3LYP Pb-O bond length of 2.31 Å. They utilized a different computational method of investigation, (the Perdew-Burke-Ernzerhof generalized gradient approximation (PBE-GGA) of DFT).

Hofer et al.[75] have reported Pb-O bond distances for $[Pb(H_2O)]^{2+}$, from HF, MP2 and B3LYP level calculations to be 2.32 Å, 2.30 Å and 2.28 Å, respectively. Hofer et al[75] utilized different pseudopotential (PP) for Pb (SBKJC VDZ ECP) and smaller basis set for water (6-31+G*) compared to the SDD/6-311+G* basis sets utilized in this thesis. This in turn accounts for the slightly smaller Pb-O bond distances reported by Hofer et al.[75].

The optimized Pb-O bond lengths obtained in this work for the dihydrate, $[Pb(H_2O)_2]^{2+}$, are 2.423 Å (HF), 2.403 Å (MP2) and 2.399 Å (B3LYP). The $[Pb(H_2O)_2]^{2+}$ ion with C_2 symmetry was found to be the most stable at all of the levels of theory investigated. The Pb-O bond lengths have increased slightly compared to the monohydrate values. The results obtained for the Pb-O bond distances are consistent with previous computational research. However, subtle differences in the values are attributed to the smaller basis sets used by previous researchers, as well as variations in the software used and the levels of theory investigated. Hofer et al.[75] obtained computed Pb-O bond distances at the HF, MP2 and B3LYP levels of theory to be 2.35 Å, 2.34 Å and 2.32 Å, respectively. Hofer et al.[75] also observed a trend where increasing the number of water ligands coordinated to a lead (Pb(II)) resulted in elongation of the Pb-O bonds. The bond distances reported by Hofer et a.l[75] were shorter than our results.

Juan et al.[76] also reported a shorter Pb-O bond distance for $[Pb(H_2O)_2]^{2+}$ than ours, of 2.36 Å at the B3LYP level of theory. This subtle difference has been attributed to the fact that Juan et al.[76] utilized a completely different computational method of investigation (PBE-GGA of DFT). Furthermore, Wander et al.[21] reported the Pb-O bond length to be 2.38 Å at the B3LYP level of theory, which is again slightly shorter distance than the one reported here.

The most stable structure for the trihydrate complex, $[Pb(H_2O)_3]^{2+}$, proved to be that with C_3 symmetry for all of the levels of theory (HF, MP2 and B3LYP) studied in this work. The Pb-O bond distances for $[Pb(H_2O)_3]^{2+}$ were found to be 2.462 Å, 2.438 Å and 2.442 Å at the HF, MP2 and B3LYP levels of theory, respectively. These bond lengths are all longer when compared to either the mono and dihydrate values. Once

again increasing the number of water ligands has resulted in a further elongation of the Pb-O bonds. Hofer et al.[75] have also shown that increasing number of water molecules from two to three further increases the length of such Pb-O bonds. The optimized Pb-O bond lengths reported by Hofer et al.[75] are 2.36 Å, 2.35 Å and 2.33 Å at the HF, MP2 and B3LYP levels of theory, respectively. These Pb-O bond lengths are slightly shorter than the ones reported in this thesis. These subtle differences in the Pb-O values are attributed to the use of smaller basis sets compared to our basis sets, as well as the presence of a second hydration sphere ($[Pb(H_2O)_9^{I}\ (H_2O)_{24}^{II}]^{2+}$, both of which contribute to the observed Pb-O bond length decrease.

Juan et al.[76] have also demonstrated that increasing the number of water ligands from two to three, increases the Pb-O bond distances. This is consistent with our finding. However, Juan et al.[76] reported a slightly lower Pb-O bond distance (2.40 Å compared to 2.442 Å reported here) at the B3LYP level of theory. This is understandable, since Juan et al.[76] utilized different computational software (PBE-GGA).

In addition to these findings, Wander et al.[21] obtained a B3LYP optimized Pb-O bond lengths of 2.42 Å for $[Pb(H_2O)_3]^{2+}$. This is only slightly lower in value than our obtained value of 2.442 Å.

The tetrahydrate species, $[Pb(H_2O)_4]^{2+}$, was found to be the most stable with C_2 symmetry for all of the levels of theory calculated. The average Pb-O bond lengths are 2.538 Å, 2.508 Å and 2.515 Å for the HF, MP2 and B3LYP levels of theory, respectively. The bond lengths are consistently longer when compared to the mono-, di- and trihydrate values. Wander et al.[21] have reported an average bond length of 2.49 Å for B3LYP

optimized $[Pb(H_2O)_4]^{2+}$. The optimized Pb-O bond length is again smaller when compared to B3LYP value reported in this thesis.

Juan et al.[76] reported the average Pb-O bond length in $[Pb(H_2O)_4]^{2+}$ to be 2.47 Å at the B3LYP level, which is smaller than our reported value. This is attributed to the different computational software and basis sets used.

Hofer et al.[75] reported average Pb-O bond lengths of 2.45 Å, 2.42 Å and 2.38 Å for HF, MP2 and B3LYP level calculations, respectively. These results again substantiate the trend of increasing Pb-O bond lengths with increasing lead coordination number (a finding once again consistent with ours). The optimized Pb-O bond distances obtained by Hofer et al.[76] are only slightly smaller than our optimized bond lengths.

The pentahydrate species, $[Pb(H_2O)_5]^{2+}$, proved to be the most stable with C_s symmetry for all of the levels of theory studied. The calculated average Pb-O bond lengths are 2.578 Å, 2.538 Å and 2.623 Å at the HF, MP2 and B3LYP levels of theory, respectively. Wander et al.[21] has reported the average Pb-O bond length to be 2.53 Å for the B3LYP optimized $[Pb(H_2O)_5]^{2+}$ complex. Juan et al.[76] reported the average Pb-O bond length for the B3LYP level of theory to be 2.53 Å. Both of these studies confirmed that increasing the coordination number, by increasing the number H_2O ligands, results in elongation of the Pb-O bond distances (findings consistent with our own).

The most stable geometry for the hexahydrate complex, $[Pb(H_2O)_6]^{2+}$, proved to have C_3 symmetry for all of the levels of theory investigated. The average Pb-O bond lengths for these structures were found to be 2.679 Å and 2.640 Å for the HF and MP2 level calculations, respectively. The B3LYP optimized $[Pb(H_2O)_6]^{2+}$ structure was found to be unstable and resulted in the formation of $[Pb(H_2O)_3]^{2+}$ plus 3 detached water

molecules, which were hydrogen bonded to a neighbouring water ligands. The unstable nature of $[Pb(H_2O)_6]^{2+}$ at the B3LYP level is consistent with the results from a structural optimization performed by Wander et al.,[21] where B3LYP/LANL2DZ/aug-cc-pvdz molecular optimization of $[Pb(H_2O)_6]^{2+}$ resulted in $[Pb(H_2O)_3]^{2+}$ and 3 dissociated H_2O ligands. However, when Wander et al.[21] replaced the large-core 78 electron LANL2DZ basis set for lead with the small-core 60 electron aug-cc-pvdz-PP basis set, stable $[Pb(H_2O)_6]^{2+}$ was obtained. The unstable B3LYP optimized structure can be attributed to the choice of basis set, where a large-core basis set like SDD results in dissociation of 3 water ligands.

This finding is also consistent with the results from a study performed by Gourlaouen et al.,[22] where the $[Pb(H_2O)_6]^{2+}$ complex was optimized at the B3LYP/SDD/6-31+G** level and which resulted in the dissociation of 2 water ligands (one water ligand was lost at a time close to 4 ps and the second ligand was dissociated during the time interval of 8.5 ps). Wander et al.[21] reported the Pb-O bond distance for the stable $[Pb(H_2O)_6]^{2+}$ structure at the B3LYP/ aug-cc-pvdz-PP/ aug-cc-pvdz level to be 2.62 Å. Furthermore, Juan et al.[76] reported the B3LYP optimized Pb-O bond distance to be 2.65 Å. These results are in good agreement with our obtained Pb-O results for $[Pb(H_2O)_6]^{2+}$ at the HF and MP2 levels (keeping in mind that our B3LYP value was not extracted due to the ligand dissociation). Hofer et al.[75] reported the Pb-O bond lengths to be 2.56 Å, 2.54 Å and 2.52 Å at the HF, MP2 and B3LYP levels, respectively. These HF and MP2 results are consistent with our HF and MP2 optimized Pb-O bond length values.

The heptahydrate species, $[Pb(H_2O)_7]^{2+}$, was desymmetrized from a C_{2v} symmetry structure to one with C_s symmetry. However, it contained imaginary modes of frequency

suggesting further desymmetrization to a C_1 symmetry structure was required. The C_1 symmetry structure was found to be unstable and resulted in decomposition to $[Pb(H_2O)_4]^{2+}$ plus 3 dissociated water ligands. These results were not comparable to previous computational results, since our C_1 structure containing real modes of frequencies was unstable.

The octa-hydrated species, $[Pb(H_2O)_8]^{2+}$, was found to be stable with C_4, C_2 and S_8 symmetries for all of the levels of theory studied. That is, positive (real) frequency modes were obtained at the HF, MP2 and B3LYP levels of theory for all of the 3 indicated symmetries. The optimized Pb-O bond lengths for the C_4 symmetry structure are 2.783 Å, 2.735 Å and 2.762 Å at the HF, MP2 and B3LYP levels, respectively. The Pb-O bond distances for the C_2 symmetry structure are 2.773 Å, 2.726 Å and 2.760 Å at the HF, MP2 and B3LYP levels of theory, respectively. The optimized bond distances for S_8 symmetry complex are 2.773 Å, 2.725 Å and 2.756 Å for the HF, MP2 and B3LYP levels, respectively. The bond lengths are longer when compared to the mono-, di, tri-, tetra-, penta-, hexa- and heptahydrate values. This result can be attributed to the increased number of water ligands, these induce repulsion thus forcing the bonds to be longer. Wander et al.[21] also showed that increased coordination number results in increasing Pb-O bond lengths. They reported an average Pb-O bond length of 2.71 Å for B3LYP optimized $[Pb(H_2O)_8]^{2+}$. This result is in good agreement with our Pb-O bond distance at the B3LYP level of theory.

Juan et al.[76] reported the average Pb-O bond length in the same complex to be 2.73 Å at the B3LYP level of theory, which is the closest to our S_8 $[Pb(H_2O)_8]^{2+}$ structure. Hofer et al.[75] reported average Pb-O bond lengths of 2.63 Å, 2.60 Å and 2.58 Å from

calculations at the HF, MP2 and B3LYP levels, respectively. These results show the same trend of increasing Pb-O bond lengths with increasing number of coordinated water ligands (a finding consistent with ours). Hofer et al.[75] obtained only slightly shorter Pb-O bond distances than we did. This was attributed to the smaller basis sets used by the Hofer et al.[78] (SBKJC VDZ ECP/ 6-31+G*).

The enneahydrate species, $[Pb(H_2O)_9]^{2+}$, contained real frequencies for a structure of C_3 symmetry at the HF level of theory. However, this structure resulted from the dissociation of 3 water ligands that remained hydrogen bonded to the neighbouring attached water molecules. $[Pb(H_2O)_9]^{2+}$ was desymmetrized to a C_1 symmetry structure at the MP2 and B3LYP levels of theory, however it too was found to be unstable. One water ligand underwent dissociation at the MP2 level of theory and two water ligands were dissociated at the B3LYP level of theory. Wander et al.[21] performed a geometry optimization of unconstrained $[Pb(H_2O)_9]^{2+}$, which resulted in the dissociation of one water ligand, while optimization of the C_3 symmetry structure yielded a fully attached 9 coordinated complex. However, this C_3 structure, even though fully attached, contained imaginary frequency modes, implying that the potential energy surface search did not reach the lowest energy minima structure for $[Pb(H_2O)_9]^{2+}$.

Juan et al.[76] have shown in their computational study that the $[Pb(H_2O)_9]^{2+}$ structure is unstable and hence they concluded that the highest possible coordination number for an aqualead (II) complex is 8. This finding is also consistent with the findings of Wander et al.[78] and most importantly with our computational findings. The highest possible coordination number for an aqualead (II) complex is 8, and not 9, as previously proposed by Hofer et al.[75]

The highest, stable coordination number identified in this thesis for aqualead (II) complexes, $[Pb(H_2O)_n]^{2+}$, is $[Pb(H_2O)_8]^{2+}$. All of the previous computational studies regarding the optimized Pb-O bond lengths of aqualead (II) complexes are in a good agreement with the results that we have found. The subtle differences observed in the Pb-O bond distances can be a result of the varying software, levels of theory and different basis sets utilized. Geometry comparison of aqualead (II) complexes between our results and previous research data , ($[Pb(H_2O)_n]^{2+}$ where n = 1 – 9) is summarized in the following tables 1, 2 and 3.

Table 1: Geometry comparison of $[Pb(H_2O)_n]^{2+}$, where n = 1 – 9, at B3LYP level of theory. All bond lengths (Å) are averages where appropriate.

Optimized Pb-O Bond Length (Å)							
Complex	**Devereux et al.[77]**	**Gourla-ouen et al.[81]**	**Shi et al.[80]**	**Wander et. al.[21]**	**Juan et al.[76]**	**Hofer et al.[75]**	**Our results**
$[Pb(H_2O)]^{2+}$	2.359	2.339	2.330	2.340	2.310	2.280	2.357
$[Pb(H_2O)_2]^{2+}$	2.399	-	-	2.380	2.360	2.320	2.399
$[Pb(H_2O)_3]^{2+}$	-	-	-	2.420	2.400	2.330	2.442
$[Pb(H_2O)_4]^{2+}$	-	-	-	2.490	2.470	2.380	2.515
$[Pb(H_2O)_5]^{2+}$	-	-	-	2.530	2.530	-	2.623
$[Pb(H_2O)_6]^{2+}$	-	-	-	2.620	2.650	2.520	N/A
$[Pb(H_2O)_7]^{2+}$	N/A	N/A	N/A	N/A	N/A	N/A	N/A
$[Pb(H_2O)_8]^{2+}$	-	-	-	2.710	2.730	2.58	2.762
$[Pb(H_2O)_9]^{2+}$	N/A	N/A	N/A	N/A	N/A	N/A	N/A

Table 2: Geometry comparison of $[Pb(H_2O)_n]^{2+}$, where n = 1 – 9, at MP2 level of theory. All bond lengths (Å) are averages where appropriate.

Optimized Pb-O Bond Length (Å)		
Complex	**Hofer et al.[75]**	**Our results**
$[Pb(H_2O)]^{2+}$	2.300	2.365
$[Pb(H_2O)_2]^{2+}$	2.340	2.403
$[Pb(H_2O)_3]^{2+}$	2.350	2.438
$[Pb(H_2O)_4]^{2+}$	2.420	2.508
$[Pb(H_2O)_5]^{2+}$	-	2.538
$[Pb(H_2O)_6]^{2+}$	2.540	2.640
$[Pb(H_2O)_7]^{2+}$	N/A	N/A
$[Pb(H_2O)_8]^{2+}$	2.600	2.735
$[Pb(H_2O)_9]^{2+}$	N/A	N/A

Table 3: Geometry comparison of $[Pb(H_2O)_n]^{2+}$, where n = 1 – 9, HF level of theory. All bond lengths (Å) are averages where appropriate.

Complex	**Devereux et al.[77]**	**Gourlaouen et al.[81]**	**Hofer et al.[75]**	**Our results**
$[Pb(H_2O)]^{2+}$	2.384	2.364	2.320	2.382
$[Pb(H_2O)_2]^{2+}$	-	-	2.350	2.423
$[Pb(H_2O)_3]^{2+}$	-	-	2.360	2.462
$[Pb(H_2O)_4]^{2+}$	-	-	2.450	2.538
$[Pb(H_2O)_5]^{2+}$	-	-	-	2.578
$[Pb(H_2O)_6]^{2+}$	-	-	2.560	2.679
$[Pb(H_2O)_7]^{2+}$	N/A	N/A	N/A	N/A
$[Pb(H_2O)_8]^{2+}$	-	-	2.630	2.762
$[Pb(H_2O)_9]^{2+}$	N/A-	N/A	N/A	N/A

From the optimized MP2 and B3LYP geometries for aqualead (II) complexes reported in this thesis, it was evident that the water ligands prefer sterically hindered (uneven) conformation around the central Pb^{2+} atom. This uneven arrangements of water ligands appears to be largely influenced by lone pair-ligand repulsion from the stereo active Pb lone pair ($6s^2$). The lone pair-ligand repulsion is clearly predominant over ligand-ligand electrostatic repulsion.

Vibrational stretching frequencies were also calculated for this set of aqualead (II) complexes as shown in Figures 6 - 9. The plotted Pb-O vibrational stretching frequencies include the $[Pb(H_2O)_{1-9}]^{2+}$ complexes. The 7 and 9 coordinate species were found to be unstable and hence were not plotted. One of the reasons for calculating these frequencies is so that they can be compared to experimental Raman studies that have been or will be completed. Specifically, simulated Raman spectra will be passed to Dr. Peter Tremaine who will perform high temperature and pressure Raman experiments on various lead (II) complexes at the University of Guelph in Ontario. These vibrational stretching frequencies can be used to confirm, or disprove, any experimental Raman findings that cannot be otherwise unambiguously assigned to a specific complex.

Comparable solution Raman data that could only be found for the monohydrate complex, $[Pb(H_2O)]^{2+}$. Gourlaouen et al.[84] performed B3LYP/SDD/6-31+G** level of calculations and reported the Pb-O vibrational stretching mode to be 335 cm^{-1}, which is consistent with our results of 318 cm^{-1}, 335 cm^{-1} and 334 cm^{-1} for the HF, MP2 and B3LYP levels of theory, respectively.

Some general trends can be drawn from our plots of bond lengths and stretching frequencies shown in Figures 7 - 9. Concerning the bond lengths, as more water ligands are added to the central lead atom, the Pb-O bond lengths show a general elongation trend. This is caused by overcrowding of the lead center resulting in electrostatic repulsion between the water ligands. The opposite trend is observed in the Pb-O vibrational stretching frequencies. As the Pb-O bond lengths increase, the vibrational stretching frequencies decrease. This trend makes sense, because if the bond is longer it

will take less energy to cause it to vibrate and hence the corresponding vibrational frequency is also lower.

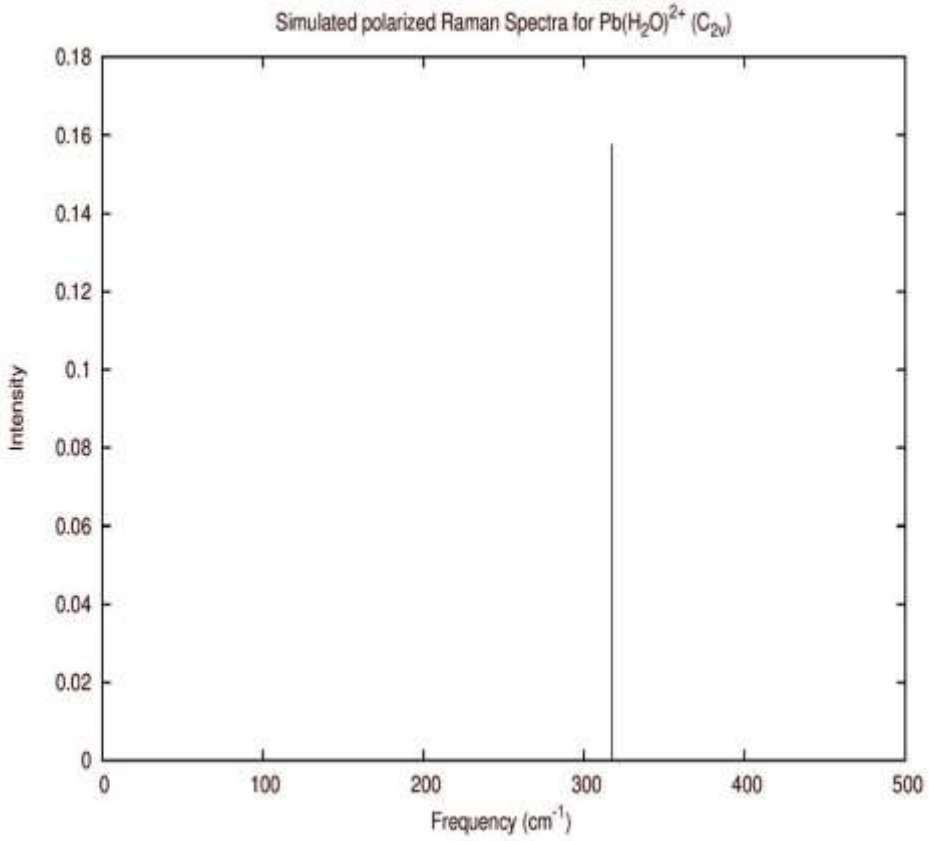

Figure 6: Simulated Raman spectrum of the monoaqualead (II) complex, $[Pb(H_2O)]^{2+}$, based on our HF/SDD/6-311+G* frequency calculation.

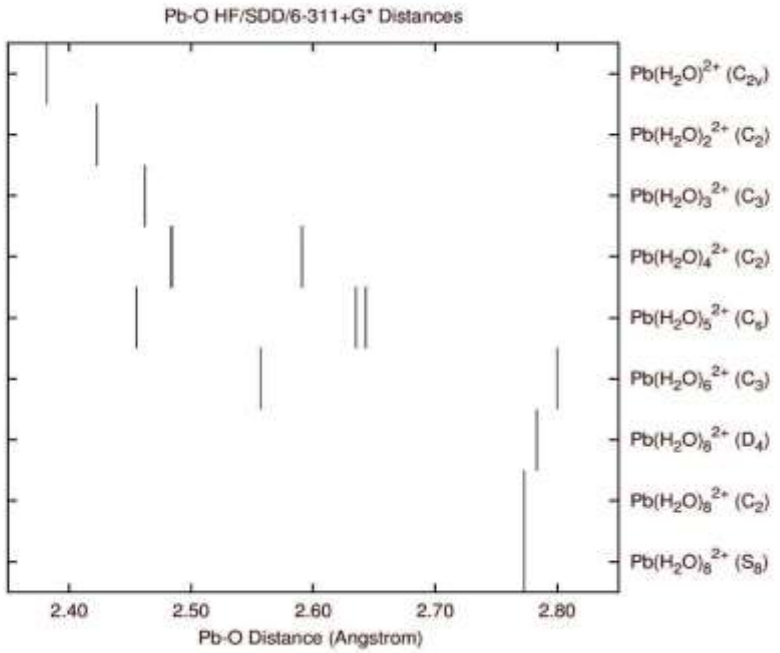

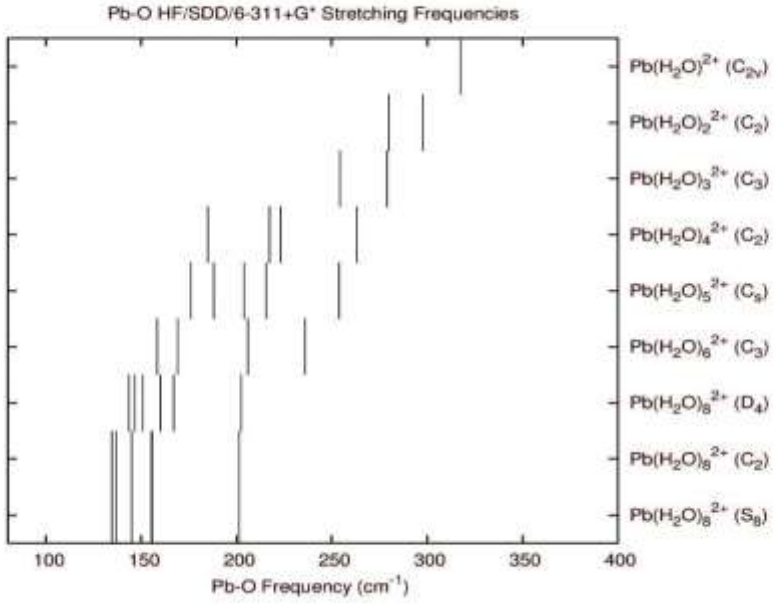

Figure 7: Pb-O bond lengths and vibrational stretching frequencies for $[Pb(H_2O)_n]^{2+}$, where n=1-8, calculated at the HF/SDD/6-311+G*level of theory.

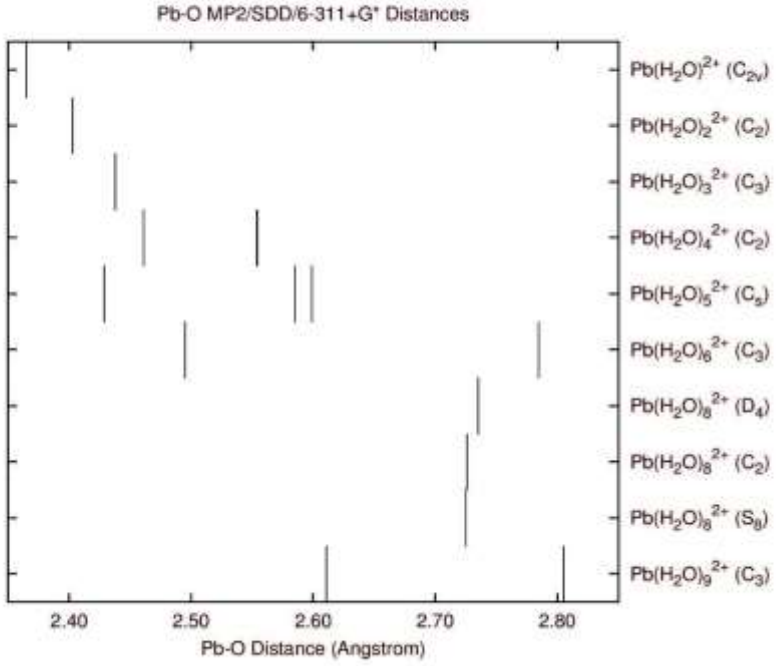

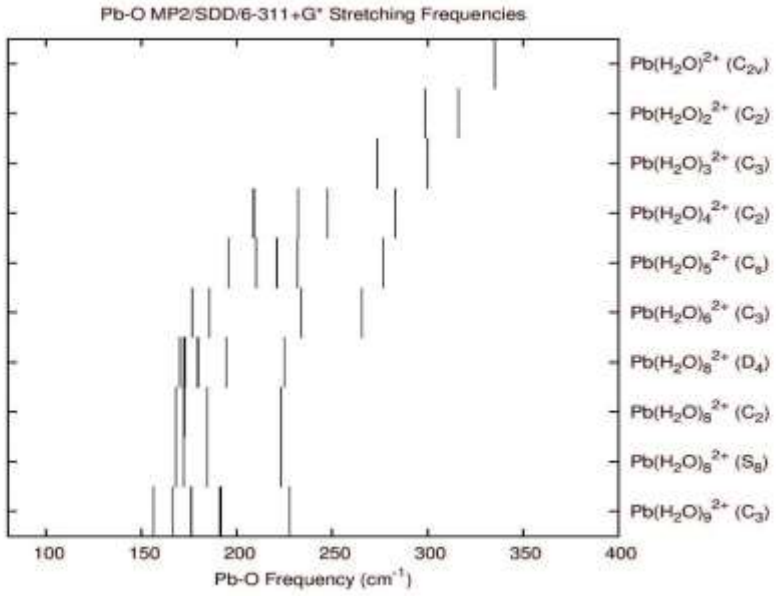

Figure 8: Pb-O bond lengths and vibrational stretching frequencies for $[Pb(H_2O)_n]^{2+}$, where n=1-8, calculated at the MP2/SDD/6-311+G*level of theory.

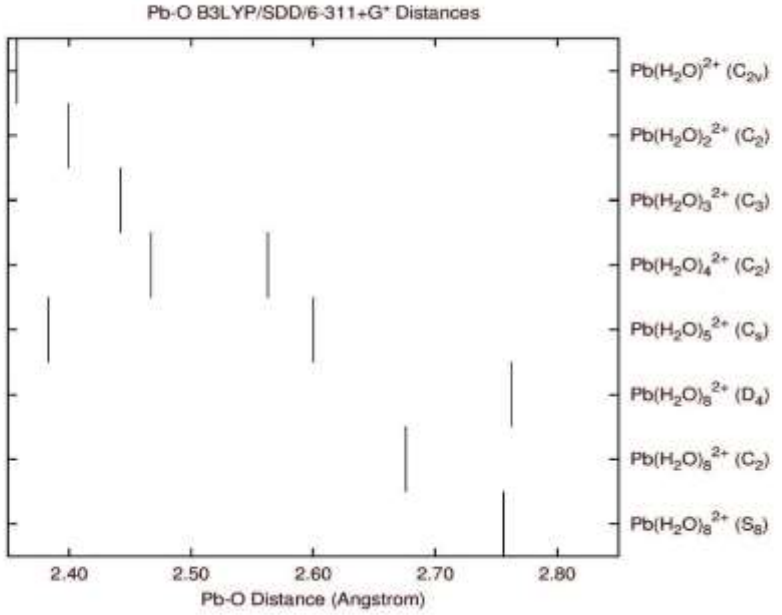

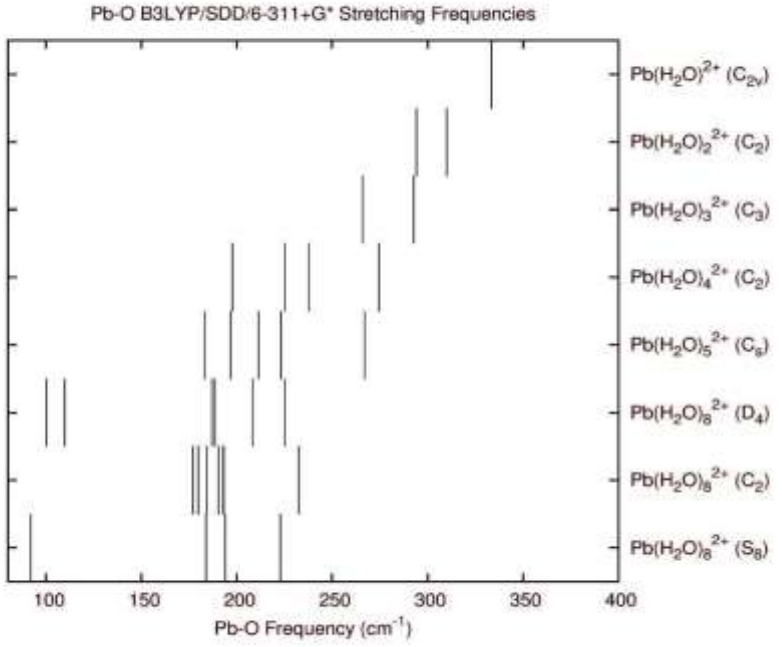

Figure 9: Pb-O bond lengths and vibrational stretching frequencies for $[Pb(H_2O)_n]^{2+}$, where n=1-8, calculated at the B3LYP/SDD/6-311+G*level of theory.

Chapter 4: Chlorolead (II) Complexes, $[PbCl_m(H_2O)_n]^{2-m}$

This *ab initio* investigation was carried on lead (II) complexes involving chloride ligands (with and without water). The formation of these species and their transport through a supercritical water-cooled (SCW) reactor core may result in the corrosion of the reactor's construction material. In order to assure the sustainability of the nuclear reactor, it is essential to understand the bonding properties of aquachlorolead (II) species in order to gain control over corrosion associated with the formation of these metal ligand species.

This chapter includes computational results and a discussion of the chlorolead (II) complexes, up to and including six-coordinate species $[PbCl_m(H_2O)_n]^{2-m}$, where m =1 - 4, n = 0 - (6-m). Water molecules were added to the chlorolead (II) complexes to probe how hydration affects the stability of the given species. All of the results discussed within this thesis (i.e., total energies, bond lengths and corresponding vibrational frequencies) come from calculations carried out the HF, MP2 and B3LYP levels of theory coupled to an SDD basis set for Pb and 6-311+G* for water and chloride. All calculations were carried out at zero Kelvin, in the gas-phase. All simulated Raman spectra are from vibrational frequency data obtained at the HF/SDD/6-311+G* level. The structures shown are the absolute energy minima located at the MP2 and B3LYP levels of theory at SDD/6-311+G*, unless other local minima were obtained that had pronouncedly different geometries.

4.1 Literature Review

The motivation behind our research on lead chlorides is the fact that lead (Pb^{2+}) is a highly toxic, heavy metal and its complexes are a serious health hazard and environmental pollutants.[82, 83] Mapping of lead poisoning and designing chelating ligands to prevent lead poisoning requires an in-depth understanding of lead's binding properties, stability, as well as a detailed spectral analysis. Structural investigations of lead chlorides and their hydration species are very poorly documented in the literature and thus require a comprehensive structural investigation on the molecular level.

The crystal structure of lead chloride was investigated by Braekken et al.[84] as early as 1932. Sass et al.[85] doubted the results obtained by Braekken et al.[84] and hence reinvestigated the lead chloride structure using single crystal, X-ray diffraction aiming for a more reliable set of interatomic distances. $PbCl_2$ was found to have Pb-Cl in plane bond distances of 3.04 Å, 3.09 Å and 2.80 Å and out of plane Pb-O bond distances of 2.91 Å, 3.05 Å and 3.70 Å. However, the typical Pb-Cl bond distances recorded in the Cambridge Structural Database[86] is 2.839 Å with a standard deviation of 0.160 Å. Neutral and ionic compounds containing lead and chloride that have been known for a long time are $PbCl_2$ and $PbCl_4$, as well as their derivative $PbCl_6^{2-}$.[87]

Saghatforoush et al.[88] reported the synthesis and crystal structure of a new coordination polymer identified as [Pb(TpyCl)Cl] [Pb(TpyCl)Cl_2] [$PbCl_3$] (CH_3OH), where TpyCl is the 4'-chloro-2,2':6',2"-terpyridine ligand. This yellow crystal was obtained by the branched tube method and its structure determined using single-crystal X-ray diffraction. The crystal structure revealed three complexes, the cationic $[Pb(TpyCl)Cl]^+$, the neutral [Pb(TpyCl)Cl_2] and the anionic $[PbCl_3]^-$, which were

connected via bridging chlorides and hydrogen bonds. The structural arrangement of the surrounding ligands bonded to a central metal atom (Pb^{2+}) suggested the presence of a stereo active lone pair. Within the neutral complex, $[Pb(TpyCl)Cl_2]$, the first lead atom (Pb1) is five-coordinate. It forms three bonds via coordination to the TpyCl ligand, with Pb-N bond distances of 2.490 Å, 2.502 Å and 2.507 Å, Pb1 is also coordinated to two chloride anions with Pb-Cl bond distances of 2.818 Å and 2.858 Å. In addition, two bridging oxygen atoms are linked to Pb1 and the Pb-O bond lengths were identified as 3.169 and 3.393 Å, respectively. The second lead (II) centre (Pb2) was identified within the cationic complex $[Pb(TpyCl)Cl]^+$. Pb2 is five coordinate, including a stereo-active lone pair of electrons on the lead. Pb 2 is coordinated through 3 Pb-N bonds of a second TpyCl ligand, where the Pb-N bond distances were measured to be 2.560 Å, 2.564 Å and 2.567 Å, respectively. The final coordination is through another Pb-Cl bond (2.774 Å). The third lead (II) atom (Pb3), from the anionic complex $[PbCl_3]^-$, was identified by its three Pb-Cl bonds (2.576 Å, 2.650 Å and 2.742 Å). The anionic $[PbCl_3]^-$ complex is arranged in a tetrahedral structure. Bridging chloride ligands, from the cationic and neutral complex, are coordinated to Pb3 and through longer Pb-Cl bonds (3.132 Å and 3.296 Å respectively).

Freza et al.[89] performed *ab inito* calculations to investigate the structural and physiochemical properties of the lead chlorides ($PbCl_x$; x=1-5) and their chloroplumbate derivatives ($PbCl_y^n$; y = 1 - 7, n = 1 - 4), as well as the thermodynamic and kinetic properties of these species. Specifically, calculations were performed at the MP2 and MP2 (PCM) levels of theory, coupled to LANL2DZ basis sets for Pb and 6-311+G* basis sets for water. Freza et al.[89] identified electronically, energetically and thermodynamically

stable species in a gaseous system. These included lead chlorides involving $PbCl_x$ (x = 1 - 5), singly charged anions with the formula $PbCl_y^-$ (y=2-6) and the doubly charged anions $PbCl_y^{2-}$ (y = 4 - 6), while the species $PbCl_5^{3-}$, $PbCl_6^{3-}$, and $PbCl_7^{2-}$ were found to be stable in the aqueous phase. The attachment of Cl^- to neutral molecules was found to be free of any kinetic activation barrier, whereas the attachment to anions involved moderate kinetic activation barriers. Cl_2 was found to attach in a constructive two-step fashion involving an initial complex formation followed by an unconcerted substitution. Theoretical prediction showed that the maximum ionic valence of electronically stable species in the gaseous stable is two (e.g. $PbCl^{2-}$), while in an aqueous environment chloroplumbate anions with an ionic valence of more than two can occur. Crystal structures were predicted for $PbCl_5^{3-}$ and $PbCl_6^{4-}$ implying that these structures should be stable in crystalline solid phase. These observations were attributed to the strong repulsive electrostatic interactions which prevent the formation of highly charged chloroplumbate anions in the gaseous phase, while these electrostatic repulsions are significantly reduced in an aqueous environment.[88]

4.2 Results

Stable structures were found for all of the anhydrous chlorolead (II) complexes up to and including those with four chloride ligands. These chlorolead complexes were further hydrated and investigated up to, and including a hexacoordinate species (species with 6 ligands). Water molecules were added with the aim of probing how the hydration affects the stability of a given complex. The highest stable coordination number of the hydrated chlorolead (II) complexes proved to be largely dependent on the number of chloride ligands involved.

The hydrated monochlorolead (II) complexes were found to be stable up to, and including, the penta-coordinate species. The hexa-coordinated species were investigated, but these were unstable with respect to dissociation of one or two of the water molecules (depending on the symmetry investigated). The hydrated dichlorolead (II) complexes were found to be stable up to, and including, the tetra-coordinate species. The penta- and hexa- coordination of the hydrated dichlorolead (II) species were attempted, but they underwent dissociation of one or more of the ligands (chloride and/or water). Therefore, stable structures for penta- and hexacoordinated dichlorolead (II) complexes were not found. Furthermore, no stable structures were found for either trichlorolead (II) complexes or tetrachlorolead (II) complexes when water was added. All of these structures showed either a chloride or water molecule dissociating from the rest of the molecule.

All of the results (total energies, bond distances and stretching frequencies) discussed in this thesis are from calculations carried out at the HF, MP2 and B3LYP levels of theory with SDD/6-311+G* basis sets. The total energies of the stable structures, as well as those of the others that were attempted, can be found in Tables 4A.1- 4A.9 of the Supplementary Materials section. The absolute minimum energy structures are presented for the MP2 and B3LYP optimizations and can be found in Figures 10, Figure 11, Figure 12 and Figure 13 for the monochlorolead (II) complexes, the dichlorolead (II) complexes, the trichlorolead (II) complexes and the tetrachlorolead (II) complexes respectively.

The anhydrous monochlorolead (II) complex, $[PbCl]^+$, did not cause any symmetry problems as the highest symmetry $C_{\infty v}$ structure was found to be the most

stable at all of the levels of theory studied. The monohydrate, $[PbCl(H_2O)]^+$, was desymmetrized from C_{2v}, along the imaginary B_1 mode, a skeletal deformation mode, to a preferred C_s symmetry. $[PbCl(H_2O)]^+$ was the most stable with C_s symmetry for all of the levels of theory studied. The dihydrate, $[PbCl(H_2O)_2]^+$, was initially constrained to have C_{2v} symmetry (two forms). Subsequently, the lower energy C_{2v} #2 structure was desymmetrized along the B_1 and B_2 modes, skeletal deformation modes, to C_s #1 and C_s #2 respectively. These subsequently converged to the same structure with the same absolute energy minimum. Hence, the dihydrate, $[PbCl(H_2O)_2]^+$, was the most stable at C_s symmetry for all of the levels of theory studied. The trihydrate, $[PbCl(H_2O)_3]^+$, was investigated under the constraint of C_{3v} symmetry (two forms). The C_{3v} #2 structure was found to be at the lowest energy minimum for the HF and B3LYP levels, while the MP2 level results contained imaginary frequency modes. Subsequently, the C_{3v} #2 structure was desymmetrized along the imaginary A_2, water twisting mode, to a C_3 structure. The C_3 structure was stable at the HF level of theory, but contained imaginary E modes at the MP2 level of calculations; this suggested that further desymmetrization to the C_s structure would be necessary. Subsequently, the C_3 structure was desymmetrized at the MP2 level of theory along the E mode, a skeletal deformation mode, to the stable C_s symmetry. Hence, C_s symmetry was identified as giving the most stable structure for the $[PbCl(H_2O)_3]^+$ species at the MP2 level of theory The tetrahydrate complex, $[PbCl(H_2O)_4]^{1+}$, was investigated under the constraint of C_{4v} symmetry (two forms). The C_{4v} #2 structure was found to give the lowest energy minimum for all of the levels of theory studied. The pentahydrate complex, $[PbCl(H_2O)_5]^{1+}$, was initially constrained to have C_{2v} symmetry (five forms). The C_{2v} #4 and C_{2v} #5 structures were unstable, resulting

in the dissociation of one H_2O ligand in each case. The C_{2v} #1 structure was the lowest in energy and hence was desymmetrized to C_s #1, based on the B_1 imaginary mode at the HF and MP2 levels and to C_s #2 based on the B_2 imaginary mode at the B3LYP level. In addition, the C_{2v} structure of $[PbCl(H_2O)_5]^+$ was desymmetrized along the A_2 imaginary mode to the C_2 #1 structure at the HF and MP2 levels of theory, while being desymmetrized to C_2 #2 at the B3LYP level. These C_2 and C_s structures contained imaginary frequencies, suggesting further desymmetrization was required to even lower symmetry structures. Subsequently, the C_s structure was desymmetrized along the A" imaginary mode to a C_1 structure. The C_1 structure did contain real frequency modes, but resulted in the dissociation of one water ligand at the HF and MP2 levels and dissociation of two water ligands at the B3LYP levels of theory. Hence, the C_1 symmetry of $[PbCl(H_2O)_5]^+$ species was found to be unstable at all levels of theory.

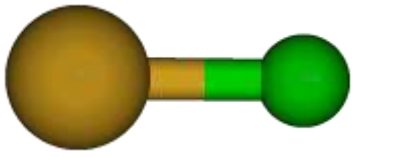

$C_{\infty v}$

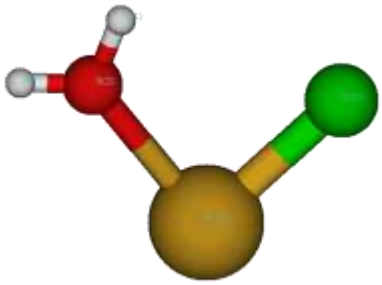

C_s

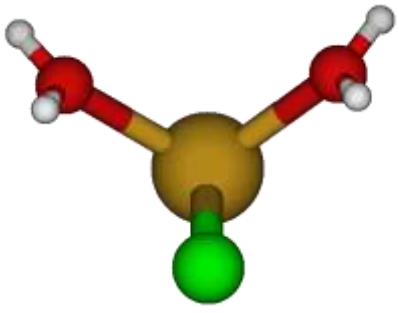

C_s

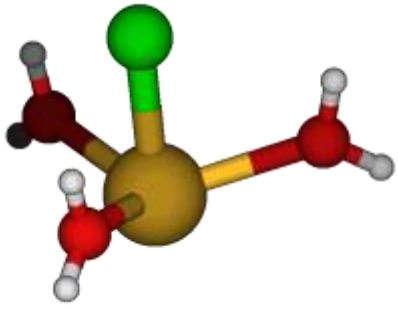

C_{3v} #2*

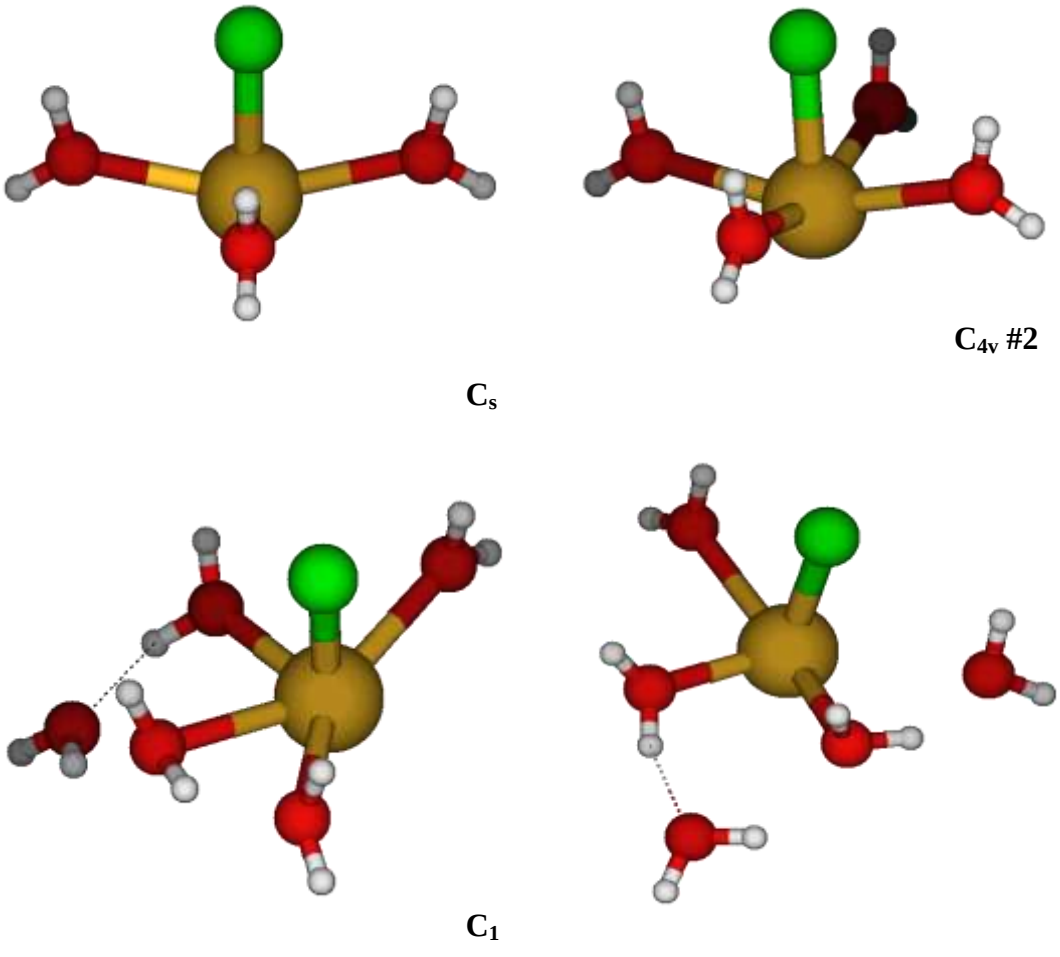

Figure 10: Optimized MP2 and B3LYP geometries for stable structures of $[PbCl_m(H_2O)_n]^{2-n}$, where m=1 and n=0- (6-m). All symmetries marked with "*" indicates B3LYP level results, "a" indicates MP2, otherwise the MP2 and B3LYP derived structures are similar.

The anhydrous dichloro complex, $[PbCl_2]^0$ was initially constrained to the highest possible $D_{\infty h}$ symmetry. This structure was desymmetrized along a $\prod_{1u}$ imaginary mode, a skeletal deformation mode, to C_{2v} symmetry. Hence, C_{2v} symmetry was identified as the most stable for $[PbCl_2]^0$.

The monohydrate, $[PbCl_2(H_2O)]^0$, was investigated under the constraint of C_{2v} symmetry (two forms). Both of these forms had A_2 imaginary modes (indicative of a C_2

structure), as well as B_1 and B_2 imaginary modes (indicative of two C_s structures). Both the C_2 and C_s structures contained imaginary frequency modes at all of the levels of theory, suggesting that further desymmetrization was required. Subsequently, the lower symmetry C_s structure was desymmetrized along the A" imaginary mode, a structural deformation mode, to the C_1 unconstrained structure. Hence, $[PbCl_2(H_2O)]^0$ was found to be the most stable at C_1 symmetry.

The dihydrate complex, $[PbCl_2(H_2O)_2]^0$, was initially constrained to have D_{2h} symmetry (2 forms). The lower energy D_{2h} structure was desymmetrized along the imaginary skeletal deformation modes, B_{1u} and B_{2u}, to C_{2v} #1 and C_{2v} #2 symmetries, respectively. Frequency analysis revealed that the C_{2v} #1 symmetry is the most stable form for $[PbCl_2(H_2O)_2]^0$ at all of the levels of theory studied.

The trihydrate, $[PbCl_2(H_2O)_3]^0$, was reverted from D_{3h} along the A_2" imaginary mode to a C_{3v} symmetry structure, which was, in turn, desymmetrized along the A_2 (water twisting mode) and E (skeletal deformation mode) to C_3 and C_s structures, respectively. The C_3 structure was found to be unstable with one detached chloride ligand. The C_s structure was stable, but contained an imaginary A" mode (indicative of a C_1 structure). The trihydrate, $[PbCl_2(H_2O)_3]^0$, was initially constrained to the highest possible symmetry, a D_{3h} structure (2 forms). The lower energy D_{3h} structure was desymmetrized along the A_2" mode, a skeletal deformation mode, to C_{3v} symmetry. The C_{3v} structure was then further desymmetrized along the A_2 imaginary frequency mode (water twisting mode) and the E imaginary frequency mode (skeletal deformation mode) to C_3 and C_s structures, respectively. However, the C_3 structure was found to be unstable, with the dissociation of one chloride ligand ultimately resulting in the formation of

$[PbCl_1(H_2O)_3]^0$. On the other hand, the C_s structure was found to be fully attached, but contained the imaginary A" frequency mode; further desymmetrization resulted in a C_1 symmetry structure. The HF optimization of the C_1 structure was skipped due to the dissociation of the remaining chloride ligand. The C_1 structure was optimized at the MP2 and B3LYP levels of theory, where real frequency modes were obtained. However, it was unstable, resulting in the formation of $[PbCl_2(H_2O)_2]^0$ and one detached H_2O molecule. Therefore, a stable structure for the $[PbCl_2(H_2O)_3]^0$ complex was not found.

The tetrahydrate, $[PbCl_2(H_2O)_4]^0$, was initially investigated under a D_{4h} symmetry constraint (two forms). Subsequently, the lower energy D_{4h} structure was desymmetrized along A_{2g}, a water wagging mode, to C_{4h} symmetry, along A_{2u}, a skeletal deformation mode, to C_{4v} symmetry and along B_{2u}, a skeletal deformation mode, to D_{2d} symmetry. The C_{4v} structure was found to be fully attached at the HF level of theory but contained imaginary frequency modes. The same structure lost one chloride ligand when optimized at the MP2 and B3LYP levels of theory. The tetrahydrate, $[PbCl_2(H_2O)_4]$ was desymmetrized along the imaginary E_u mode, to a C_{2v} symmetry structure. The C_{2v} symmetry $[PbCl_2(H_2O)_4]^0$ structure lost one water ligand when optimized at the HF and MP2 levels of theory, while the C_{2v} structure optimized at the B3LYP level lost two chloride ligands and one water molecule through dissociation. The D_{4h} #1 form of $[PbCl_2(H_2O)_4]^0$ was reverted along the E_g mode, a water twisting mode, to C_s symmetry. The C_s structure was fully attached at the HF and MP2 levels of theory, while the B3LYP optimized structure had lost one chloride ligand. The C_s structure contained an imaginary A" mode at the HF and MP2 levels of theory suggesting desymmetrization to the C_1 structure was required. Subsequently, the $[PbCl_2(H_2O)_4]^0$ complex was desymmetrized to

a C_1 symmetry, unconstrained structure. This resulted in the detachment of one chloride ligand at the HF level of theory, while optimization at the MP2 and B3LYP levels was skipped due to the dissociation of ligands. Hence, a stable structure for the $[PbCl_2(H_2O)_4]^0$ complex was not found.

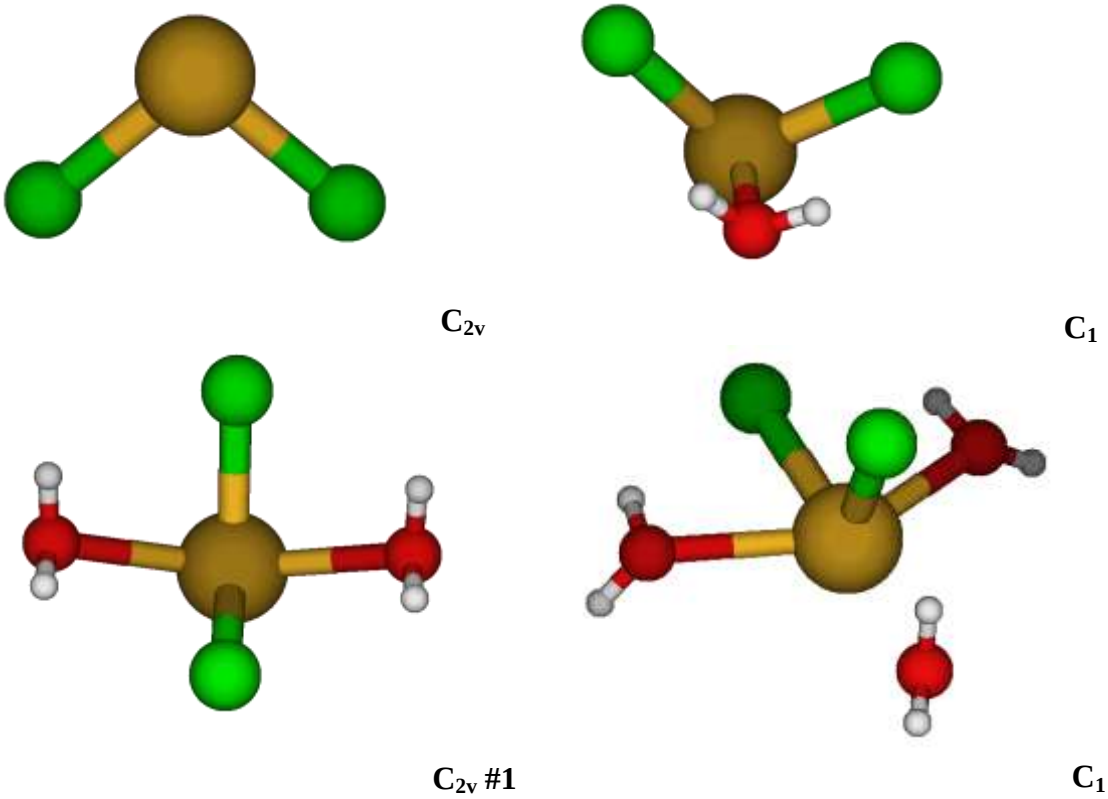

Figure 11: Optimized MP2 and B3LYP geometries for stable structures of $[PbCl_m(H_2O)_n]^{2-n}$, where m=2 and n=0- (6-m). All symmetries marked with "*" indicates B3LYP level results, "a" indicates MP2, otherwise the MP2 and B3LYP derived structures are similar

The anhydrous trichloro complex, $[PbCl_3]^-$ was reverted from the initially constructed D_{3h} structure, along the imaginary A" mode, a skeletal deformation mode, to give a structure with C_{3v} symmetry. The structure with C_{3v} symmetry was found to be the most stable form for the $[PbCl_3]^-$ complex.

The monohydrate, $[PbCl_3(H_2O)]^-$, was initially constrained under C_{2v} symmetry (two forms). Subsequently, the lower energy C_{2v} #1 structure was desymmetrized along the B_1 and B_2 modes to symmetries of C_s #1 and C_s #2, respectively. Optimization of the C_s #1 structure resulted in dissociation of one water ligand that appeared to be then hydrogen bonded to two neighboring attached chloride ligands ($[PbCl_3]^-$ + 1 H_2O detached). On the other hand, the C_s #2 structure was not optimized at the HF/MP2/B3LYP/SDD/6-311+G* levels, due to problematic steps that showed the dissociation of ligands. Hence, the C_s #1 and C_s #2 structures were unstable and no further desymmetrization was performed due to the dissociation of ligands. No stable structure was found for $[PbCl_3(H_2O)]^-$.

The dihydrate complex, $[PbCl_3(H_2O)_2]^-$, was initially optimized under the constraint of C_{2v} symmetry (two forms). Subsequently, the lower energy structure, C_{2v} #2, was desymmetrized along the A_2 frequency mode to a C_2 structure. The C_2 structure contained an imaginary B mode (indicative of a C_s structure). Subsequently, the C_s #1 and C_s #2 structures were optimized, but were proven to be unstable. Optimization of both of the C_s structures of $[PbCl_3(H_2O)_2]^-$ resulted in the formation of $[PbCl_3(H_2O)]^-$ and the detachment of one H_2O ligand. Since the $[PbCl_3(H_2O)_2]^-$ complex was found to be unstable with C_s symmetry, no further desymmetrization was performed.

The trihydrate complex, $[PbCl_3(H_2O)_3]^-$, was initially constrained to have C_{3v} symmetry (4 forms). All these forms were unstable and resulted in dissociation of 3 H_2O molecules ($[PbCl_3]^-$ + 3 H_2O detached). The trihydrate, $[PbCl_3(H_2O)_3]^-$, was also constrained under C_{2v} symmetry (4 forms). The C_{2v} #1 structure turned out to be unstable, resulting in the detachment of one chloride molecule, while the other 3 forms gave C_{2v}

structures that were fully attached. These C_{2v} structures contained imaginary frequency modes (B_1 and A_2 suggesting desymmetrization to C_s and C_2, respectively). Desymmetrization of the C_{2v} structure along the A_2 mode resulted in a structure of C_2 symmetry, which was fully attached but contained an imaginary B frequency mode, suggesting further desymmetrization to the lower C_s symmetry was required. However, optimization of the C_s structure was skipped at the HF and MP2 levels of theory due to the dissociation of ligands, while the B3LYP optimization was found to be unstable, giving the $[PbCl_3(H_2O)]^-$ structure and 2 detached H_2O molecules. Hence, no further desymmetrization was performed for the $[PbCl_3(H_2O)_3]^-$ complex and no stable structure was identified.

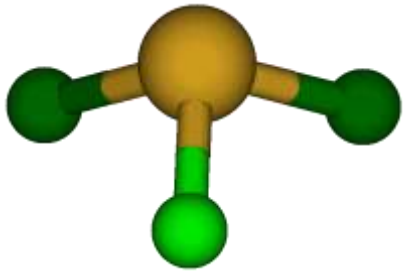

C_{3v}

Figure 12: Optimized MP2 and B3LYP geometries for stable structures of $[PbCl_m(H_2O)_n]^{2-n}$, where m = 3 and n = 0 - (6-m). There was no distinction between the structures for the MP2 and B3LYP levels of theory.

The anhydrous tetrachloro complex, $[PbCl_4]^{2-}$ was initially investigated under the constraint of D_{4h} symmetry. There were A_{2u} and B_{2u} imaginary frequencies. Subsequently, the D_{4h} structure was desymmetrized along the A_{2u} mode, a skeletal deformation mode, to a structure of C_{4v} symmetry, which contained imaginary frequency modes and along B_{2u}, a skeletal deformation mode, to a D_{2d} symmetry structure. However, the D_{2d} structure converged to a T_d structure. Hence, $[PbCl_4]^{2-}$ was found to be

at the lowest energy minima for T_d symmetry. The hydrated tetrachloro complexes, $[PbCl_4(H_2O)]^{2-}$ and $([PbCl_4(H_2O)_2]^{2-}$, were found to be unstable. These complexes showed dissociation of either a chloride ligand or a water molecule from the rest of the molecule.

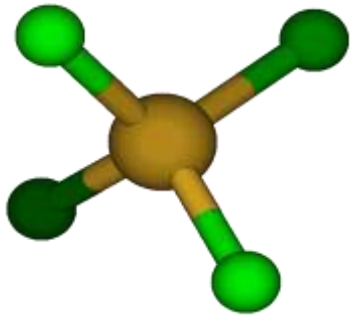

T_d

Figure 13: Optimized MP2 and B3LYP geometries for stable structures of $[PbCl_m(H_2O)_n]^{2-n}$, where m = 4 and n =0 - (6-m). There was no distinction between the structures for the MP2 and B3LYP levels of theory.

No stable structures were found for the pentachlorolead (II) complex. The geometry attempted showed dissociation of chloride ligands.

From the optimized geometries, both MP2 and B3LYP levels of theory, it was clear that the chloride and water ligands prefer to arrange themselves in a sterically hindered conformation around the central lead (II), which appears to be largely influenced by the stereo active Pb lone pair ($6s^2$).

Plots of the Pb-O and Pb-Cl bond lengths and vibrational stretching frequencies were constructed and can be seen in Figure 14, Figure 15 and Figure 16 for the HF, MP2 and B3LYP calculations, respectively. Within these plots, the dashed lines indicate which bond lengths and vibrational stretches involve chloride ligands. Simulated polarized Raman spectra were also created for the stable HF structures and can be found in Figure 4A-1 of the Supplementary Materials section.

4.3 Discussion and Literature Comparison

The information on the structure, stability and spectral properties of chlorolead (II) complexes acquired through the work in this thesis creates a convenient framework within which to gain a more detailed understanding of the bonding properties and behavior of the most stable chlorolead (II) species. Computationally predicted geometries and spectral properties of the chlorolead (II) complexes (anhydrous) have been compared with the data available in the literature (both computational and experimental), to show the extent to which the characteristics of these complexes correspond to each other. Unfortunately, no literature data was available for hydrated chlorolead (II) complexes.

The most stable geometry for the anhydrous monochlorolead (II) complexes, $[PbCl]^+$ was identified as that having $C_{\infty v}$ symmetry for all of the levels of theory studied in this work (HF, MP2 and B3LYP). This finding is consistent with the results from the computational study by Freza et al.[89], who identified both [PbCl] and $[PbCl]^-$ species as having $C_{\infty v}$ geometries. Freza et al.[89] performed *ab initio* investigations of lead chlorides ($PbCl_x$; x = 1 - 5) and their chloroplumbate derivatives ($PbCl_y^n$; y = 1 - 7, n = 1 - 4) at the MP2 level of theory, using a 6-311+G* basis set for Cl and a LANL2DZ basis set for Pb. Subsequently, Freza et al.[89] identified the Pb-Cl bond length in PbCl to be 2.479Å, which is in close agreement with our 2.379 Å, 2.379 Å and 2.390 Å distances from the HF, MP2 and B3LYP calculations, respectively. Freza et al.[89] obtained slightly longer Pb-Cl bond distances and this can be attributed to their choice of basis set for Pb, which was a small-core pseudo potential (PP) LANL2DZ set compared to the large-core PP SDD set we

used. Furthermore, Freza et al.[89] identified the Pb-Cl bond length in $[PbCl]^-$ to be slightly longer (2.691 Å). The elongation of the bond length for the anionic $[PbCl]^-$ can be attributed to the electrostatic repulsion between of stereo active lone pair on Pb and the negative charge on Cl.

Saghatforoush et al.[88] studied the crystal structure of $[Pb(TpyCl)Cl][Pb(TpyCl)Cl_2][PbCl_3](CH_3OH)$ and found it to contain three complexes: cationic $[Pb(TpyCl)Cl]^+$, neutral $[Pb(TpyCl)Cl_2]$ and anionic $[PbCl_3]^-$. The Pb-Cl bond length identified within the cationic complex, $[Pb(TpyCl)Cl]^+$, was 2.774(3) Å, which is slightly longer than the value of 2.433 Å we report for $[PbCl]^+$ at B3LYP. These differences can be attributed to the fact that our calculations involved a single molecule in the gas phase, whereas Saghatforoush et al.[88] performed experiments on a solid single crystal, where longer range interactions occur, thus involving greater electrostatic repulsion and elongating the observed Pb-Cl bond lengths.

The most stable geometry found for the anhydrous dichloro complex, $[PbCl_2]$, had C_{2v} symmetry. This finding is in excellent agreement with the results obtained by Freza et al.[89] who identified the most stable geometry for $PbCl_2$ to be of C_{2v} symmetry as well. Freza et al.[89] characterized $PbCl_2$ from the obtained Pb-Cl bond length of 2.457 Å. The Pb-Cl bond lengths reported in this thesis for $PbCl_2$ are 2.505 Å, 2.498 Å and 2.518 Å at the HF, MP2 and B3LYP levels of theory, respectively. The overall Pb-Cl bond length has increased when compared to the anhydrous monochlorolead (II) complex ($[PbCl]^+$).

Saghatforoush et al.[88] reported the Pb-Cl bond distances for the neutral $[Pb(TpyCl)Cl_2]$ complex to be 2.818(3) Å and 2.858(3) Å. The structure of this complex was identified as having five-coordinate lead including a stereo-active lone-pair on the

lead (II) center. The Pb-Cl bond distances obtained by Saghatforoush et al.[88] are higher than the ones reported in this thesis (2.505 Å, 2.498 Å and 2.518 Å at the HF, MP2 and B3LYP levels of theory, respectively). Again, our calculations were performed on a single molecule ($[PbCl_2]$) in the gas phase whereas Saghatforoush et al.[88] calculated optimized geometries for the cationic complex ($[Pb(TpyCl)Cl]^+$) within the solid state crystal resulting in a larger electrostatic repulsion.

The most stable geometry for the anhydrous trichlorolead (II) complex, $[PbCl_3]^-$ proved to be that with C_{3v} symmetry for all of the levels of theory studied (HF, MP2 and B3LYP). The Pb-Cl bond lengths determined in this work for $[PbCl_3]^-$ are 2.645 Å, 2.621 Å and 2.659 Å for the HF, MP2 and B3LYP respectively. These bond lengths are longer than the analogous anhydrous mono- and dichlorolead (II) values. The Pb-Cl bond lengths reported here are consistent with an *ab initio* study by Freza et al.[89], who performed calculations at the MP2/LANL2DZ/6-311+G* level on $[PbCl_3]^-$ and identified the most stable structure to have C_{3v} symmetry. Freza et al.[89] obtained a slightly shorter Pb-Cl bond length of 2.581 Å.

Saghatforoush et al.[88] identified $[PbCl_3]^-$ within their more complex single crystal, to be tetrahedral in structure with three coordinated chloride anions. Subsequently, the Pb-Cl bond lengths were identified to be 2.576(3) Å, 2.650(3) Å and 2.742(3) Å. These Pb-Cl values are in a close agreement with our values, however the bond lengths obtained by Saghatforoush et al.[88] are slightly longer. These differences can be attributed to the fact that our geometry optimization was done on a single molecule in the gas phase, whereas Saghatforoush et al.[88] investigated $[PbCl_3]^-$ within the larger solid state crystal resulting in elongation of the Pb-Cl bond lengths.

The anhydrous tetrachloro species, $[PbCl_4]^{2-}$, that proved to be the most stable has T_d symmetry. The Pb-Cl bond lengths in it are 2.937 Å, 2.877 Å and 2.911 Å from the HF, MP2 and B3LYP calculations, respectively. These bond lengths are longer when compared to those in the lower coordination species like the anhydrous mono-, di- and trichloro lead (II) complexes. These differences can be attributed to the increased number of chloride ligands, which affect the electrostatic repulsion forcing the bonds to elongate. Freza et al.[89] identified the most stable structures for $[PbCl_4]^{2-}$ to have T_d and C_{3v} symmetries, with Pb-Cl bond lengths of 2.844 Å and 2.886 Å, respectively. These results are similar to the results reported here (2.937 Å, 2.877 Å and 2.911 Å at HF, MP2 and B3LYP level, respectively), while the bond lengths obtained by Freza et al.[89] are slightly lower than our values.

Table 4: Geometry comparison of chloride lead complexes (MP2 and B3LYP levels) with results reported by Freza et al.[89] All bond lengths (Å) are averages where appropriate.

Complex	**Symmetry Point Group**	**Optimized Pb-Cl Bond Lengths (Å)**			
		Freza et al.[89]	**Our Results**		
		MP2	**HF**	**MP2**	**B3LYP**
$PbCl^+$	**$C_{\infty v}$**	-	2.379	2.379	2.390
PbCl	**$C_{\infty v}$**	2.479	-	-	-
$PbCl^-$	**$C_{\infty v}$**	2.691	-	-	-
$PbCl_2$	**C_{2v}**	2.457	2.505	2.498	2.518
$PbCl_3^-$	**C_{3v}**	2.581	2.645	2.621	2.659
$PbCl_4^{2-}$	**T_d**	2.886	2.937	2.877	2.911

All previous computational studies regarding optimized Pb- O and Pb- Cl bonds of aquachlorolead (II) complexes are in a good agreement with the results reported in this thesis. The Pb-Cl values obtained by Freza et al.[89] are slightly lower than our values. These subtle difference can be attributed to the different choice of pseudo potentials (LANL2DZ) utilized at MP2 level of theory by Freza et al.,[89] while we used a large-core PP SDD at HF, MP2 and B3LYP levels of theory, thus resulting in a slight elongation of the Pb-Cl bond lengths. The geometry comparison of chloride lead complexes (MP2 and B3LYP levels) with results reported by Freza et al.[89] is summarized in Table 4.

Vibrational stretching frequencies were calculated for this set of hydrated chlorolead (II) complexes as seen in Figures 14 - 16. Freza et al.[89] computationally calculated the vibrational frequencies to be 289 cm^{-1} and 194 cm^{-1} for [PbCl] and $[PbCl]^-$, respectively. The vibrational stretching frequencies reported for the $[PbCl]^+$ species in this thesis are 361 cm^{-1}, 363 cm^{-1} and 348 cm^{-1} for the HF, MP2 and B3LYP levels of theory, respectively.

Freza et al.[89] computationally calculated the harmonic vibrational frequencies for the stable $PbCl_2$ species having C_{2v} symmetry. Specifically, the frequency modes b_2 and a_1 were obtained at 288 cm^{-1} and 305 cm^{-1}, respectively. The vibrational stretching frequencies reported in this thesis are 283 cm^{-1} (b_2 mode) and 305 cm^{-1} (a_1 mode) for $PbCl_2$ (C_{2v} symmetry) calculated at the HF level of theory. Our HF results are in excellent agreement with the values obtained by Freza et al.[89].The MP2 optimized vibrational stretching frequencies obtained for $PbCl_2$, constrained under C_{2v} symmetry, in this thesis are 290 cm^{-1} (b_2 mode) and 309 cm^{-1} (a_1 mode). The B3LYP optimized vibrational stretching frequencies for $PbCl_2$ reported in this thesis are 273 cm^{-1} (b_2 mode) and 293

cm^{-1} (a_1 mode). Hence, the vibrational frequencies obtained at the MP2 and B3LYP levels of theory are in very good agreement with the computational values obtained by Freza et al.[89]

The anhydrous trichlorolead (II) complex, $[PbCl_3]^-$ was found to be the most stable with C_{3v} symmetry. This species was characterized and found to have the following vibrational frequencies at the HF level of theory: 216 cm^{-1} (e mode) and 251 cm^{-1} (a_1 mode). The MP2 optimized vibrational frequencies for $[PbCl_3]^-$ with C_{3v} symmetry were 231 cm^{-1} (e mode) and 260 cm^{-1} (a_1 mode). Furthermore, the B3LYP optimized vibrational frequencies for $[PbCl_3]^-$ at C_{3v} symmetry reported in this thesis are: 212 cm^{-1} (e mode) and 242 cm^{-1} (a_1 mode). These results are in close agreement with the frequency values reported by Freza et al.[89] for the $[PbCl_3]^-$ structure having C_{3v} symmetry. Specifically, these vibrational frequency values included 226 cm^{-1} (e mode) and 254 cm^{-1} (a_1 mode).

The anhydrous tetrachloro complex, $[PbCl_4]^{2-}$, was found to be the most stable with T_d symmetry. The HF optimized vibrational frequencies obtained for this $[PbCl_4]^{2-}$ complex are: 133 cm^{-1} (b_2 mode), 133 cm^{-1} (e mode) and 180 cm^{-1} (a_1 mode). The MP2 optimized vibrational frequency values for T_d constrained $[PbCl_4]^{2-}$ are: 148 cm^{-1} (b_2 mode), 148 cm^{-1}(e mode) and 190 cm^{-1} (a_1 mode). The B3LYP optimized vibrational frequencies obtained for the $[PbCl_4]^{2-}$ species constrained under T_d symmetry are: 140 cm^{-1} (b_2 mode), 140 cm^{-1} (e mode) and 178 cm^{-1} (a_1 mode). Freza et al.[89] calculated vibrational frequencies for the $[PbCl_4]^{2-}$ complex constrained under T_d and C_{3v} symmetries. Specifically, the vibrational frequencies obtained for the $[PbCl_4]^{2-}$ complex constrained under T_d symmetry are: 143 cm^{-1} (t_2 mode) and 186 cm^{-1} (a_1 mode). The

reported frequency values for the $[PbCl_4]^{2-}$ complex constrained to have C_{3v} symmetry are 128 cm^{-1}(e mode), 154 cm^{-1} (a_1 mode) and 226 cm^{-1} (a_1 mode).

Table 5: Stretching vibrational frequencies comparison of anhydrous chlorolead (II) complexes with results reported by Freza et al.[89]

Complex	**Symmetry Point Group**	**Stretching Vibrational Frequency (cm^{-1}) (Frequency mode)**			
		Freza et al.[89]	**Our Results**		
		MP2	**HF**	**MP2**	**B3LYP**
$PbCl^+$	**$C_{\infty v}$**	-	361 (σ_g)	363 (σ_g)	348 (σ_g)
PbCl	**$C_{\infty v}$**	289 (σ_g)	-	-	-
$PbCl^-$	**$C_{\infty v}$**	194 (σ_g)	-	-	-
$PbCl_2$	**C_{2v}**	288 (b_2) 305 (a_1)	283 (b_2) 305 (a_1)	290 (b_2) 309 (a_1)	273 (b_2) 293 (a_1)
$PbCl_3^-$	**C_{3v}**	226 (e) 254 (a_1)	216 (e) 251 (a_1)	231 (e) 260 (a_1)	212 (e) 242 (a_1)
$PbCl_4^{2-}$	**T_d**	143 (t_2) 186 (a_1)	133 (t_2) 180 (a_1)	148 (t_2) 189 (a_1)	140 (t_2) 178 (a_1)

The vibrational frequencies reported by Freza et al.[89] are slightly different in value compared to the results reported in this thesis and can be attributed to the fact that Freza et al.[89] utilized different pseudopotential (LANL2DZ) basis set, while the SDD basis set was utilized in this thesis. Please refer to a Table 5 for comparison purposes (our vibrational frequency data vs. Freza et al.[89] frequency results).

Plots containing the Pb-O and Pb-Cl bond lengths and the vibrational stretching frequencies have been created and can be found in Figures 14 to 16. From these plots a general trend can be determined, where increasing the number of coordinated water

molecules around the central lead atom results in increase of the Pb-O and Pb-Cl bond lengths. This general trend can be accounted for an increase in the ligand-ligand repulsion when the number of water ligands is increased. However, when the number of coordinated chloride ligands is increased, there is a greater tendency for ligand dissociation (water and chloride) to occur, with subsequent hydrogen bonding to a neighboring chloride and/or water in coordinated molecules. These observed trends are consistent with the theoretical/computational predictions made by Freza et al.[89] where it was shown that in an aqueous environment chloroplumbate anions with a valence of more than two can occur, while, the highest ionic valence for the electronically stable anhydrous species is two (for example $PbCl_4^{2-}$). Such findings have been attributed to the repulsive electrostatic interactions which prevent the formation of highly charged chloroplumbate anions ($PbCl_y^{x}$) in the gas phase. These are substantially reduced in an aqueous environment due to the strong ion-dipole stabilizing interactions that can occur in such conditions. A similar effect on the stability of multiply charged anions when the number of coordinated water molecules is increased has been reported by other authors.[90, 91]

Vibrational stretching frequency plots accompanying the bond length plots in Figures 14-16. An inverse relationship between the bond length and the magnitude of the associated vibrational frequency is observed. That is, as more water molecules are added to the complex there is a decrease in the vibrational stretching frequency values. The explanation of such behavior is attributed to the elongation of the bond lengths. This reduces the stabilization of a given species (slightly increasing the total energy), thus

making bond distances longer. In turn, less energy is needed for a bond to stretch vibrationally, ultimately resulting in a lower frequency of vibration.

Simulated polarized Raman plots have been constructed based on intensities calculated at the HF level of theory. These can be found in Figure 4A-1 in the Supplementary Materials section. Currently, there is no Raman data found in the literature and hence cannot be compared. However, the ultimate goal is to compare the simulated Raman intensities generated in this work with experimental Raman studies that will be completed by our colleagues at the University of Guelph in Ontario. Subsequently, the computationally-calculated Raman intensities will be utilized to confirm or refute any ambiguous experimental Raman data. At the present time there is no experimental data available with which to compare the simulated Raman intensities obtained in this thesis.

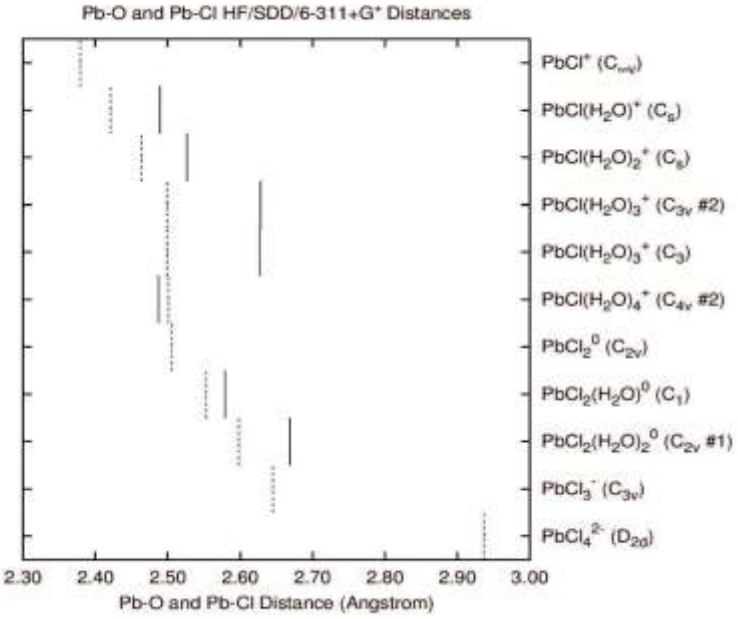

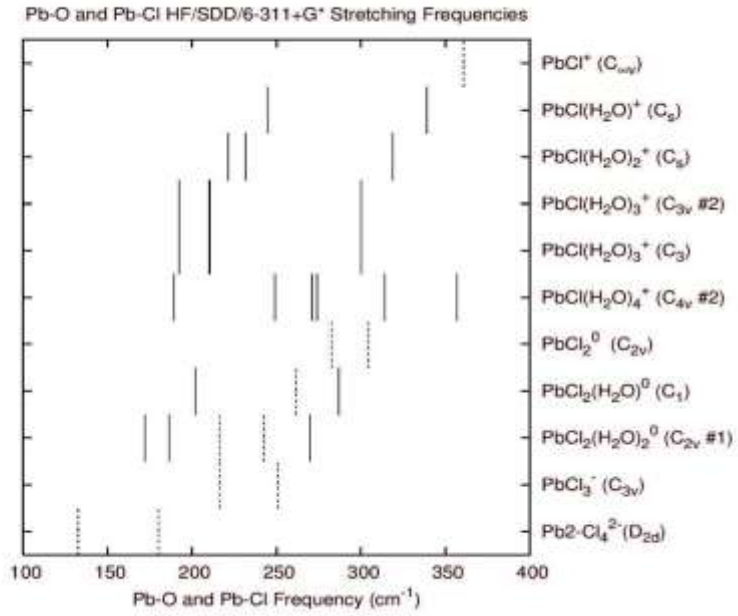

Figure 14: Pb-O (solid line) and Pb-Cl (dashed line) bond lengths and vibrational stretching frequencies for $[PbCl_m(H_2O)_n]^{2-m}$, where m =1 - 4, n = 0 - (6-m), calculated at the HF/SDD/6-311+G* level of theory.

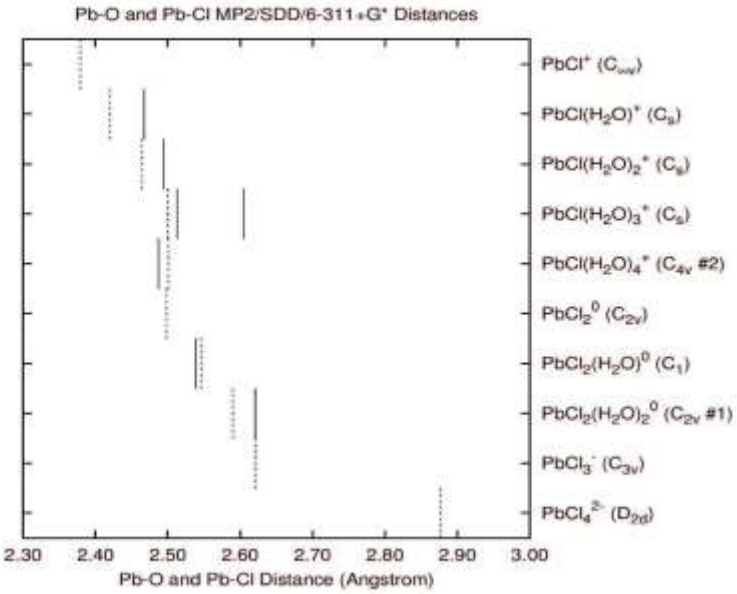

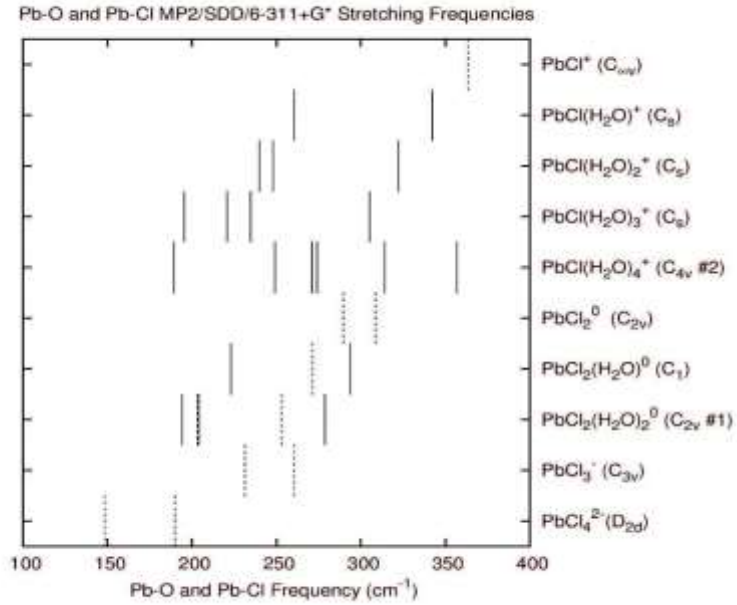

Figure 15: Pb-O (solid line) and Pb-Cl (dashed line) bond lengths and vibrational stretching frequencies for $[PbCl_m(H_2O)_n]^{2-m}$, where m =1 - 4, n = 0 - (6-m), calculated at the MP2/SDD/6-311+G* level of theory.

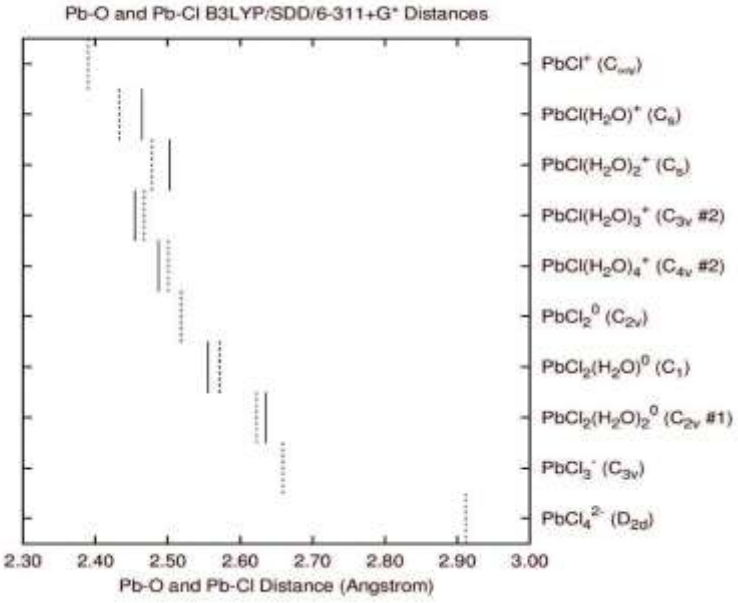

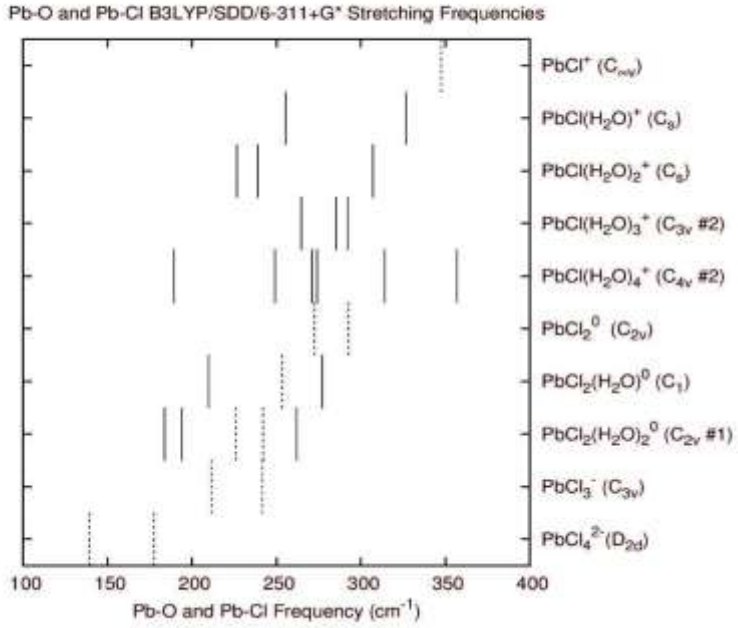

Figure 16: Pb-O (solid line) and Pb-Cl (dashed line) bond lengths and vibrational stretching frequencies for $[PbCl_m(H_2O)_n]^{2-m}$, where m = 1 - 4, n = 0 - (6-m), calculated at the B3LYP/SDD/6-311+G* level of theory.

Chapter 5: Hydroxylead (II) Complexes

Hydroxylead (II) complexes are metal-ligand corrosion products predicted to form under extreme temperature and pressure conditions within the supercritical water-cooled reactor (SCWR). No detailed investigation of all possible stable hydroxylead (II) complexes has been documented up until now. This thesis summarizes the very first catalogue of systematically optimized hydroxylead (II) complexes and the very first catalogue of computationally predicted vibrational spectra of each stable lowest energy minima structure. This chapter includes computational results and a discussion of the hydroxylead (II) complexes, up to and including six-coordinate species, $[Pb(OH)_m(H_2O)_n]^{2-m}$, where m = 1-4, n= 0- (6-m).

5.1 Literature Review

Lead is widely scattered throughout our ecosystem as a result of its continuing industrial use.[92,93] The common oxidation state of lead (Pb (II)) is highly mobile in nature, and thus presents a serious health hazard to all living species.[93] The importance of understanding the mechanism of lead transport in the natural environment has been a driving force behind previous research regarding the structural characterization of hydroxylead (II) compounds.[94]

At high pH, Pb (II) is largely hydrolyzed to $Pb_p(OH)_q^{(2p-q)+}$ (both mononuclear (p=1) and polynuclear (p>1) species).[93,95] In 1969, Spiro et al.[96] hydrolyzed a lead (II) perchlorate solution isolating a compound of composition $Pb_6O(OH)_6(ClO_4)_4 \cdot H_2O$, which was subsequently crystalized and characterized by single-crystal X-ray diffraction. Discrete hexanuclear complexes, $[Pb_6O(OH)_6^{4+}]$, were identified in the structure, with

lead atoms at the corners of three face-sharing tetrahedral, thus forming the boat-shaped metal atoms clusters. That is, 4 lead atoms are found in the central tetrahedron while the remaining two lead atoms cover two of the tetrahedral faces.[96.]The structural arrangement of the hexanuclear cluster was predicted *a priori* from Raman spectroscopic data to be octahedral.[96] Following the study by Spiro et al.[96], Johansson and Olin[97] performed an X-ray scattering study on hydrolyzed lead (II) perchlorate solutions. The scattering data revealed a tetrahedral arrangement of the lead atoms within the polynuclear hydrolysis complex. The structures of these complexes were in close agreement with the previously reported discrete hexa-nuclear complex, $[Pb_6O(OH)_6^{4+}]$, reported by Spiro et al.[96] Inspired by the previous research of Spiro et al.[96], where the α-form of the $[Pb_6O(OH)_6](ClO_4)_4 \cdot H_2O$ crystal was investigated, Olin et al.[98] probed the β-form of the very same crystal. Olin et al.[101] utilized X-ray diffraction spectroscopy to determine the crystal structure of β-$[Pb_6O(OH)_6](ClO_4)_4 \cdot H_2O$. The crystal was identified as having an orthorhombic lattice. Within the β-$[Pb_6O(OH)_6](ClO_4)_4 \cdot H_2O$ crystal structure, discrete $[Pb_6O(OH)_6^{4+}]$ units were identified, with six lead atoms arranged at the corners of three distorted tetrahedral connected to each other by common faces.[98] The oxygen atom were arranged at the center of the central tetrahedron, while the outer unit contained hydroxide oxygen atoms outside each of the six unshared faces. These discrete six-nuclear units, $[Pb_6O(OH)_6^{4+}]$ were identical to the ones identified within the α-$[Pb_6O(OH)_6](ClO_4)_4 \cdot H_2O$ crystal identified by Spiro et al.[96.]

In 1973, Hong and Olin[99] determined the crystal structure of $[Pb_4(OH)_4]_3(CO_3)(ClO_4)_{10} \cdot 6H_2O$ utilizing X-ray diffraction spectroscopy. The crystal was identified as being of hexagonal symmetry and composed of discrete slightly distorted

tetrahedral $[Pb_4(OH)_4^{4+}]$ units with four lead ions (Pb^{2+}) occupying its corners, while hydroxide (OH^-) groups were located outside the given unit. Hong and Olin[99] concluded that the observed atomic distances between the perchlorate groups and the $[Pb_4(OH)_4^{4+}]$ units are in a close agreement with the bond distances of α- and β-$[Pb_6O(OH)_6](ClO_4)_4 \cdot H_2O$ obtained by Spiro et al.[96] and Olin et al.[98] respectively. The average Pb-O bond distance obtained for solid $[Pb_4(OH)_4^{4+}]$ was 2.38 Å. Hence, Hong and Olin[99] concluded that two $[Pb_4(OH)_4^{4+}]$ units may combine to form a six-nuclear unit building block, $[Pb_6O(OH)_6^{4+}]$, obtained in both the α- and β-$[Pb_6O(OH)_6](ClO_4)_4 \cdot H_2O$ complexes with two lead centres and one oxygen in common.[99.]

In 1974, Hong and Olin[100] reported the crystal structure of $[Pb_4(OH)_4](ClO_4)_4 \cdot 2H_2O$. The crystal structure was determined by X-ray diffraction. Discrete $[Pb_4(OH)_4^{4+}]$ units were identified in the structure, with each having slightly distorted tetrahedral geometries. The authors noted that the very same $[Pb_4(OH)_4^{4+}]$ unit had been identified in a previous study involving $[Pb_4(OH)_4]_3(CO_3)(ClO_4)_{10} \cdot 6H_2O$. The locations of the lead atoms (located at the corners of a tetrahedron) and the hydroxide groups (located outside the faces of the tetrahedron) within the $[Pb_4(OH)_4^{4+}]$ units were found to be identical within both $[Pb_4(OH)_4](ClO_4)_4 \cdot 2H_2O$ and $[Pb_4(OH)_4]_3(CO_3)(ClO_4)^{10} \cdot 6H_2O$. The Pb-O bond lengths within the $[Pb_4(OH)_4^{4+}]$ units were identified to be in the range of 2.35 and 2.47 Å, depending on the lead and oxygen atoms involved in the bonding.

Baes and Mesmer[95] concluded, based on their comprehensive review, that the highest possible coordination number of a hydrolyzed mononuclear lead (II) complex to be three, with the resulting $Pb(OH)_3^-$ structure. Specifically, at a Pb (II) concentration of

approximately 10 μM, $Pb(OH)_q^{(2-q)+}$ species with q≤3 and $Pb_3(OH)_4^{2+}$ were identified. However, Perera et al.[93] suggested further investigation of the highest mononuclear complexes was necessary. Perera et al.[93] utilized UV-Vis spectrophotometric-potentiometric titrations to probe the Pb (II)/OH^- system within $NaClO_4$ media at $[Pb(II)]_T \leq 10\mu M$. At low pH, Pb (II) was hydrolyzed into $Pb_p(OH)_q^{(2p-q)+}$ with the possibility of its existing as a mononuclear species where p = 1 or a polynuclear species where p is greater than 1. At pH ≤ 10.4, absorbance from 216 to 300 nm confirmed the existence of the following species: Pb^{2+}, $Pb(OH)^+$, $Pb(OH)_2^0$, or $Pb(OH)_3^-$. At higher pH, one more species, $Pb(OH)_4^{2-}$ was detected. The highest coordination number for a hydrolyzed mononuclear lead (II) complex was identified to be $Pb(OH)_4^{2-}$. No evidence was found for higher order complexes nor for the existence of any polynuclear species at $[Pb(II)]_T \leq 10\mu M$. It was concluded, that the important species that are present within our biosphere are the four species, $Pb(OH)^+$, $Pb(OH)_2^0$, $Pb(OH)_3^-$ and $Pb(OH)_4^{2-}$. A Pb-NMR study and Raman spectroscopy utilized to investigate the Pb(II)/OH^- systems gave only semi-quantitative confirmations, indicating that these methods are not suitable for such investigation. Perera et al.[93] argued that Baes and Mesmer's model[95] was underestimated with respect to the highest mononulcear species and overestimated with respect to the polynuclear species at $[Pb(II)]_T \leq 10\mu M$.

Based on the literature review, the highest coordination number studied for the anhydrous hydroxylead (II) species in this thesis is four.

Breza et al.[94] utilized Gaussian 94 software to probe the molecular geometries of the $[Pb_4(\mu_3\text{-}OH)_n]^q$ and $[Pb_4O(\mu_3\text{-}OH)_n]^{q-2}$ complexes (where q = 8-n and n= 2, 3, 4), subsequently followed by investigation of species where the μ_3-OH bridges were

removed. Computational calculations were done at the HF, MP2 and B3LYP levels of theory coupled to basis sets, cc-pVDZ for O and H atoms and LANL2DZ effective core potential for Pb. Geometry optimization revealed the highest symmetry for $[Pb_4(\mu_3\text{-}OH)_4]^{4+}$ and $[Pb_4O\ (\mu_3\text{-}OH)_4]^{2+}$ to be T_d (tetrahedral structures), while the highest symmetry for both $[Pb_4(\mu_3\text{-}OH)_3]^{5+}$ and $[Pb_4O(\mu_3\text{-}OH)_3]^{3+}$ was C_{3v}. The Pb-O bonds holding the clusters together were identified as being relatively weak. The $[Pb_4(\mu_3\text{-}OH)_3]^{5+}$ and $[Pb_4O(\mu_3\text{-}OH)_3]^{3+}$ complexes were found to be stable. On the other hand, $[Pb_4(\mu_3\text{-}OH)_2]^{6+}$ and $[Pb_4O(\mu_3\text{-}OH)_2]^{4+}$ were found to be unstable, which was attributed to their insufficient number of μ_3-OH bridges, needed to hold the tetrahedral complexes together. The Pb-O bond lengths reported for $[Pb_4(\mu_3\text{-}OH)_4]^{4+}$ were identified as 2.41 Å, 2.42 Å and 2.44 Å at the HF, MP2 and B3LYP levels of theory, respectively. The Pb-O bond lengths of $[Pb_4(\mu_3\text{-}OH)_3]^{5+}$ were identified as 2.45 Å, 2.48 Å and 2.48 Å at HF, MP2 and B3LYP levels respectively.

Gourlaouen et al.[81] computationally probed the complex $[Pb(OH)]^+$, the most likely Pb (II) species besides $[Pb(H_2O)]^{2+}$ to be present in our atmosphere. The driving force behind this research was unravelling the molecular significance of the Pb^{2+} ion as a polluting agent in environment. Gourlaouen et al.[81] utilized Gaussian03 to perform calculations at the HF and B3LYP levels of theory coupled to different basis sets (6-31++G* for the O and H atoms; scalar relativistic pseudo potentials LANL2DZ and SDD (large core relativistic pseudo potentials), as well as CRENBS were used to describe Pb^{2+}). For the sake of comparison, all-electron (AE) calculations were performed utilizing Faegri's basis sets (double zeta quality basis set) on Pb^{2+}.[101] The four-component calculations were performed using DIRAC code,[102] subsequently utilizing DB3LYP/AE

(Dirac-Hybrid Density Functional all electron calculations)[103]. Furthermore, Gourlaouen et al.[81] performed population analysis (natural bond orbital (NBO) and atoms in molecule calculations (AIM) with the objective to gain a more detailed understanding of the bonding nature (covalent or electrostatic) between the Pb^{2+} cation and the OH^- ligand. These studies were followed by a topological analysis of the electron localization function (ELF).

Based on the population analysis, Gourlaouen et al.[81] suggested covalent bonding between the Pb^{2+} cation and the OH^- ligand. The authors also emphasized that up until this study no spectroscopic data (rotational or vibrational) had been reported for the $[Pb(OH)]^+$ complex. Geometry optimization showed $[Pb(OH)]^+$ to be the lowest energy minima for the $C_{\infty v}$ (linear structure) and for the C_s (bent structure), largely depending on the computational method utilized. The $[Pb(OH)]^+$ complex preferred $C_{\infty v}$ symmetry at all HF levels except HF/LANL2DZ, which preferred C_s symmetry. However, all MP2 and B3LYP levels identified the lowest energy minima as a bent structure (C_s), except the B3LYP/SDD level where the linear structure ($C_{\infty v}$) was preferred. The authors observed a very small inversion barrier from the C_s structure to the $C_{\infty v}$ structure, implying that such a small barrier could be overcome at high temperatures. The SDD and CRENBS optimized geometries for $[Pb(OH)]^+$ were in close agreement with one another (especially the Pb-O bond distance). The calculations involving population analysis, including NBO, AIM and ELF, gave results that are in very close agreement with one another as well. SDD and CRENBS basis sets were identified as a great choice for calculating the molecular geometries of the $[Pb(OH)]^+$ complex. On the other hand, Gourlaouen et al.[81] advised against utilization of the LANL2DZ basis set, since it showed non-precise

reproduction of DB3LYP/AE (Dirac-B3LYP level of theory with all-electron (AE) calculations) offering unreliable results. This was attributed to the small expansion associated with LANL2DZ basis sets.[81]

5.2 Results

This chapter includes computational results and discussion regarding molecular optimization of hydroxylead (II) complexes with maximum 4 hydroxide (OH) ligands up to and including hexa-coordinated species. Water molecules were added to investigate how hydration influences the stability of a given species. Total energies are summarized in Tables 5A.1-5A.9 of the supplementary material section and include all 27 levels of theory investigated. These 27 levels include HF, MP2 and B3LYP coupled to the basis sets, CEP-121G, LANL2DZ and SDD for Pb and 6-31G*, 6-31+G* and 6-311+G* for H and O. However, the results reported and discussed in sections 5.2 and 5.3 of this thesis are the only those involving SDD/6-311+G*. Large core pseudo potential SDD was chosen based on a previous, successful computational study involving the lead cation (Pb^{2+}) coordinated to ligands containing hydrogen and oxygen atoms.[21] The optimized geometries presented here are those found for the lowest energy minima at MP2 and B3LYP/6-311+G*/SDD levels, unless other local minima were obtained with significantly different geometries. These are shown in Figure 17, Figure 18 and Figure 19 for the monohydroxy- , dihydroxy- and trihydroxylead (II) complexes, respectively. All calculations were carried out at 0 Kelvin, in the gas phase.

The coordination number of the hydroxide ligands was limited to four or less. However, stable structures were found for the anhydrous hydroxide complexes up to and

including the trihydroxyspecies $[Pb(OH)_3]^-$. The anhydrous tetrahydroxo complex, $[Pb(OH)_4]^{2-}$, showed dissociation of one hydroxide (OH^-) ligand, and an affinity to exist as ion pair. A stable structure for this ion pair complex was not found. The anhydrous hydroxide complexes were further hydrated and investigated up to and including hexa-coordinated species. Hydration was performed to investigate whether addition of water perturbs the stability of a given complex.

The hydrated monohydroxylead (II) complexes were stable up to and including the penta-coordinate species, $[Pb(OH)_1(H_2O)_4]^+$. Geometry optimization of the hexa-coordinated species of $[Pb(OH)_1(H_2O)_5]^+$ resulted in the dissociation of one water molecule. The diaquadihydroxolead (II) complex, $[Pb(OH)_2(H_2O)_2]^0$, was identified as the lowest energy minima structure for the hydrated dihydroxylead (II) complexes. All of the other hydrated dihydroxolead (II) complexes were found to be unstable with dissociation of one or more water ligands (depending on the level of theory investigated). No stable structures were found for either the trihydroxylead (II) complexes or the tetrahydroxylead (II) complexes when water ligands were added. All of these tri- and tetra- hydroxolead (II) species showed dissociation of hydroxide (OH^-) and/or water (H_2O) ligands from the rest of the molecule.

The anhydrous monohydroxo complex, $[Pb(OH)]^+$, preferred the linear $C_{\infty v}$ structure at all levels of theory (HF, MP2 and B3LYP).

The monohydrate, $[Pb(OH)(H_2O)]^+$ was initially investigated under the constraint of C_{2v} symmetry. Desymmetrization of $[Pb(OH)(H_2O)]^+$ was performed along the imaginary skeletal deformation modes, B_1 and B_2, to C_s #1 and C_s #2 respectively. The

most stable geometry for the monohydrate, $[Pb(OH)(H_2O)]^+$, was C_s #1 at the HF, MP2 and B3LYP levels of theory.

The dihydrate, $[Pb(OH)(H_2O)_2]^+$, was initially constrained at C_{2v} symmetry (two forms). The C_{2v} #1 structure was lower in symmetry and was subsequently desymmetrized along the imaginary modes B_1 and B_2 to C_s #1 and C_s #2 respectively. The most stable structure (the lowest energy structure) for $[Pb(OH)(H_2O)_2]^+$ was proven to be C_s #1 at all of the levels of theory investigated (HF, MP2 and B3LYP).

The trihydrate, $[Pb(OH)(H_2O)_3]^+$, was investigated under the constraint of C_{3v} symmetry (two forms). The lower energy structure, C_{3v} #1, was desymmetrized along the imaginary skeletal deformation E mode to C_s symmetry (two forms). These C_s structures were further desymmetrized along the imaginary A" frequency mode to C_1, #1 and #2 structures. C_1 #1 and C_1 #2 structures converged into the same C_1 conformation. The most stable (the lowest energy minima) structure for $[Pb(OH)(H_2O)_3]^+$ was found to be C_s, #1 at HF, C_1 at both MP2 and B3LYP levels of theory.

The tetrahydrate, $[Pb(OH)(H_2O)_4]^+$, was initially investigated under the constraint of C_{4v} symmetry (two forms). The lower energy structure, C_{4v} #1, was desymmetrized along the imaginary water twisting (A_2) and the skeletal deformation (E) frequency mode, to C_4 and C_s symmetry, respectively. All of these structures contained imaginary frequencies, suggesting further desymmetrization was required. Hence, C_s was reverted along the imaginary A" frequency mode to C_1 symmetry. The results gave all real (positive) frequencies at all levels of theory. However, even though the HF optimized geometry of $[Pb(OH)(H_2O)_4]^+$ contained all positive frequencies, the resulting structure suggested dissociation of one H_2O ligand, which was hydrogen bonded to a neighbouring

water molecule. Hence, at C_1 symmetry $[Pb(OH)(H_2O)_4]^+$ was stable at the HF level of theory, although through the secondary hydration shell. Secondary hydration shell stabilization is not of interest of this thesis. On the other hand, C_1 symmetry of $[Pb(OH)(H_2O)_4]^+$, was found to be at the lowest energy minima and fully attached at both MP2 and B3LYP levels of theory.

The pentahydrate, $[Pb(OH)(H_2O)_5]^+$, was primarily investigated under C_{2v} symmetry (4 forms). The lowest energy structure, C_{2v} #1, was desymmetrized along the imaginary water twisting (A_2) and skeletal deformation (B_1 and B_2) frequency modes to the C_2, C_s #1 and C_s #2 structures, respectively. The lowest energy structure, C_s #2, was desymmetrized along the imaginary A" mode, to C_1 symmetry. HF and MP2 optimization of the C_1 structure indicated stabilization through the secondary shell, characterized by real (positive) frequency modes and dissociation of one or more water ligands. These are hydrogen bonded to the remaining $[Pb(OH)(H_2O)_3]^+$ complex. Geometry optimization was skipped for C_1 symmetry at the B3LYP level of theory due to dissociation of ligands. Hence, no lowest energy minima structure was identified for $[Pb(OH)(H_2O)_5]^+$.

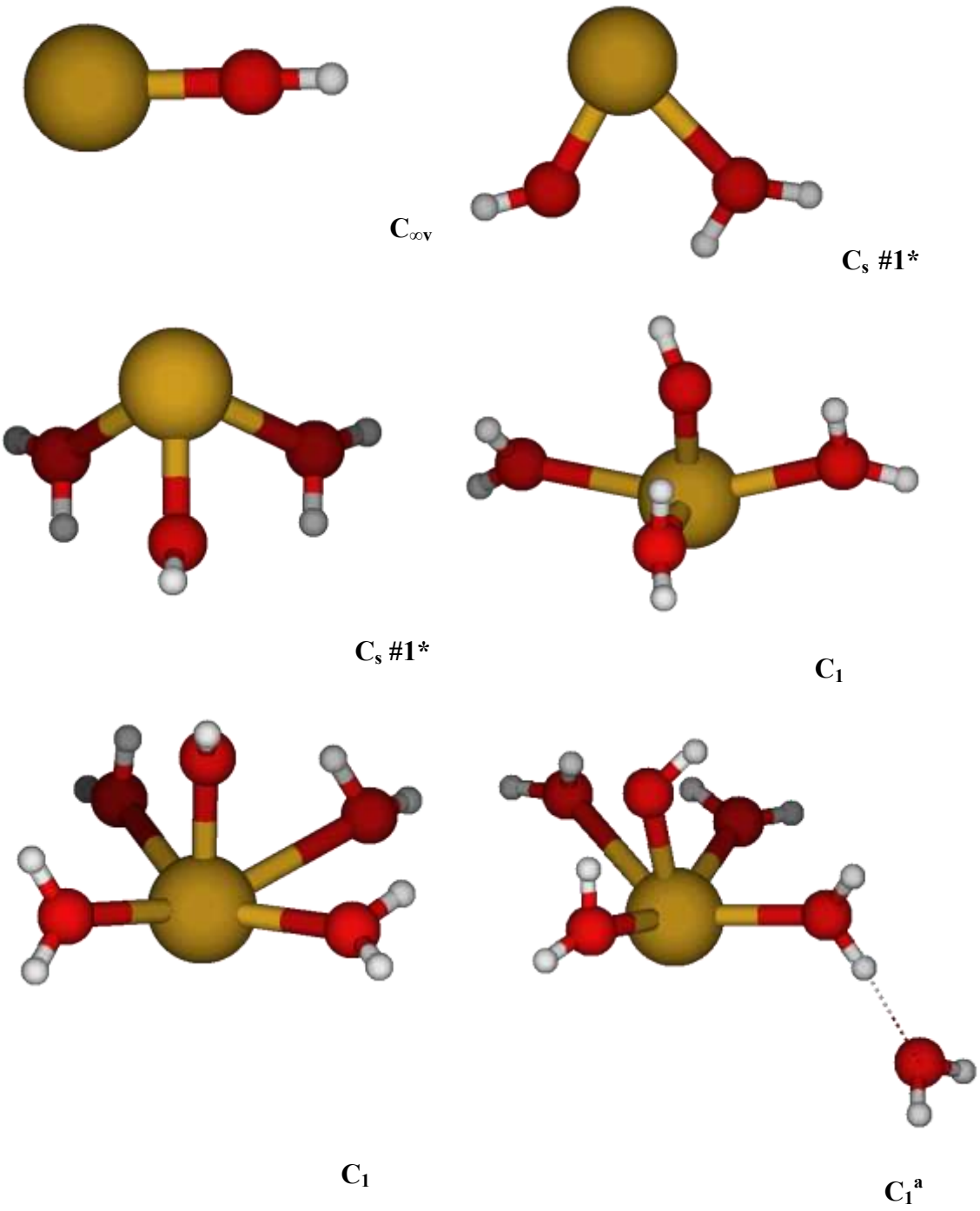

Figure 17: Optimized MP2 and B3LYP geometries for stable structures of $[Pb(OH)_m(H_2O)_n]^{2-m}$, where m=1 and n=0- (6-m). All symmetries marked with a "*" indicates B3LYP, "a" indicates MP2 otherwise all MP2 and B3LYP structures are very similar.

The anhydrous dihydroxo complex, $[Pb(OH)_2]^0$, was initially constrained under $D_{\infty h}$ symmetry. The resulting $D_{\infty h}$ structure had imaginary Π_u, which suggests desymmetrization had occurred to C_{2v} symmetry. The C_{2v} form of $[Pb(OH)_2]^0$ was stable and fully attached at all of the levels of theory investigated (HF, MP2 and B3LYP).

The monohydrate, $[Pb(OH)_2(H_2O)]^0$, was initially investigated under C_{2v} symmetry constraint (2 forms). Both forms were characterized by negative imaginary frequencies and dissociation of one water ligand, implying unstable structures. No further desymmetrization of $[Pb(OH)_2(H_2O)]^0$ was performed. Hence, no stable lowest energy minima structure was identified for the $[Pb(OH)_2(H_2O)]^0$ complex.

The dihydrate complex, $[Pb(OH)_2(H_2O)_2]^0$, was initially constrained to D_{2h}, symmetry (2 forms). The lower energy structure, D_{2h} #2, was desymmetrized along the imaginary stretching mode, B_{1g}, to C_{2h} symmetry and along the imaginary skeletal deformation mode, B_u, to C_{2v} symmetry (5 forms). The C_{2h} structure was stable, but not at the lowest energy minima, and was characterized by imaginary frequency modes. The C_{2v} #2 and C_{2v} #5 structures were unstable at all levels of theory with one water ligand detached. The C_{2v} #4 structure was found to be unstable at the B3LYP level of theory with one hydroxide (OH^-) ligand detached. The lowest energy minima structure for the dihydrate complex, $[Pb(OH)_2(H_2O)_2]^0$, was identified as the structure with C_{2v} #3 symmetry at all of the levels of theory investigated (HF, MP2 and B3LYP).

The trihydrate, $[Pb(OH)_2(H_2O)_3]^0$, was initially investigated under constraint of D_{3h} symmetry (2 forms). The lower energy trihydrate complex, D_{3h} #2, was desymmetrized to C_{3h} symmetry along the imaginary A_2' frequency mode. The C_{3h}

structure was fully attached, but contained imaginary frequency modes. The D_{3h} #2 form of $[Pb(OH)_2(H_2O)_3]^0$ was also desymmetrized to C_{2v} symmetry (3 forms) along skeletal deformation mode, A'. The C_{2v} #1 structure was unstable at the HF and MP2 levels of theory with one water ligand dissociated. The C_{2v} #1 structure was fully attached at the B3LYP level, but contained imaginary modes indicating that this was not the lowest energy minima structure. Furthermore, the C_{2v} #2 and C_{2v} #3 structures were unstable at the HF, MP2 and B3LYP levels of theory, thus resulting in dissociation of one or two water ligands, depending on the level of theory investigated. The D_{3h} form of $[Pb(OH)_2(H_2O)_3]^0$ was also desymmetrized along the imaginary skeletal deformation E" mode to C_s symmetry. The C_s symmetry structure was unstable at all levels of theory, resulting in dissociation of one water molecule. Hence, no lowest energy minima structure was identified for the $[Pb(OH)_2(H_2O)_3]^0$ complex.

The tetrahydrate complex, $[Pb(OH)_2(H_2O)_4]^0$, was initially constrained under D_{4h} symmetry (2 forms). Interestingly, the D_{4h} #1 form was found to be unstable at the B3LYP level resulting in the dissociation of 4 water ligands. Hence, the lower energy form, D_{4h} #2, was reverted along the water wagging mode, A_{2g}, to C_{4h}. The C_{4h} symmetry of $[Pb(OH)_2(H_2O)_4]^0$ was fully attached, but contained imaginary levels of theory. Hence, D_{4h} #2 was reverted along the skeletal deformation E_u mode to C_{2v} symmetry. The C_{2v} structure was unstable resulting in the dissociation of 2 water ligands. The C_{4h} structure was reverted to a C_s structure along the imaginary skeletal deformation E_u mode. However, no energetics were obtained for the C_s structure at the HF, MP2 and B3LYP levels of theory, since these levels of calculations were skipped due to dissociation.

Hence, no lowest energy minima structure was identified for the $[Pb(OH)_2(H_2O)_4]^0$ complex.

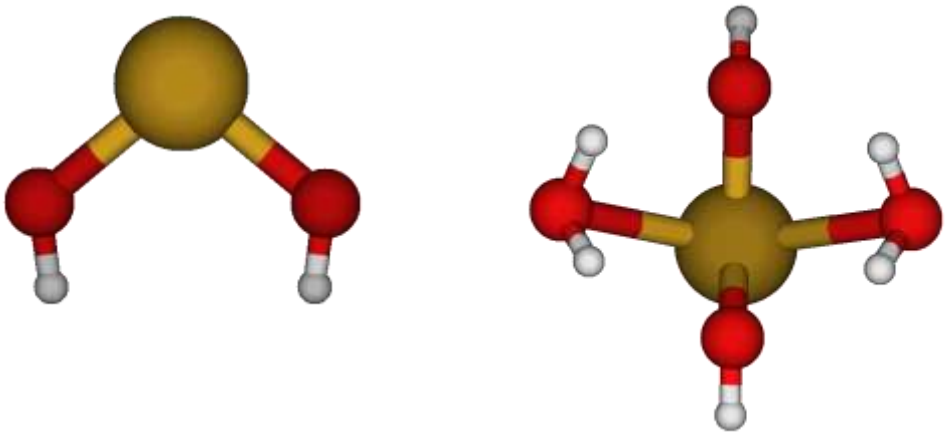

C_{2v} **C_{2v} #3**

Figure 18: Optimized MP2 and B3LYP geometries for stable structures of $[Pb(OH)_m(H2O)_n]^{2-m}$, where m=2 and n=0- (6-m). All MP2 and B3LYP optimized geometries are nearly identical.

Many stable (fully attached) geometries were found for the anhydrous trihydroxo lead (II) complexes, $[Pb(OH)_3]^-$, with the highest symmetry being D_{3h} and the lowest symmetry being C_3. The anhydrous $[Pb(OH)_3]^-$ complex was reverted from D_{3h} symmetry along the imaginary skeletal deformation, A_2", to C_{3v} and along the hydroxide wagging mode, A_2', to the C_3 structure. Both the C_{3h} and C_{3v} structures were stable, however, they both contained imaginary frequency modes, suggesting further desymmetrization was necessary. Hence, the C_{3v} structure was desymmetrized along the imaginary hydroxide twisting mode, A_2, to the C_3 structure, which proved to be the most stable (lowest energy minima structure) at all of the levels investigated (HF, MP2 and B3LYP).

The monohydrate, $[Pb(OH)_3(H_2O)]^-$ was initially investigated at the highest symmetry, C_{2v} (2 forms). Geometry optimization of the C_{2v} #1 structure was skipped due

to dissociation of a water ligand at the HF level of theory. However, the MP2 and B3LYP levels could be optimized for C_{2v} #1, but resulted in dissociation of one water ligand. The dissociated ligand was a hydrogen bond acceptor (oxygen from the dissociated water is hydrogen bonded to two adjacent attached hydrogens). On the other hand, $[Pb(OH)_3(H_2O)]^-$ constrained under C_{2v} #2 symmetry was found to be stable at all of the levels of theory investigated, but contained imaginary frequencies. Hence, $[Pb(OH)_3(H_2O)]^-$ was desymmetrized from C_{2v} #2 along the imaginary skeletal deformation modes, B_1 and B_2, to symmetries C_s #1 and C_s #2 respectively. The C_{2v} #2 structure was also desymmetrized along the imaginary water twisting mode, A_2, to C_2. All three, C_2, C_s #1 and C_s #2, symmetry structures of $[Pb(OH)_3(H_2O)]^-$, were unstable at all levels of theory, resulting in dissociation of the water ligand. In case of C_s #1 geometry optimization was simply skipped at the MP2 and B3LYP levels due to dissociation. Based on these research findings, no lowest energy minima structure was identified for the $[Pb(OH)_3(H_2O)]^-$ complex.

The dihydrate, $[Pb(OH)_3(H_2O)_2]^-$, proved to be unstable at the highest symmetry constraint, that is at C_{2v} (2 forms). Geometry optimization for the C_{2v} #1 form of $[Pb(OH)_3(H_2O)_2]^-$ was skipped at all levels of theory (HF, MP2 and B3LYP) due to the dissociation of ligands. The C_{2v} #2 structure resulted in dissociation of one hydroxide (OH^-) ligand at all levels of theory. Hence, no further desymmetrization of the C_{2v} symmetry was performed and no lowest energy minima for $[Pb(OH)_3(H_2O)_2]^-$ was identified.

The trihydrate, $[Pb(OH)_3(H_2O)_3]^-$, initially constrained under C_{3v} symmetry (4 forms). Two forms of the C_{3v} symmetry products were oriented in a prismatic

conformation and the other two in an anti-prismatic conformation. Geometry optimizations of the C_{3v} #1 and C_{3v} #3 structures (prismatic and anti-prismatic with dihedral hydrogen (from H_2O) angles of 0.0° and 180.0°) were both skipped at all of the calculation levels due to dissociation of ligands. On the other hand, the C_{3v} #2 and C_{3v} #4 structures (prismatic and anti-prismatic with dihedral hydrogen angles (from H_2O) being of 90.0° and -90.0°) were found to be unstable with 3 water ligands dissociated form the central Pb^{2+} cation. These dissociated water ligands were hydrogen bonded, in a donor fashion, where the hydrogens from the detached water ligands are bonded to the neighboring oxygen atoms of attached hydroxide ligands. The C_{3v} #2 structure was characterized by imaginary modes of frequency as expected. Surprisingly, the C_{3v} #4 form of $[Pb(OH)_3(H_2O)_3]^-$ even though unstable was characterized by real frequency modes at the HF, MP2 and B3LYP levels of theory. This observation was again attributed to secondary hydration stabilization. Secondary hydration stabilization is not of interest in this thesis. Subsequently, no further desymmetrization of $[Pb(OH)_3(H_2O)_3]^-$ was performed. No lowest energy minima structure stabilized by a primary hydration shell was found for the $[Pb(OH)_3(H_2O)_3]^-$ complex.

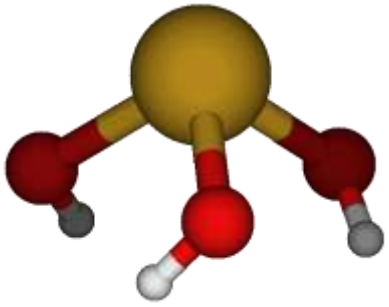

C_3

Figure 19: Optimized MP2 and B3LYP geometries for stable structures of $[Pb(OH)_m(H_2O)_n]^{2-m}$, where m=3 and n=0- (6-m). All of the MP2 and B3LYP optimized geometries are nearly identical.

The anhydrous tetrahydroxo lead (II) complex, $[Pb(OH)_4]^{2-}$, was initially investigated under the constraint of T_d symmetry. Subsequently, the T_d structure was desymmetrized along the imaginary skeletal deformation E mode to a D_{2d} structure. The D_{2d} structure was found to be stable but contained imaginary frequency modes implying that further desymmetrization was required. $[Pb(OH)_4]^{2-}$ was also reverted from T_d symmetry along the imaginary skeletal deformation mode, T_2, to C_{3v} and C_{2v} symmetries and along the imaginary water twisting mode, T_1, to C_3 symmetry. Geometry optimization was skipped for both the C_{3v} and C_3 structures at the HF, MP2 and B3LYP levels of theory due to dissociation of ligands. On the other hand, the C_{2v} structure was found to be stable but with imaginary frequencies at the HF and B3LYP levels, while one hydroxide (OH^-) ligand was observed to dissociate at the MP2 level of theory. Subsequently, the C_{2v} structure was desymmetrized along the imaginary skeletal deformation mode, B_1, to a C_s structure. The C_s structure was found to be unstable at all levels of theory, resulting in one hydroxide (OH^-) ligand becoming detached. Consequently, no stable lowest energy minima structure was found for the $[Pb(OH)_4]^{2-}$ complex.

The monohydrate, $[Pb(OH)_4(H_2O)]^{2-}$, was desymmetrized from its highest symmetry, C_{2v}, along the imaginary skeletal deformation B_1 mode to C_s symmetry and along the imaginary water twisting mode to the C_2 structure. The C_2 structure was not optimized at the HF level of theory, because a problematic level was skipped due to dissociation of ligands. However, the C_2 structure was optimized at the MP2 level, resulting in dissociation of two hydroxide ligands. The C_2 structure was only stable at the B3LYP level, but even here it contained imaginary frequencies suggesting further

desymmetrization would be necessary. Geometry optimization of the C_s structure was skipped due to ligand dissociations at all of the levels of theory studied. Hence, no further desymmetrization was possible; overall the results suggest that there is no stable lowest energy structure for the $[Pb(OH)_4(H_2O)]^{2-}$ complex.

The dihydrate, $[Pb(OH)_4(H_2O)_2]^{2-}$, was initially investigated at its highest possible symmetry, giving a D_{2h} structure. The D_{2h} structure was found to be unstable at the HF and MP2 levels of theory, resulting in the detachment of one hydroxide and one of the water ligands. However, the D_{2h} structure of $[Pb(OH)_4(H_2O)_2]^{2-}$ was found to be stable at the B3LYP level, but with imaginary frequencies. Subsequently, the D_{2h} structure was reverted, along the skeletal deformation modes, B_{1u} and B_{2u}, to the C_{2v} #1 and C_{2v} #2 structures, respectively. Both forms of the C_{2v} structures were identified as unstable. All levels of theory were skipped for both forms of C_{2v} structures owing to dissociation of some of the ligands. Again, this implies that there is no stable lowest energy minima structure for the $[Pb(OH)_4(H_2O)_2]^{2-}$ complex.

As mentioned earlier, no stable structures were found for the complexes with more than three hydroxide ligands. These complexes showed preference for the formation of ion pairs. Most of the levels of calculation had to be skipped due to dissociation of ligands, which made the calculations very difficult. Hence, these complexes will not be discussed further in the following section of this chapter.

Bond length and vibrational frequency data for the stable lowest energy hydroxylead (II) complexes has been tabulated in the supplementary material section. Based on these data, plots of Pb-O bond lengths and vibrational stretching frequencies are presented in Figures 20, 21 and 22 for the HF, MP2 and B3LYP levels of theory,

respectively. Simulated polarized Raman spectra (frequency data obtained at HF/6-311+G*/SDD) can be found in Figure 5A.1 of the supplementary material.

5.3 Discussion and Literature Comparison

The easiest way to confirm that the calculated geometries are reliable is to compare the obtained optimized geometries (stable symmetry, bond lengths, energies and vibrational frequencies) to literature results where they are available. The optimized geometries obtained for hydroxylead (II) complexes in this work are primarily confirmed by comparison to available data, taken mainly from the computational studies involving anhydrous hydroxylead (II) complexes by Gourlaouen et al.[81] and Breza et al.[94].

The highest coordination number for the anhydrous hydroxylead (II) complexes considered in this thesis was four, $[Pb(OH)_4]^{2-}$, as suggested by Perera et al.[93]. However, the obtained results indicate that the highest coordination number for a stable anhydrous hydroxylead (II) complex should actually be three, $[Pb(OH)_3]^-$, which is in agreement with the results obtained by Baes and Mesmer[95] and in disagreement with the research finding by Perera et al.[93.]

The lowest energy minima structure found for the anhydrous mono-hydroxylead (II) complex, $[Pb(OH)]^+$, reported in this thesis was $C_{\infty v}$ for all of the levels of theory investigated (HF, MP2 and B3LYP). The B3LYP optimized results are consistent with the computational study by Gourlaouen et al.,[81] who identified $[Pb(OH)]^+$ to be the most stable form ($C_{\infty v}$ symmetry at the B3LYP/SDD level). Specifically, Gourlaouen et al.[81] utilized Gaussian03[65] to perform *ab initio* calculations to optimize $[Pb(OH)]^+$ at the HF and B3LYP levels coupled to LANL2DZ and SDD relativistic pseudopotentials. The

authors emphasize that LANL2DZ basis sets gave unreliable results, while SDD based calculations are reliable when compared to four-component DB3LYP/AE calculations (refer to section 5.1 of this thesis). This non-precise reproduction of the data by B3LYP/LANL2DZ was attributed to the small expansion of the Gaussian basis set using this pseudopotential.[81] Gourlaouen et al.[81] identified the lowest energy minima of HF/SDD optimized $[Pb(OH)]^+$ to be the C_s structure, which is characterized by a bending of the Pb-O-H bond angle. This is in disagreement with our findings, which indicated that the $[Pb(OH)]^+$ structure preferred $C_{\infty v}$ symmetry at the HF level of theory. This discrepancy can be attributed to the slightly lower quality basis set (6-31+G**) used for the O and H atoms by Gourlaouen et al.,[81] compared to the 6-311+G* basis set used in this research. The values we have calculated for the Pb-O bond lengths are 1.943 Å, 1.966 Å and 1.963 Å for the HF, MP2 and B3LYP/6-311+G*/SDD levels, respectively. These Pb-O bond lengths can be found in Table 5A.10 within the supplementary materials section. Gourlaouen et al.[81] calculated Pb-O bond lengths of 1.949 Å and 1.957 Å at the HF and MP2/6-31+G**/SDD levels, respectively. These Pb-O bond lengths are nearly identical to our values, obtained at the HF and B3LYP/SDD levels of theory and coupled to a slightly larger 6-311+G* basis set for the O and H atoms. However, Breza et al.[94] reported elongated Pb-O bond lengths in $[Pb_4(\mu_3\text{-}OH)_4]^{4+}$ to be 2.413, 2.419 and 2.436 Å for the HF, MP2 and B3LYP levels of theory, respectively. The elongation of the Pb-O bonds in the $[Pb_4(\mu_3\text{-}OH)_4]^{4+}$ cation can be attributed to the multiple Pb atoms and OH ligands present (owing to higher electrostatic repulsion between atoms), as well as the fact that Breza et al.[94] utilized a small-core pseudopotential (LANL2DZ) to describe the Pb atom and a smaller cc-pVDZ basis set for the O and H atoms.

Unfortunately, no literature reports were found regarding the remaining hydroxylead (II) complexes which have been investigated in this study; no further literature comparison was thus possible.

It is very important to note that only the $[Pb(OH)]^+$ complex was found to be linear ($C_{\infty v}$ symmetry). Addition of water molecules, as well as increasing the number of hydroxide ligands (OH^-) resulted in bending of the Pb-O-H angles. From the optimized MP2 and B3LYP geometries for hydroxylead (II) complexes with coordination number between 2 and 6 (both anhydrous and hydrated complexes), it was evident that ligands arrange themselves in sterically hindered (uneven) conformations around the central Pb^{2+} cations. This uneven ligand coordination around a central atom gives a hemi-directed conformation. In other words, the hemi-directed arrangement of ligands is largely influenced by lone pair-ligand repulsion (stereo active Pb lone pair ($6s^2$)), which prevails over ligand-ligand electrostatic repulsion. For the optimized MP2 and B3LYP geometries of the hydroxylead (II) complexes referred to in this thesis please see section 5.2 (Figures17, 18 and 19).

Plots were constructed of the Pb-O bond lengths and vibrational stretching frequencies and can be found in Figures 20-22. Each plot suggests that there is an inverse relationship between the bond lengths and the corresponding vibrational frequencies. Specifically, as the number of water molecules, as well as number of hydroxide ions is increased, there is an observed elongation of the bond lengths corresponding to the increased coordination number. This, in turn, reduces the stabilization of species with higher coordination numbers. The elongation of the Pb-O bond lengths corresponds to a

decrease of the vibrational frequencies, due to formation of weaker Pb-O bonds, which require less energy to vibrate.

The Pb-OH bonds within hydroxylead (II) complexes, $[Pb(OH)_m(H_2O)_n]^{2-m}$ with m = 1-4 and n = 0- (6-m), investigated in this thesis are significantly shorter than the bond lengths in Pb-OH_2 complex, due to the stronger attraction between Pb and OH in the former. This was further characterized by a Pb-OH vibrational stretching frequency notably larger than those for Pb-OH_2, by 200-400 cm^{-1} (please refer to the Pb-O bond length and vibrational frequency tables in the Chapter 5 appendix of the supplementary materials).

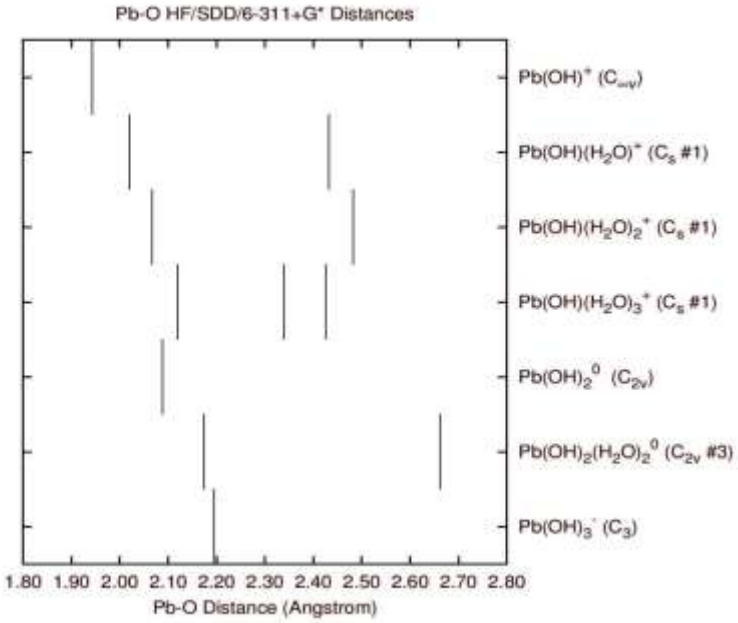

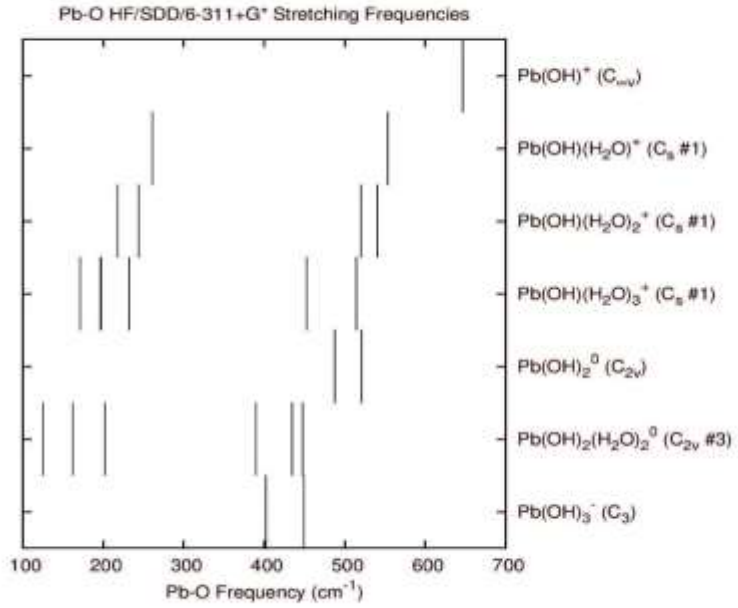

Figure 20: Pb-O bond lengths and vibrational stretching frequencies for $[Pb(OH)_m(H_2O)_n]^{2-m}$, where m = 1-3 and n = (0-(6-m)), calculated at the HF/SDD/6-31+G* level.

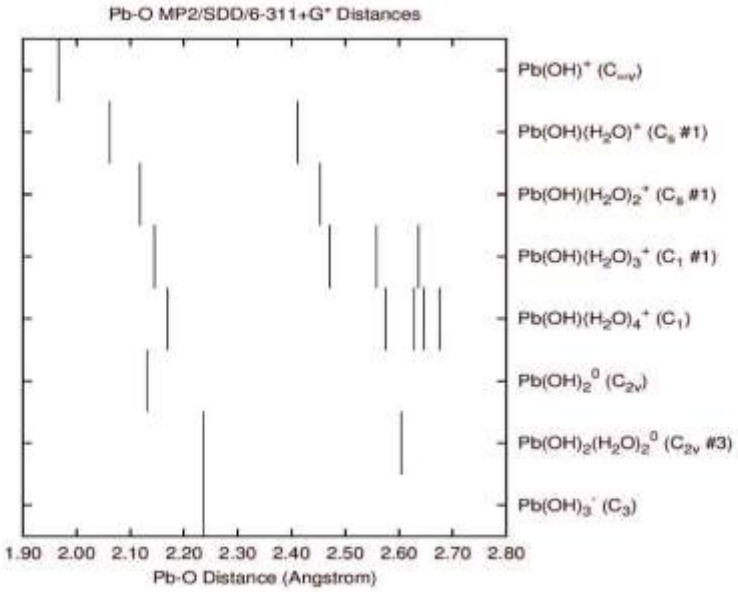

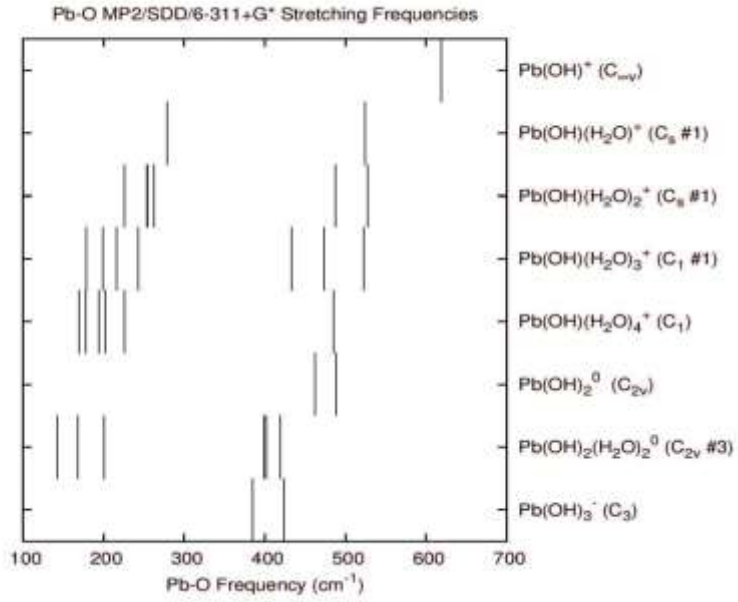

Figure 21: Pb-O bond lengths and vibrational stretching frequencies for $[Pb(OH)_m(H_2O)_n]^{2-m}$, where m = 1-3 and n = (0-(6-m)), calculated at the MP2/SDD/6-31+G* level.

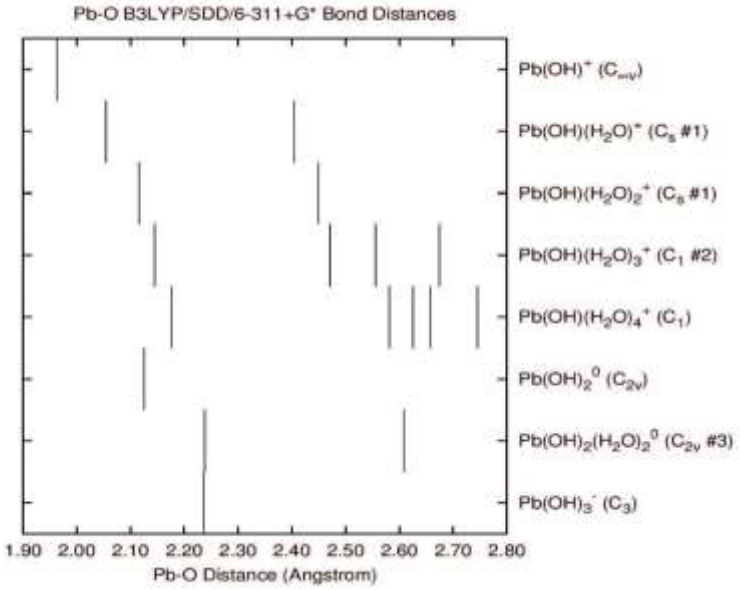

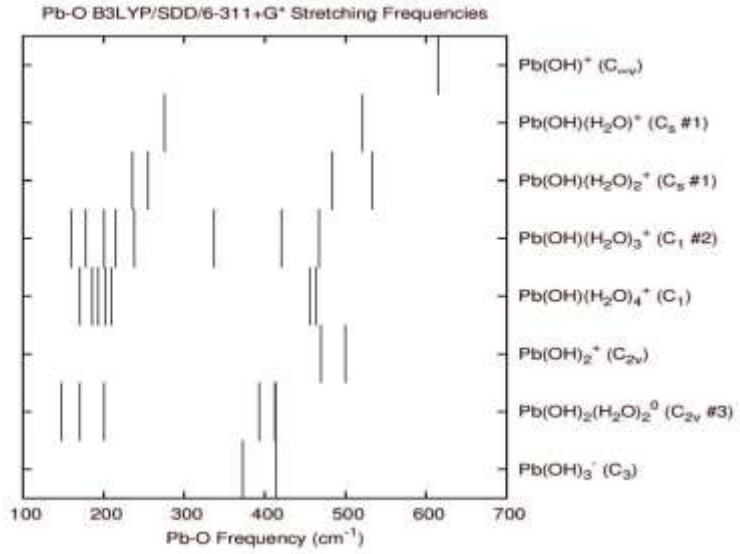

Figure 22: Pb-O bond lengths and vibrational stretching frequencies for $[Pb(OH)_m(H_2O)_n]^{2-m}$, where m=1-3 and n=0-(6-m), calculated at the B3LYP/SDD/6-311+G* level.

Gourlaouen et al.[81] computationally investigated the nature of the stationary points encountered during the geometry optimization of $[Pb(OH)]^+$ by means of vibrational frequency analysis within the harmonic approximation. They reported the vibrational frequencies of $[Pb(OH)]^+$ to be 87 cm^{-1} (Pb-O stretching mode) and 623 cm^{-1} (Pb-O bending mode) at the B3LYP/SDD/6-31+G** level. The vibrational frequencies for $[Pb(OH)]^+$ reported in this thesis are 646.9 cm^{-1}, 618.9 cm^{-1} and 614.0 cm^{-1} (Pb-O stretching mode) at the HF, MP2 and B3LYP/SDD/6-311+G* levels, respectively. The vibrational frequencies obtained in this research can be found in Tables 5A.11-5A.13 in the supplementary materials section. Values for the Pb-O stretching mode frequencies obtained at the MP2 and B3LYP levels in this thesis are very similar to the Pb-O bending mode frequency at the B3LYP/SDD level reported by Gourlaouen et al.[81]. The HF frequency value obtained in this thesis is not comparable to a frequency value obtained at the B3LYP level of theory by Gourlaouen et al.[81]. This can be attributed to the fact that the HF level of theory, unlike the B3LYP level, lacks electron correlation effects, as well as the fact that Gourlaouen et al.[81] utilized a smaller, 6-31+G**, basis set for the O and H atoms, compared to the basis set used for the O and H atoms in this thesis (6-311+G*). There are no other literature reports on vibrational frequency modes comparable to those of the remaining hydroxolead (II) complexes which have been investigated in this study; no further vibrational frequency comparison is possible.

Simulated polarized Raman spectra have been constructed based on intensities calculated at the HF level of theory and can be found in Figure 5A-1 of the supplementary materials section. These computationally obtained Raman active bands will be a valuable tool for interpreting experimental Raman spectra on hydroxolead (II) species, a means of

confirming or negating any ambiguous experimental data. Experimental Raman spectroscopy on these complexes is to be performed in the near future by Dr. Peter Tremaine at Guelph University, Ontario. Currently, there are no literature reports regarding polarized Raman spectra of these hydroxylead (II) complexes.

Chapter 6: Amminelead (II) Complexes

Ammonia may be added to the supercritical water-cooled reactor (SCWR) for pH adjustment. Amminelead (II) complexes, $[Pb(NH_3)_m(H_2O)_n]^{2+}$, are one type of metal-ligand species, expected to form as corrosion products under the harsh operating conditions within the supercritical water-cooled reactor (SCWR). Development of an appropriate water control strategy for the SCWR (and the subsequent elimination of corrosion) relies on a thorough understanding of the formation of such metal-ligand complexes. Amminelead (II) complex formation requires comprehensive insight of ammine-lead chemistry on a molecular level. No experimental or computational literature reports of amminelead (II) complexes have been documented up until now. Hence, no comparison to the literature is possible at this moment. As a result, the discussion section of this chapter is limited to our findings regarding molecular geometries, bond lengths and vibrational stretching frequency trends.

This thesis is the very first extensive study of amminelead (II) complexes carried out on the molecular level. It offers the very first comprehensive catalogue of computationally predicted molecular geometries for amminelead (II) complexes and their corresponding simulated vibrational spectra. This chapter includes computational results and a discussion of the amminelead (II) Complexes, $[Pb(NH_3)_m(H_2O)_n]^{2+}$, up to and including six-coordinate species, where m = 1 - 6, n = 0- (6-m).

The lead (II) ammine complexes studied included up to hexa-coordinate species with and without water molecules. Based on this research, aqualead(II) complexes were unstable when seven water ligands were added. Ammine (NH_3) ligand is neutral ligand

just like water (H_2O), hence the coordination number of the ammine ligands was limited to six. Water molecules were added to the lead (II) complexes with the aim of probing the how hydration affects stabilities of the given complexes.

6.1 Results

The total energies of the successfully optimized amminelead (II) complexes have been tabulated and can be found in Tables 6A.1-6A.9 in the Supplementary Materials section. These energy tables contain calculations from all 27 levels of theory studied, as described in Section 2.2 of this thesis. However, the molecular geometry analysis and the discussion are limited to the results from the HF, MP2 and B3LYP levels of calculation, utilizing 6-311+G* and SDD basis sets for the small atoms (H, O and N) and the large atom (Pb), respectively. Specifically, 6-311+G*/SDD basis set calculations were expected to give the most reliable results based on previous research regarding basis set performance (refer to a chapter 2 of this thesis).

The optimized geometries of the stable structures can be found in Figures 23-26 for the mono-, di-, tri- and tetraammine complexes, respectively. Pb-N and Pb-O bond lengths for the stable geometries of the amminelead(II) complexes have been tabulated in Table 6A.10 of the Supplementary Materials section. Furthermore, the Pb-N and Pb-O vibrational stretching frequencies of the lowest energy minima amminelead (II) complexes have been tabulated in Tables 6A.11, 6A.12 and 6A.13 for the HF, MP2 and B3LYP/6-311+G*/SDD levels of calculations, respectively.

The anhydrous monoammine, $[Pb(NH_3)]^{2+}$, was stable in the highest possible symmetry, C_{3v}, at all of the levels of theory investigated (HF, MP2 and B3LYP).

The monohydrate monoammine, $[Pb(NH_3)(H_2O)]^{2+}$, was initially optimized to a C_s symmetry structure (two forms). The lower energy C_s structure was desymmetrized along the A" imaginary frequency mode to the lowest energy minima structure, C_1, for all of the levels of theory investigated (HF, MP2 and B3LYP).

The dihydrate monoammine complex, $[Pb(NH_3)(H_2O)_2]^{2+}$, was initially constrained to have C_s symmetry, but it was subsequently desymmetrized along the imaginary A" frequency mode to a C_1 structure. The C_1 structure was found to be the most stable conformation of $[Pb(NH_3)(H_2O)_2]^{2+}$ for all of the levels of theory investigated (HF, MP2 and B3LYP).

The trihydrate monoammine, $[Pb(NH_3)(H_2O)_3]^{2+}$ was initially optimized under C_{3v} symmetry constraints (four forms). The lowest energy C_{3v} structure was desymmetrized along the A_2 imaginary mode, water and ammine twisting mode, to a C_3 structure and along the E imaginary mode, skeletal deformation mode, to a C_s structure. The C_3 symmetry conformation of $[Pb(NH_3)(H_2O)_3]^{2+}$ was found to be at the lowest energy minima at B3LYP level of theory. However, the C_s structure was further desymmetrized along imaginary A" frequency mode to a C_1 structure. Ultimately, the C_1 structure of was found to be the most stable (the lowest energy minima) at all of the levels of theory investigated (HF, MP2 and B3LYP).

The tetrahydrate monoammine complex, $[Pb(NH_3)(H_2O)_4]^{2+}$ was initially optimized under the highest possible C_s symmetry constraints (two forms). The lower energy structure was desymmetrized along the A" frequency mode, a structural deformation mode, to a C_1 structure. The C_1 structural arrangement of $[Pb(NH_3)(H_2O)_4]^{2+}$

was found to be at the lowest energy minima (the most stable structure) for all of the levels of calculations carried out (HF, MP2 and B3LYP).

The pentahydrate monoammine complex, $[Pb(NH_3)(H_2O)_5]^{2+}$, was primarily investigated under the constraint of C_s symmetry (two forms). The C_s structure was subsequently desymmetrized along an imaginary skeletal deformation mode, A", to a C_1 structure. The C_1 structure had real frequency modes, suggesting that the structure was at the lowest energy minimum. However, the C_1 structure also resulted in a dissociation of one or two H_2O ligands (depending on the level of theory investigated). Further, these were hydrogen bonded to a neighboring attached water molecule. Hence, the C_1 conformation of $[Pb(NH_3)(H_2O)_4]^{2+}$ was stabilized through the secondary hydration shell. Secondary hydration shell stabilization is not of interest in this thesis and shall not be discussed any further. The highest overall coordination number for a stable hydrated monoammine lead (II) structure was determined to be five, with $[Pb(NH_3)(H_2O)_4]^{2+}$ being the obtained structure.

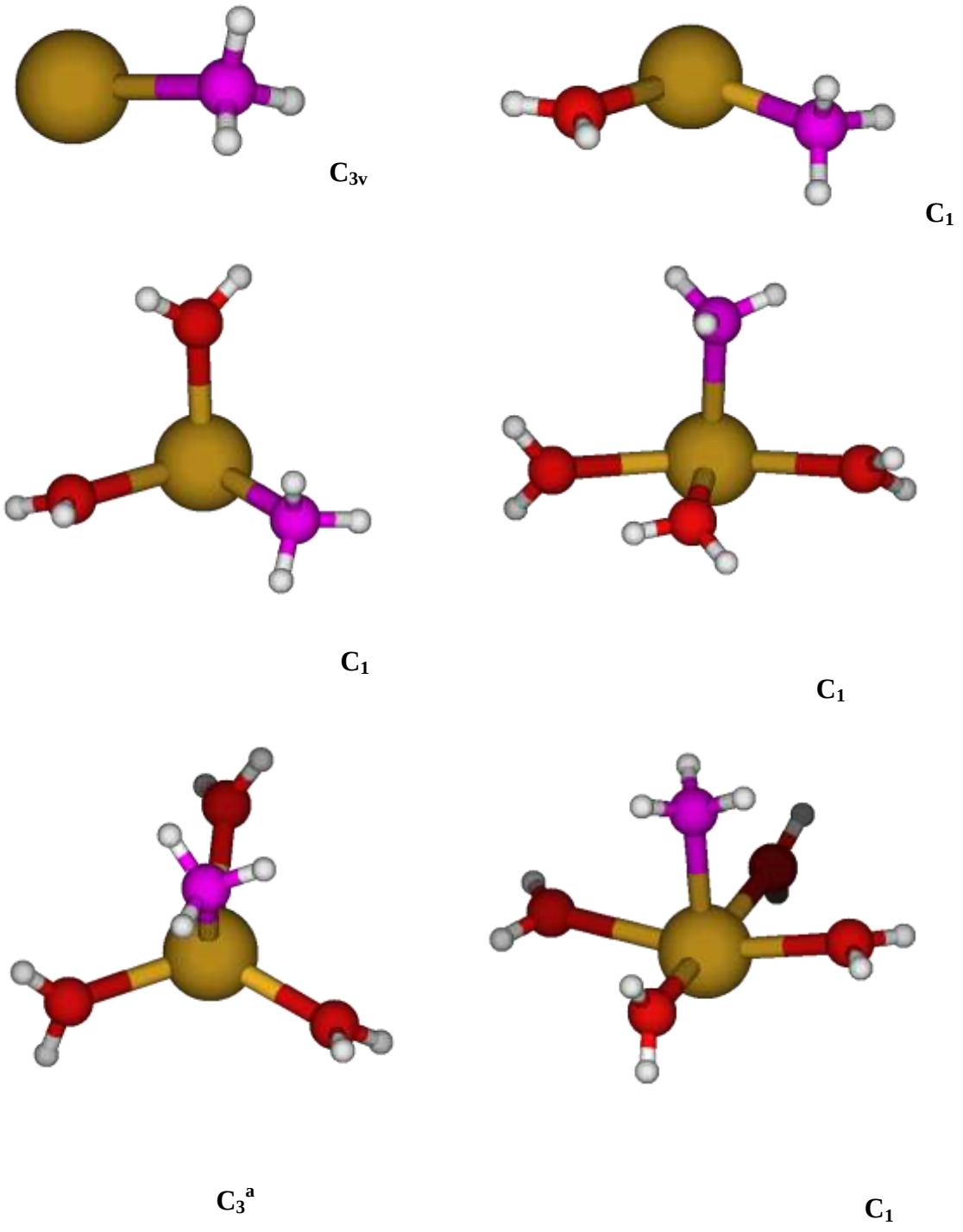

Figure 23: Optimized MP2 and B3LYP geometries for stable structures of $[Pb(NH_3)_m(H_2O)_n]^{2+}$ complexes, where m =1, n =0 - (6-m). "a" indicates one only stable at the B3LYP level.

The anhydrous diammine, $[Pb(NH_3)_2]^{2+}$, was initially investigated constrained under D_{3h} and D_{3d} symmetries, but these contained various imaginary frequency modes suggesting that desymmetrization to lower symmetry structures was required. Subsequently, the following lower symmetry structures were attempted, D_3, C_{2v} and C_2. $[Pb(NH_3)_2]^{2+}$ ultimately preferred C_2 symmetry at the HF and MP2 levels of theory (the lowest energy minima structures). On the other hand, the C_2 structure was not preferred at the B3LYP level of theory and was characterized by an imaginary frequency (B) suggesting that a lower symmetry structure was required. Hence, the C_1 conformation of $[Pb(NH_3)_2]^{2+}$ was found to be the most stable at the B3LYP level of theory. In conclusion, $[Pb(NH_3)_2]^{2+}$ under the constraint of C_2 symmetry was the most stable form at the HF and MP2 levels of theory, while the C_1 structure prevailed at the B3LYP level.

Four different structures of C_{2v} symmetry were studied for the monohydrate complex, $[Pb(NH_3)_2(H_2O)]^{2+}$. All of the C_{2v} structures were characterized by imaginary frequencies suggesting desymmetrization should be applied. The lower symmetry structures, C_s #1, C_s #2 and C_2 were attempted based on the imaginary frequency modes (B_1, B_2 and A_2 respectively). The presence of new imaginary frequency modes indicated that further desymmetrization was required. In conclusion, $[Pb(NH_3)_2(H_2O)]^{2+}$ ultimately preferred the C_1 symmetry structure at all of the levels of theory investigated (HF, MP2 and B3LYP).

The dihydrate, $[Pb(NH_3)_2(H_2O)_2]^{2+}$, was initially investigated under the constraint of C_{2v} symmetry (four forms). The presence of imaginary frequency modes suggested desymmetrization to lower symmetries with the aim of finding the lowest energy minima structure. Two forms of C_s symmetry were investigated, based on B_1 and B_2 imaginary

modes, respectively. The C_1 conformation of $[Pb(NH_3)_2(H_2O)_2]^{2+}$ was the most stable (at the lowest energy minima) for all of the levels of theory investigated (HF, MP2 and B3LYP).

Four different D_{3h} symmetry structures were initially attempted for the trihydrate, $[Pb(NH_3)_2(H_2O)_3]^{2+}$. The D_{3h} symmetry structures were characterized by various imaginary frequency modes, thus hinting that the lowest energy minima structure would be found at lower symmetry. Subsequently, the following lower symmetry structures were attempted: D_3, C_{3v}, C_3, C_{2v} and C_2. All of these resulting structures were found to be fully attached, but contained imaginary frequency modes suggesting that further desymmetrization should be carried out. The C_s structure was desymmetrized from the C_{2v} structure along the B_1 frequency mode. The final C_s structure had one water molecule fully dissociated at all of the levels of theory investigated. Even though, the C_s symmetry of $[Pb(NH_3)_2(H_2O)_3]^{2+}$ was characterized by imaginary frequency modes, no further desymmetrization was performed. In conclusion, no lowest energy minima structure was obtained for $[Pb(NH_3)_2(H_2O)_3]^{2+}$.

For the tetrahydrate complex, $[Pb(NH_3)_2(H_2O)_4]^{2+}$, high symmetry structures, trans C_{2h} (two forms) and C_{2v} (four forms) were initially studied. All of the resulting structures contained imaginary frequency modes suggesting that desymmetrization (lowering of the symmetry) would be required. The energetically preferred C_{2v} structure was desymmetrized along the imaginary A_2 frequency mode, a water and ammine twisting mode, to a structure of C_2 symmetry. $[Pb(NH_3)_2(H_2O)_4]^{2+}$ was found to be at the lowest energy minima (the most stable) when constrained under C_2 symmetry at the HF and MP2/6-311+G*/SDD levels. $[Pb(NH_3)_2(H_2O)_4]^{2+}$ was also found to be stable at the

B3LYP/6-311+G*/SDD level, and it was characterized by real frequency modes. However, the resulting structure at the B3LYP level of theory was detached and the overall stabilization of the structure was attributed to a secondary shell stabilization of the detached ligands. Specifically, dissociation of two water ligands was observed, these were hydrogen bonded in an acceptor fashion (oxygen from the detached water molecules accepted hydrogen bonds from the hydrogen atoms of the neighboring attached ammine (NH_3) ligand). Secondary shell stabilization is not of interest of this thesis and will not be discussed any further.

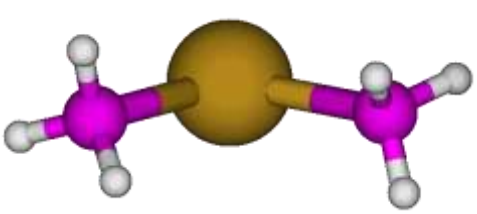

C_2*

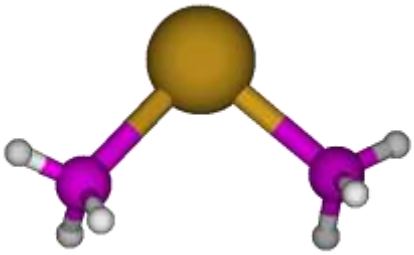

C_1[a]

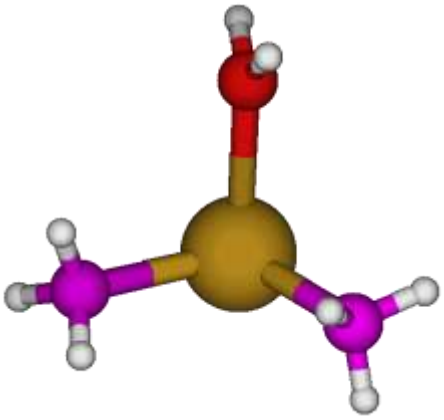

C_1

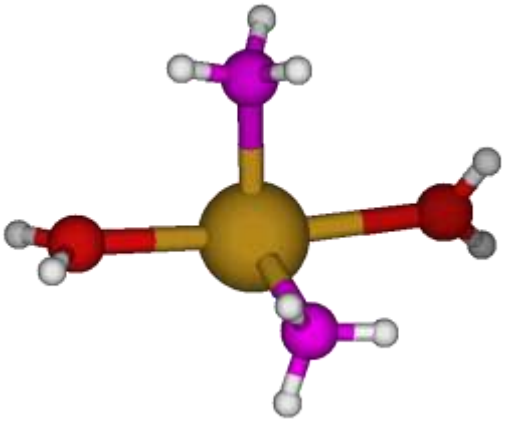

C_1

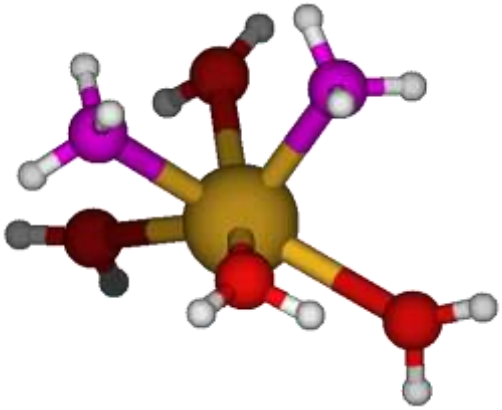

C_2*

Figure 24: Optimized MP2 and B3LYP geometries for the stable complexes of $[Pb(NH_3)_m(H_2O)_n]^{2+}$, where m = 2, n = 0 - (6-m). "*" indicates a structure only stable at the MP2 level of theory, "[a]" indicates one only stable at the B3LYP level.

The anhydrous triammine species, $[Pb(NH_3)_3]^{2+}$, was initially assigned at C_{3v} symmetry (two forms). The lower energy structure was desymmetrized along the imaginary A_2 frequency mode, a water and ammine twisting mode, to a C_3 symmetry structure. Ultimately, $[Pb(NH_3)_3]^{2+}$, was found to be the most stable when optimized with C_3 symmetry (the lowest energy minima structure) for all of the levels of theory investigated (HF, MP2 and B3LYP).

Four different structures of C_s symmetry were probed for the monohydrate, $[Pb(NH_3)_3(H_2O)]^{2+}$, but it showed imaginary frequencies at all of the levels of theory used. The lowest energy, C_s structure was desymmetrized along the imaginary A" frequency mode to a structure of C_1 symmetry. The monohydrate, $[Pb(NH_3)_3(H_2O)]^{2+}$, preferred the C_1 structure (residing at the lowest energy minima of the potential energy surface) for all of the levels of theory investigated (HF, MP2 and B3LYP).

The dihydrate, $[Pb(NH_3)_3(H_2O)_2]^{2+}$, was initially optimized under the constraint of C_s symmetry (4 forms). The C_s #4 structure was found to be at the lowest energy minima

at the HF level of theory. On the other hand, the $[Pb(NH_3)_3(H_2O)_2]^{2+}$ results contained imaginary frequencies at both the MP2 and B3LYP level of theory and were subsequently desymmetrized along the imaginary A", skeletal deformation, frequency mode, to a C_1 structure. The C_1 structure was found to be at the lowest energy minima at both the MP2 and B3LYP levels of theory. However, the C_1 structure optimized at the MP2 level was stabilized through the formation of a secondary hydration shell. Specifically, the C_1 structure of $[Pb(NH_3)_3(H_2O)_2]^{2+}$ contained one water ligand which had dissociated and subsequently hydrogen bonded in a acceptor fashion (the oxygen from the detached water ligand is hydrogen bonded to a hydrogen of a water ligand attached to the central Pb (II) atom). The secondary hydration shell stabilization is not of interest and hence will not be discussed any further. Nevertheless, the $[Pb(NH_3)_3(H_2O)_2]^{2+}$ was found to be fully attached and at the lowest energy minimum when optimized under a C_1 symmetry constraint at the B3LYP level of theory. In conclusion, $[Pb(NH_3)_3(H_2O)_2]^{2+}$ was found to be the most stable with C_s and C_1 symmetry conformations at the HF and B3LYP level of theory respectively, while the MP2 optimization resulted in the formation of a structure containing a secondary hydration shell for stabilization.

Four different forms of the highest possible symmetry, C_{3v} (two prism and two antiprism conformations), were probed for the trihydrate complex, $[Pb(NH_3)_3(H_2O)_3]^{2+}$. All of the C_{3v} symmetry structures were characterized by imaginary frequency modes requiring desymmetrization to a lower symmetry. Subsequently, the lowest energy C_{3v} antiprism structure was desymmetrized along the imaginary A_2 frequency mode to a C_3 structure. The C_3 structure contained all real frequency modes for all of the levels of theory investigated (HF, MP2 and B3LYP). This in turn implies that

$[Pb(NH_3)_3(H_2O)_3]^{2+}$.has the lowest in energy minima (i.e. is the most stable) when constrained under C_3 symmetry. The HF and MP2 optimized C_3 structures were fully attached, stable structures. However, the C_3 structure at the B3LYP level of theory was detached, after dissociation of 3 water ligands from the central Pb(II) atom. The stabilization of the C_3 structure at the B3LYP level of theory was attributed to the formation of a secondary hydration shell, hence, it will not be further discussed. In conclusion, $[Pb(NH_3)_3(H_2O)_3]^{2+}$ was determined to be the most stable as a structure with C_3 symmetry at the HF and MP2 levels of theory, while B3LYP optimization resulted in a structure with secondary hydration shell stabilization.

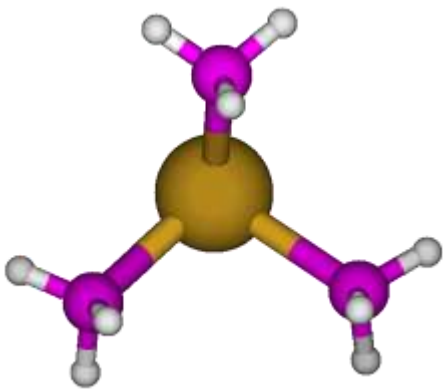

C_3

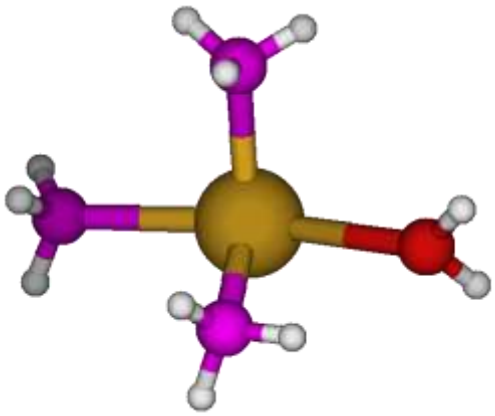

C_1

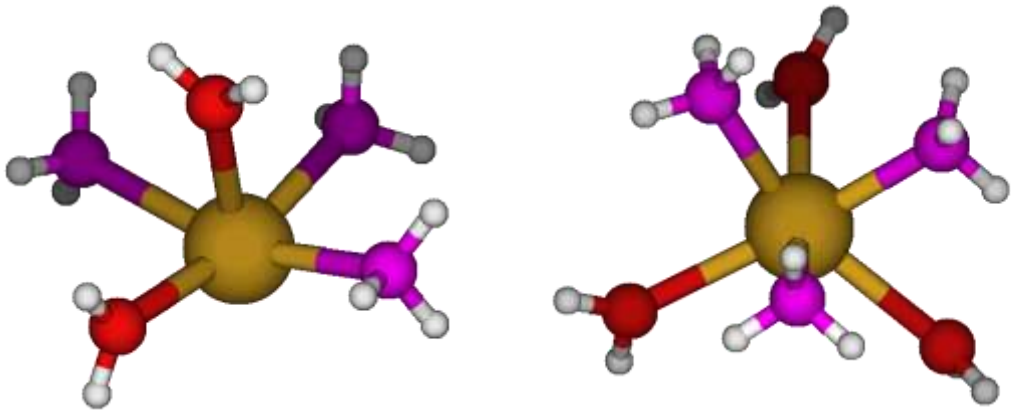

C_1[a] **C_3***

Figure 25: Optimized MP2 and B3LYP geometries for stable complexes of $[Pb(NH_3)_m(H_2O)_n]^{2+}$, where m = 3, n = 0 - (6-m). "*" indicates a structure stable at only the MP2 level of theory, "a" indicates one only stable at the B3LYP level.

The anhydrous tetraammine, $[Pb(NH_3)_4]^{2+}$, was initially investigated with the highest possible T_d symmetry (two forms). The T_d structures are characterized as having imaginary frequencies modes, thus suggesting desymmetrization to lower symmetry structures would be required. Subsequently, the $[Pb(NH_3)_4]^{2+}$ structures were investigated under lower symmetry constraints such including C_3 and C_s symmetry. Both the C_3 and the C_s symmetry structures were characterized by imaginary frequency modes. Hence, the lower symmetry structure, C_s, was desymmetrized along the skeletal deformation, A" frequency modes, to a C_1 structure. In conclusion, $[Pb(NH_3)_4]^{2+}$ was the most stable under the constraint of C_1 symmetry at all of the levels of theory studied (HF, MP2 and B3LYP).

The monohydrate complex, $[Pb(NH_3)_4(H_2O)]^{2+}$, was initially constrained to the highest possible C_{2v} symmetry structure (four forms). The C_{2v} #4 structure was found to be at the lowest energy minima (the most stable structure) at both the HF and B3LYP

levels of theory. However, the MP2 level of theory required desymmetrization of the C_{2v} #4 structure. Subsequently, the C_{2v} #4 structure was desymmetrized along the imaginary frequencies modes, A_2 and B_1, to structures of C_2 and C_s symmetry, respectively, at the MP2 level of theory. In conclusion, $[Pb(NH_3)_4(H_2O)]^{2+}$ was the most stable with C_{2v} symmetry at the HF and B3LYP levels of theory, while MP2 calculations preferred a structure with C_2 symmetry.

For the dihydrate, $[Pb(NH_3)_4(H_2O)_2]^{2+}$, optimization with C_{2h} symmetry was attempted first (two forms). The lowest energy C_{2h} structure was further desymmetrized along the imaginary frequency modes, A_u and B_u, to C_2 and C_s structures respectively. The C_2 structure was found to be at the lowest energy minima (the most stable) for $[Pb(NH_3)_4\ (H_2O)_2]^{2+}$ when optimized at the B3LYP level of theory. However, the C_2 structure contained imaginary frequency mode at the HF and MP2 levels and was subsequently desymmetrized to a C_s structures. Furthermore, the C_s structure was desymmetrized along the imaginary skeletal deformation mode, A", to a C_1 structure. In conclusion, $[Pb(NH_3)_4\ (H_2O)_2]^{2+}$ was found to be at the lowest energy minimum (the most stable) when optimized under C_1 symmetry at the HF and MP2 levels of theory and C_2 symmetry at the B3LYP level of theory.

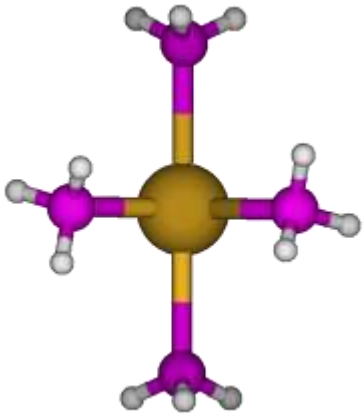

C_1

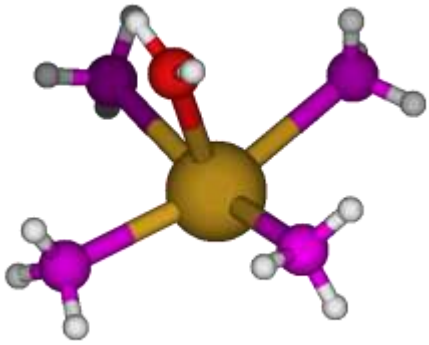

C_{2v}#4 [a]

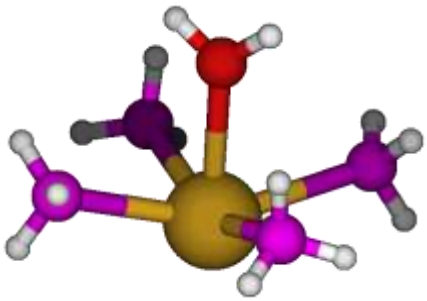

C_2*

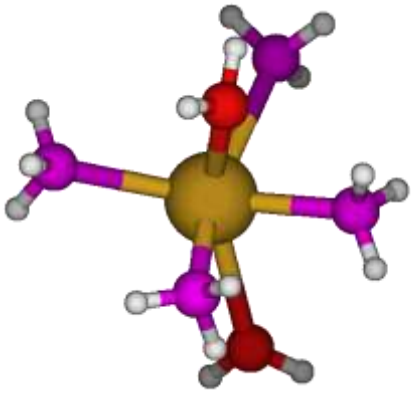

C_1*

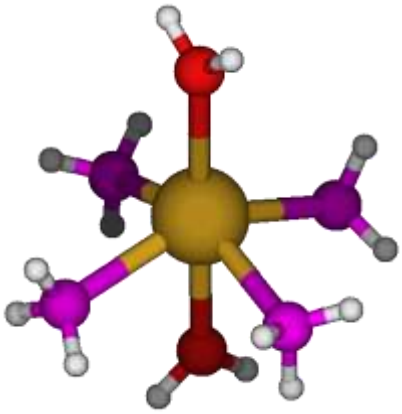

C_2 [a]

Figure 26: Optimized MP2 and B3LYP geometries for the stable complexes, $[Pb(NH_3)_m(H_2O)_n]^{2+}$, where m = 4, n = 0 - (6-m). "*" indicates structures only stable at the MP2 level of theory, "[a]" indicates ones only stable at the B3LYP level.

The anhydrous pentammine complex, was $[Pb(NH_3)_5]^{2+}$, was investigated sequentially starting with the highest possible symmetry structure towards the lowest symmetry structure in following sequence: C_{3h} (two forms), C_{3v} (two forms), C_3, C_s and C_1. Desymmetrization was performed along the imaginary frequency modes obtained within the output. The lowest energy minimum structure for $[Pb(NH_3)_5]^{2+}$ was characterized with C_1 symmetry at all of the levels of theory investigated (HF, MP2 and B3LYP).

For the monohydrate penatmmine complex, $[Pb(NH_3)_5(H_2O)]^{2+}$, optimization with C_s symmetry was attempted first (four forms). The lowest energy C_s structure was further desymmetrized along the imaginary skeletal deformation mode, A", to a C_1 structure. $[Pb(NH_3)_5(H_2O)]^{2+}$ optimized under C_1 symmetry constraint was characterized by real frequencies indicating the lowest energy minimum for all of the levels of theory investigated. However, the stabilization of C_1 symmetry structure appeared to be a result of secondary hydration, where hydrogen bonding occurred in acceptor fashion (oxygen from detached water molecule accepted hydrogen bonds from two adjacent attached hydrogens). Once again, secondary hydration is not of interest for this research.

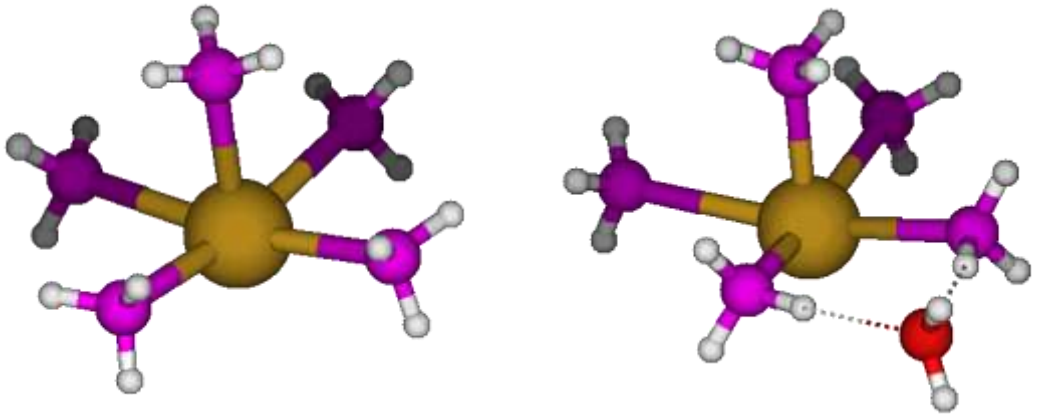

C_1 **C_1**

Figure 27: Optimized MP2 and B3LYP geometries for the stable complexes, $[Pb(NH_3)_m(H_2O)_n]^{2+}$, where m = 5, n = 0 - (6-m).

The anhydrous hexamine, $[Pb(NH_3)_6]^{2+}$, was initially constrained to the highest possible C_s symmetry structure (three forms). The lowest energy C_s structure was desymmetrized along skeletal deformation form, A", to a C_1 structure. The C_1 structure was fully attached and characterized with all real (positive) frequency modes indicating the lowest energy structure.

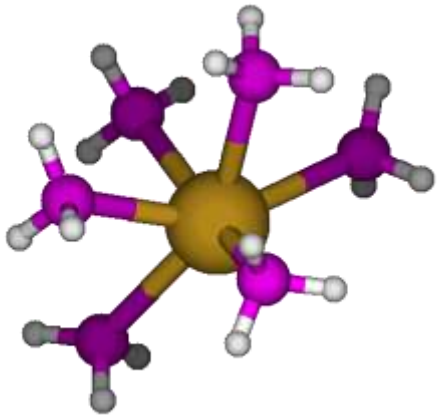

C_1

Figure 28: Optimized MP2 and B3LYP geometries for the stable complexes, $[Pb(NH_3)_m(H_2O)_n]^{2+}$, where m = 6, n = 0 - (6-m).

6.2. Discussion

The primary step when testing the reliability of research data is to compare the obtained results to available experimental and/or computational literature results. As mentioned, no such literature data (experimental nor computational) is available for amminelead (II) complexes. Hence, the discussion here is limited to a comparison of molecular geometries as well as bond lengths and stretching vibrational frequency trends for the amminelead (II) complexes we calculated. Again, this thesis offers the very first catalogue of systematically predicted amminelead (II) complexes, as well as their corresponding optimized molecular geometries (bond lengths and stretching vibrational frequencies).

A careful investigation of the lowest energy minima structures of the amminelead (II) complexes presented in Figures 23-28, shows that the orientation of the ligands around the central atom is largely affected and governed by the stereo active repulsion of the Pb (II) lone pair ($6s^2$). The Pb lone pair–ligand repulsion predominates over the ligand-ligand electrostatic repulsion resulting in an uneven distribution (hemi-directed conformation) of the attached ligands around the central atom (Pb (II)). Both types of ligand, ammonia (NH_3) and water (H_2O) are neutral, thus dissociation of the ligands is not as prevalent as it would otherwise be if one of the ligands was charged. It is also evident that hydration of ammine lead (II) complexes decreases the coordination number of the stable complexes formed. For example, the monoammine lead (II) complex was found to have a maximum coordination number of five, with the resulting structure $[Pb(NH_3)(H_2O)_4]^{2+}$, and not six as expected for all of the levels of theory investigated.

One more interesting observation is that the maximum coordination number of the hydrated diammine and triamminelead (II) complexes is dependent on the level of calculation investigated. The HF and MP2 levels of theory predict a maximum coordination number, hexa-coordinate species, for both diammine and triamminelead (II) complexes, while the B3LYP levels of calculations prefers the highest coordination number of five for both the diammine and triammine lead (II) complexes, $[Pb(NH_3)_2(H_2O)_3]^{2+}$ and $[Pb(NH_3)_3(H_2O)_2]^{2+}$, respectively.

Plots were created for the Pb-N and Pb-O bond lengths and vibrational stretching frequencies at the HF, MP2 and B3LYP levels of theory and are presented in Figures 29, 30 and 31, respectively. These plots show a trends in the bond lengths, in the corresponding vibrational stretching frequencies, as the number of ligands, either ammonia or water, are increased. As more water molecules are added to a central Pb (II) metal cation, elongation of both the Pb-O and the Pb-N bond lengths are observed. This elongation of the bond lengths can be attributed to the increased electrostatic repulsion between the ligands. The Pb-N and the Pb-O vibrational stretching frequency plots display the opposite trend from the Pb-N and Pb-O bond length plots. That is, as the number of ammonia or water ligands is increased, the vibrational stretching frequencies associated with a given ligand are decreased. Such a trend can be attributed to the fact that less energy is required for longer bonds to vibrate.

No experimental Raman data was found to compare with our simulated polarized Raman plots, which are resented in Figure 6A.1 of the Supplementary Material section. Simulated polarized Raman spectra are computationally generated from the vibrational frequency data obtained at the HF/6-311+G*/SDD level of theory. These simulated

polarized Raman plots will be a valuable reference tool for Dr. Tremaine's lab team at the University of Guelph, in Ontario, where experimental Raman data will be collected in the near future.

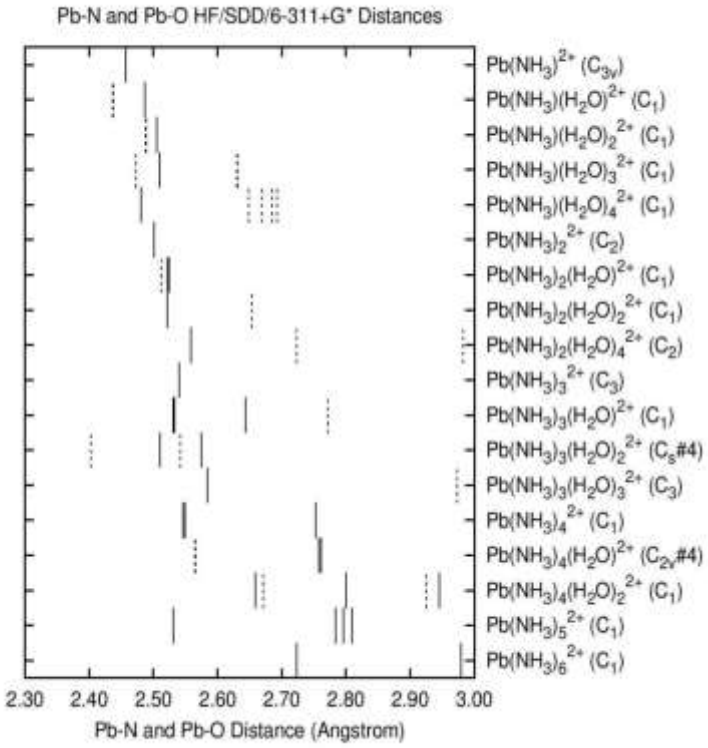

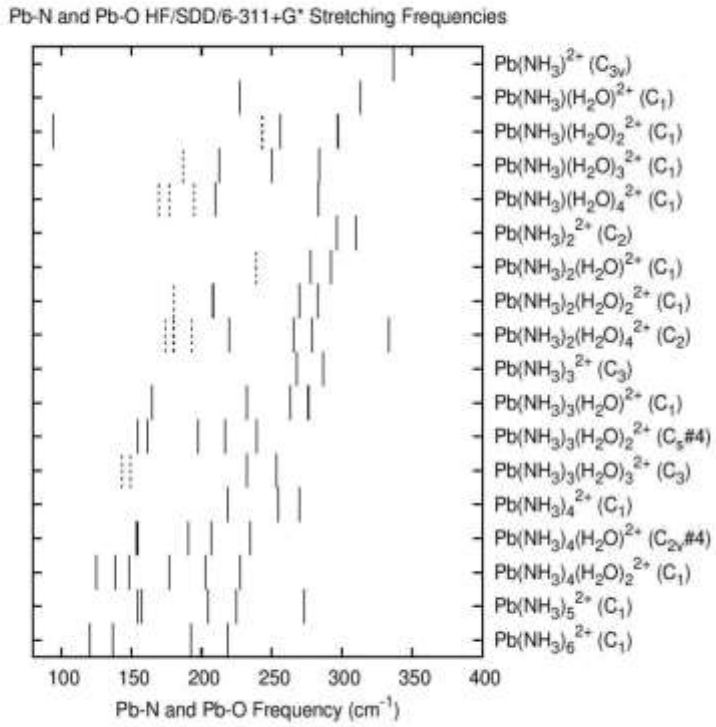

Figure 29: Pb-N (full line) and Pb-O (dashed line) bond lengths (above) and vibrational stretching frequencies (below) for $[Pb(NH_3)_m(H_2O)_n]^{2+}$, where m = 1 - 6 and n = 0 - (6-m), calculated at the HF/6-311+G*/SDD level of theory.

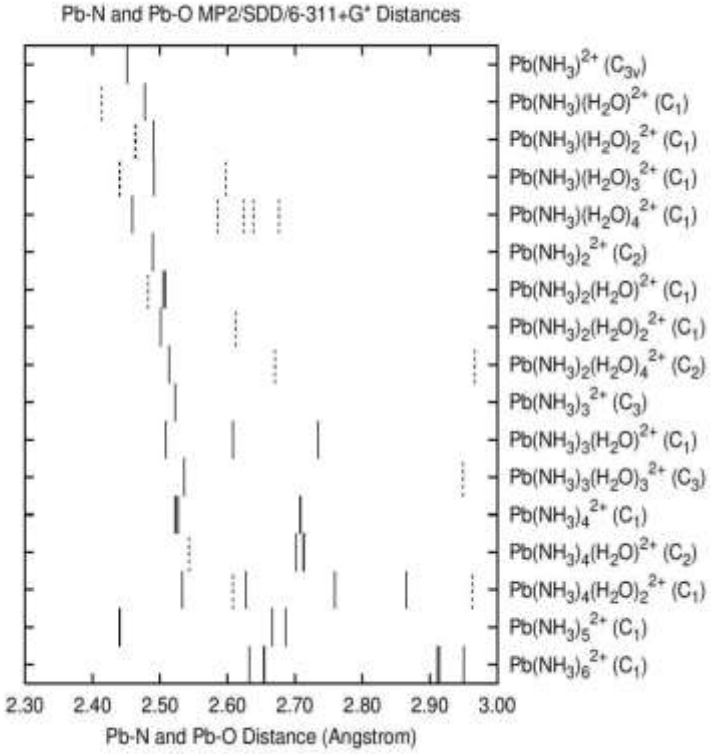
Pb-N and Pb-O MP2/SDD/6-311+G* Distances
Pb(NH3)2+ (C3v)
Pb(NH3)(H2O)2+ (C1)
Pb(NH3)(H2O)22+ (C1)
Pb(NH3)(H2O)32+ (C1)
Pb(NH3)(H2O)42+ (C1)
Pb(NH3)22+ (C2)
Pb(NH3)2(H2O)2+ (C1)
Pb(NH3)2(H2O)22+ (C1)
Pb(NH3)2(H2O)42+ (C2)
Pb(NH3)32+ (C3)
Pb(NH3)3(H2O)2+ (C1)
Pb(NH3)3(H2O)32+ (C3)
Pb(NH3)42+ (C1)
Pb(NH3)4(H2O)2+ (C2)
Pb(NH3)4(H2O)22+ (C1)
Pb(NH3)52+ (C1)
Pb(NH3)62+ (C1)
2.30
2.40
2.50
2.60
2.70
2.80
2.90
3.00
Pb-N and Pb-O Distance (Angstrom)

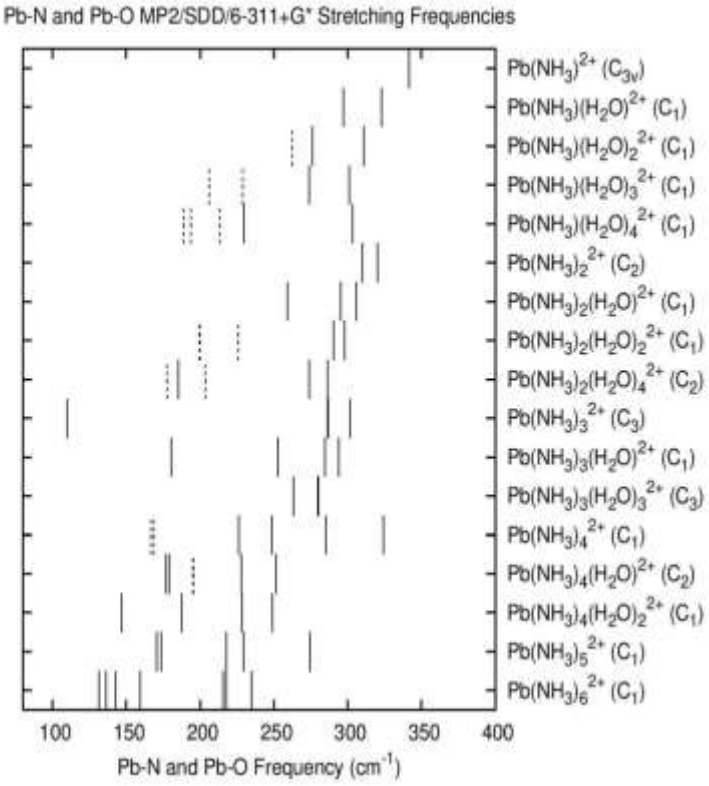

Figure 30: Pb-N (full line) and Pb-O (dashed line) bond lengths (above) and vibrational stretching frequencies (below) for $[Pb(NH_3)_m(H_2O)_n]^{2+}$, where m = 1 – 6 and n = 0- (6-m), calculated at the MP2/6-311+G*/SDD level of theory.

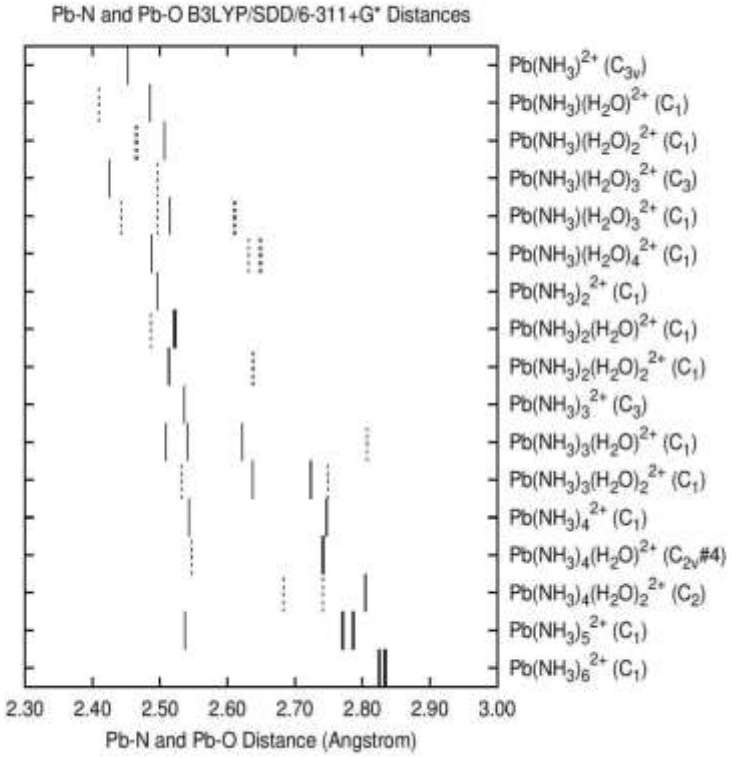
Pb-N and Pb-O B3LYP/SDD/6-311+G* Distances
Pb(NH3)2+ (C3v)
Pb(NH3)(H2O)2+ (C1)
Pb(NH3)(H2O)22+ (C1)
Pb(NH3)(H2O)32+ (C3)
Pb(NH3)(H2O)32+ (C1)
Pb(NH3)(H2O)42+ (C1)
Pb(NH3)22+ (C1)
Pb(NH3)2(H2O)2+ (C1)
Pb(NH3)2(H2O)22+ (C1)
Pb(NH3)32+ (C3)
Pb(NH3)3(H2O)2+ (C1)
Pb(NH3)3(H2O)22+ (C1)
Pb(NH3)42+ (C1)
Pb(NH3)4(H2O)2+ (C2v#4)
Pb(NH3)4(H2O)22+ (C2)
Pb(NH3)52+ (C1)
Pb(NH3)62+ (C1)
2.30
2.40
2.50
2.60
2.70
2.80
2.90
3.00
Pb-N and Pb-O Distance (Angstrom)

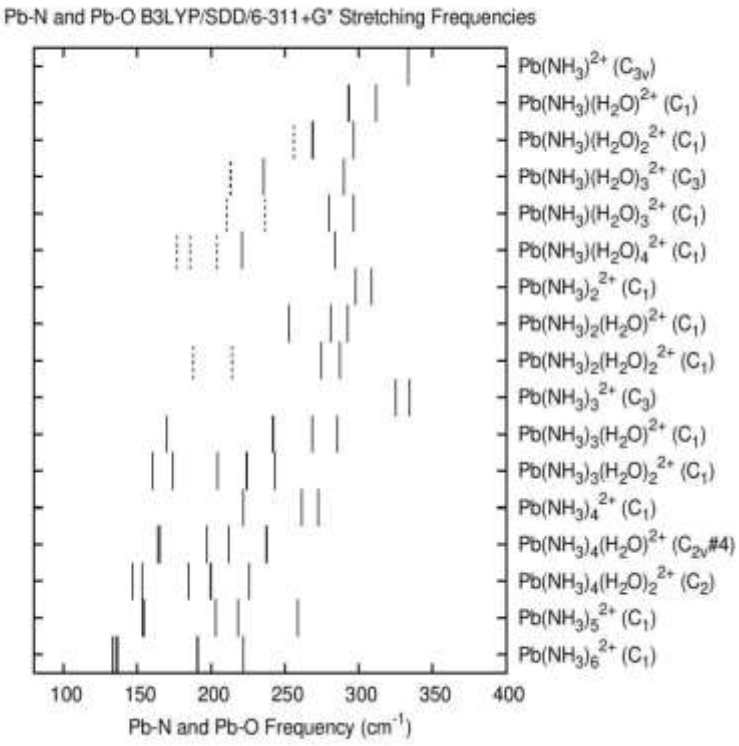

Figure 31: Pb-N (full line) and Pb-O (dashed line) bond lengths (above) and vibrational stretching frequencies (below) for $[Pb(NH_3)_m(H_2O)_n]^{2+}$, where m =1 - 6 and n = 0 - (6-m), calculated at the B3LYP/6-311+G*/SDD level of theory.

Chapter 7: Conclusion and Future Work

7.1 Conclusion

The aim of this research project was to systematically predict all possible corrosion products of lead (II) that might be formed within the CANDU GEN IV Supercritical Water-Cooled Reactor (SCWR) given all of the combinations of ligands that might be present,

(chloride (Cl^-), hydroxide (OH^-), ammonia (NH_3) and water (H_2O)). The ultimate goal of this research was to contribute to the development of a water control strategy that would limit or eliminate corrosion associated with the extreme supercritical working conditions of this Gen IV nuclear reactor.

These predications of lead (II) complexes, including their molecular geometries, total energies and vibrational stretching frequencies, were obtained from *ab initio* computational chemistry calculations. All calculations were performed using Gaussian03 software as implemented through ACEnet (Atlantic Computational Excellence Network). Simulated Raman Spectra obtained in this research will complement experimental Raman research to be completed by our colleagues at the University of Guelph in Ontario. Simulated Raman Spectra obtained in this research will complement experimental Raman research spectra obtained in this thesis, coupled to the experimental research spectra, will allow the best possible predictions for corrosive lead (II) complexes to be made.

To prepare a list of the most likely corrosion candidates, each set of lead (II) complexes investigated in this research will be critiqued.

7.2 Aqualead(II)

The highest stable coordination number determined for the aqualead(II) complex studied in this work is eight, giving the octahydrated species, $[Pb(H_2O)_8]^{2+}$. Optimization of $[Pb(H_2O)_6]^{2+}$ (at B3LYP levels), $[Pb(H_2O)_7]^{2+}$ and $[Pb(H_2O)_9]^{2+}$ resulted in dissociation of water ligands, how many depending on the level of the theory being investigated. Due to the lack of experimental literature data, the predicted aqualead(II) species in this thesis could only be compared to previous computational studies. Both, Wander et al.[21] and Juan et al.[76] determined the most stable aqualead(II) complexes as $[Pb(H_2O)_{6\text{-}8}]^{2+}$. Consequently, it can be concluded that the most likely structure to be involved in a corrosion product inside the SCWR would be octahydrated species, $[Pb(H_2O)_8]^{2+}$. However, aqualead(II) complexes have 2+ oxidation number and will need to be combined with a negatively charged anion(s) in order to form an overall neutral complex that will deposit within the super critical water (SCW) environment.

7.3 Chlorolead(II)

Chloride could possibly leak from the condenser to the SCWR environment forming corrosion products with the surrounding metal ions. In this work, stable structures were identified for each and every anhydrous (II) complex studied. The stabilities of the hydrated chlorolead(II) complexes decreased as the number of chloride ligands increased. The hydrated monochlorolead(II) complexes were found to be stable up to and including penta-coordinate species. The hydrated dichlorolead(II) complexes were found to be stable up to and including tetra-coordinate species, $[PbCl_2(H_2O)_2]$. The

optimized geometries obtained for the anhydrous dichloro complex, [$PbCl_2$], were in close agreement with those from a computational study performed by Freza et al.[89] Furthermore, no stable structures were identified for either trichlorolead(II) or tetrachlorolead(II) complexes when water ligands were added. Chlorolead(II) complexes with positive or negative charge can form deposits within the SCWR environment only when combined with other ions to give neutral complexes. Corrosive deposition requires electronically neutral species; hence, neutral complexes such as $PbCl_2$ and its stable hydration complexes are preferred (up to and including [$PbCl_2(H_2O)_2$]).

7.4 Hydroxolead(II)

Hydroxolead(II) complexes are similar to the chlorolead(II) complexes, because the ligands in both (hydroxide and chloride) have overall a single negative charge. Stable structures were found for the anhydrous hydroxide complexes up to and including the trihydroxo complex $[Pb(OH)_3]^-$. The anhydrous tetrahydroxo complex was unstable due to dissociation of one hydroxide (OH^-) ligand. In general, the hydrated hydroxylead(II) complexes showed high instability as the number of hydroxide (OH^-) and water ligands were increased. The hydrated monohydroxylead (II) complexes ware stable up to and including the penta-coordinate species, $[Pb(OH)(H_2O)_4]^+$. The dihydrate, [$Pb(OH)_2(H_2O)_2$], was the highest stable hydrated dihydroxolead(II) complex identified. No stable structures were found for the hydrated trihydroxylead(II) complexes nor for the tetrahydroxylead(II) complexes. For hydroxylead(II) species to be involved in deposition on pipes and valves of the SCW nuclear reactor, neutral complexes must be formed, thus

making $[Pb(OH)_2]$ and its hydrated complexes the best candidates. No experimental or computational studies were available for comparison purposes.

7.5 Amminelead(II)

The ammonia ligand is neutral, thus making the overall amminelead(II) complex positively charged (2+). Ammine ligands ($-NH_3$) should be considered when predicting possible corrosion products since ammonia may be introduced to the SCWR environment during pH adjustment. Stable anhydrous amminelead(II) complexes were found, up to and including the hexaamminespecies, $[Pb(NH_3)_6]^{2+}$. The highest stable hydrated monoamminelead(II) species was determined to be the penta-coordinate species, $[Pb(NH_3)(H_2O)_4]^{2+}$. In addition, the most stable hydrated form of the diamminelead(II) complexes was $[Pb(NH_3)_2(H_2O)_4]^{2+}$. $[Pb(NH_3)_2(H_2O)_3]^{2+}$ was found to be unstable, with one water ligand dissociating at all of the levels of theory investigated. Both the tri- and tetraammine hydrated lead(II) species were found to be stable, up to and including the hexa-coordinate species ($[Pb(NH_3)_3(H_2O)_3]^{2+}$ and $[Pb(NH_3)_4(H_2O)_2]^{2+}$, respectively). The anhydrous pentammine complex, $[Pb(NH_3)_5]^{2+}$ was found to be stable, while the monohydrated pentammine complex, $[Pb(NH_3)_5(H_2O)]^{2+}$, was unstable. Thus suggesting that hydration of pentammine species results in destabilization. The hexamine complex, $[Pb(NH_3)_6]^{2+}$ was found to be stable at all levels of theory invesigated. Unfortunately, neither experimental nor computational literature data on amminelead (II) complexes was available so no comparisons were possible. Once again, for corrosion products to be deposited within the SCWR environment, neutral complexes must be formed. Hence, the stable amminelead(II) cations predicted in this thesis are expected to form neutral

complexes by combining with some other small anionic species within the SCWR environment (perhaps the chloride ion).

7.6 Future work

Comprehensive *ab initio* calculations of lead (II) complexes involving four different ligands (water, chloride, hydroxide and ammonia) have been performed and are reported in this thesis. The research can be taken further by computationally probing the lead(II) complexes with mixed ligands. Suggested complexes for further investigation are: chlorohydroxolead(II) complexes ($[PbCl_n(OH)_m(H_2O)_l]^{2-n-m}$), chloroammineleadd(II) complexes ($[PbCl_n(NH_3)_m(H_2O)_l]^{2-n}$) and hydroxoammineleadd(II) complexes ($[Pb(NH_3)_n(OH)_m(H_2O)_l]^{2-m}$) up to and including the hexa-coordinated species.

References

[1]T. Abraham and S. Ion, "Generation-IV nuclear power: A review of the state of the science", *Energy Policy*, Vol. 36, 2008, pp. 4323-4330.

[2]K. C. Chow and H. F. Khartabil, "Conceptual Fuel Channel designs for CANDU-SCWR", *Nucl. Eng. Tech.*, Vol. 40, 2007, pp. 139- 146.

[3]K. L. Murty and I Charit, "Structural materials for Gen-IV nuclear reactors: Challenges and opportunities", *J. Nucl. Mater*., Vol. 383, 2008, pp. 189-195.

[4]C. Sun, R. Hui, W. Qu and S. Yick, "Progress in corrosion resistant materials for supercritical water reactors", *Corros. Sci.,* Vol. 51, 2009, pp. 2508-2523.

[5]Y. Oka and S. Koshizuka, "Supercritical-pressure, Once-through Cycle Light Water Cooled Reactor Concepts", *J. Nucl. Sci. and Tech.*, Vol. 38, 2001, pp. 1081-1089.

[6]Y. Oka, "Review of high temperature water and steam cooled reactor concepts", Proc. SCR2000 Symp., Paper No. 104, ISBN 4-901332-00-4, 2000.

[7]W. Peiman, I. Pioro and K. Gabriel, "Thermal Aspects of Conventional and Alternative Fuels in Super Critical Water-Cooled Reactor (SCWR)" Applications, Nuclear Reactors, Prof. Amir Mesquita (Ed.), ISBN: 978-953-51-0018-8, In Tech. Retrieved January 15, 2014 from http://www.intechopen.com/books/nuclear-reactors/-thermal-aspects-of-conventional-and-alternative-fuels-in-supercritical-water-cooled-reactor-scwr-ap., 2012.

[8]J. Spoelstra, "Numerical stability analysis of natural circulation driven supercritical water reactors", Master of Science Thesis, PNR-131-2012-15, Delft University of Technology, Faculty of Applied Sciences, Dept. of Radiation, Radionuclides &Reactors), 2012.

[9] Nuclear facts. Canadian Nuclear Association. Retrieved September 21, 2014, from http: // teachnuclear.ca/general_resources/facts, 2013.

[10] D. F. Torgerson, B. A. Shalaby, and S. Pang, "CANDU technology for Generation III + and IV reactors", *Nucl. Eng. Design*, Vol. 236, 2006, pp. 1565-1572.

[11] A. J. Lukomski, "Study on Linking a Super Critical Water-Cooled Nuclear Reactor to a Hydrogen Production Facility", A Thesis Submitted in Partial Fulfilment of the Requirements for the Degree of Master of Applied Science, Nuclear Engineering, The faculty of Energy Systems and Nuclear Science, University of Ontario Institute of Technology, 93 pages, 2001.

[12] I. Pioro and R. Duffey, "Heat Transfer and Hydraulic Resistance at Supercritical Pressures in Power Engineering Applications", ASME Press, New York, NY, USA, 2007, 334 pages.

[13] A Technology Roadmap for Generation IV Nuclear Energy Systems. US DOE Nuclear Energy Research Advisory Committee and the Generation IV International Forum GIF-002-00, 2002.

[14] P. Sun, "Dynamics Model Construction and Control System Design for Canadian Supercritical Water-cooled Reactors", A thesis submitted in partial fulfillment of the requirements for the degree of Doctor of Philosophy, The School of Graduate and Postdoctoral Studies, The University of Western Ontario, London, Ontario, 2012.

[15] P. Kritzer, "Corrosion in high-temperature and supercritical water and aqueous solutions: a review", *J. Supercrit. Fluids*, Vol. 29, 2004, pp. 1-29.

[16] M. I. Svischev and D. A. Guzonas, "Supercritical water and particle nucleation: Implication for water chemistry control in a GEN IV supercritical water cooled nuclear reactor", *J. Supercrit. Fluids*, Vol. 60, 2011, pp.121-126.

[17] G. Was, P. Ampornrat, G. Gupta, S. Teysseyre, E. West, T. Allen, K. Sridharan, L. Tan, Y. Chen, X. Ren, C. Pister, "Corrosion and stress corrosion cracking in supercritical water", *J. Nucl. Mater.*, Vol. 371, 2007, pp. 176-201.

[18] P. Ampornrat, G. S. Was, "Oxidation of ferritic-martenistic alloys T91, HCM12A and HT-9 in supercritical water" *J. Nucl. Mater.* , Vol. 371, 2007, pp. 1-17.

[19] F. Xiu and F. Zhang, "Recovery of copper and lead from waste printed circuit boards by supercritical water oxidation combined with electro kinetic process", *J. Hazard. Mater.*, Vol. 165, 2009, pp. 1002-1007.

[20] S. Hwang, B. Lee, J. Kim, J. Jang, "SCC and corrosion evaluations of the F/M steels for a supercritical water reactor", *J. of Nucl. Mater.*, Vol. 372, 2008, pp. 177-181.

[21] M. Wander and A. Clark, "Hydration Properties of Aqueous Pb (II) Ion", *Inorg. Chem.*, Vol. 47, 2008, pp. 8233-8241.

[22] C. Gourlaouen, H. Gerard, O. Parisel, "Exploring the hydration of Pb^{2+}: Ab Initio Studies and First-Principles Molecular Dynamics", *Chem. Eur. J.*, Vol. 12, 2006, pp. 5024-5032.

[23] X. Cheng, X-J. Liu, Y-H. Yang, "A mixed core for supercritical water-cooled reactors", *Nucl. Eng. Tech.*, Vol. 40, 2007, pp. 117-126.

[24] P. McDonald, J. Buongiorno, J. W. Sterbentz, C. Davis, R. Witt, "Feasibility Study of Supercritical Light Water Cooled Reactors for Electric Power Production", INEEL/EXT-04-02530, INEEL, January, 2005.

[25] X. Cheng, T. Schulenberg, D. Bittermann, P. Rau, "Design Analysis of Core Assemblies for Supercritical Pressure Conditions", *Nucl. Eng. Design*, Vol. 223, 2003, pp. 279-294.

[26] D. Squarera, T. Schulenberg, D. Struwea, Y. Oka, "High Performance Light Water Reactor", *Nucl. Eng. Design*, 221, 2003, pp. 167-180.

[27] L. Cao, Y. Oka, Y. Ishiwatari, Z. Shang, "Fuel, Core Design and Subchannel Analysis of a Superfast reactor", *J. Nucl. Sci. Tech.*, 2008, Vol. 45, pp. 138-148.

[28] A. Yamaji, Y. Oka, A. Koshizuka, "Three- dimensional core design of high temperature supercritical-pressure light water reactor with neutronic and thermal-hydraulic coupling", *J. Nucl. Sci. Tech.*, Vol. 42, 2005, pp. 8–19.

[29] A. Yamaji, K. Kamei, Y. Oka, "Improved core design of the high temperature supercritical-pressure light water reactor", *Ann. Nucl. Energy*, Vol. 32, 2005, pp. 651-670.

[30] M. Naidin, S. Mokry, I. Pioro, "SCW NPPs: Layouts and thermodynamic cycles", International Conference Nuclear Energy for New Europe. Bled. Slovenia, 2009.

[31] M. Naidin, S. Mokry, F. Baig, Y. Gospodinov, "Thermal-Design Options for Pressure-Channel SCWRS With Cogeneration of Hydrogen", J. Eng. for Gas Turbines and Power, Vol.131, 2008, 8 pages.

[32] S. Mokry, M. Naidin, F. Baig, Y. Gospodinov, U. Zirn, K. Bakan, I. Pioro and G. Naterer, "Conceptual Thermal-Design Options for Pressure-Tube SCWRs with Thermochemical Co-Generation of Hydrogen", ICONE16-48313, 16th International Conference on Nuclear Engineering, Orlando, Florida, Vol. 2, 2008, pp. 765-777.

[33] G. Naterer, S. Suppiah, M. Lewis, "Recent Canadian Advances in Nuclear-Based Hydrogen Production and the Thermochemical Cu-Cl Cycle", *Int. J. of Hydrogen Energy*, Vol. 34, 2009, pp. 2901-2917.

[34] Phase diagram of water (Critical point). Retrieved January 8, 2014, from http://en.wikipedia.org/wiki/Critical_point (thermodynamics), 2013.

[35] Lead and Lead Alloys. Key to Metals. The World's Most Comprehensive Metals Database. Retrieved January 15, 2014, from http://www.keytometals.com/Article10.htm, 2010.

[36] M. E. Weeks, "Discovery of the Elements: Collected Reprints of a Series of Articles Published in the Journal of Chemical Education", J. of Chem. Educ., Vol. 10, 1993, pp. 161–170. Retrieved January 15, 2014, from http://www.vanderkrogt.net/elements/element.php?sym=Pb.

[37] M. Madi, Periodic Table09. Group 14. Retrieved January 15, 2014, from http://periodictable09.wikispaces.com/Group+14., 2014.

[38] I. N. Levine, "Quantum Chemistry", Fifth Edition; Prentice Hall, New Jersey, 2000.

[39] P. Atkins, "Physical Chemistry", Sixth Edition; W.H. Freeman and Company, New York, 1999.

[40] Nobelprize.org. Nobel Prizes and Literature. The Nobel Prize in Physics 1921. Retrieved January, 15, 2014, from http://www.nobelprize.org/nobel_prizes/physics/laureates/1921/., 2013.

[41] C. L. Tag, "Fundamentals of Quantum Mechanics: For Solid State Electronics and Optics", Cambridge University Press. New York, 2005.

[42] C. J. Cramer, "Essentials of Computational Chemistry: Theories and Models", 2nd. Edition; John Wiley & Sons Ltd, England, 2002.

[43] M. Born, J. R. Oppenheimer, "On the Quantum Theory of Molecules". *Ann. Physik,* Vol. 84, 458, 1927, pp. 1-32.

[44] F. J. Bockhoff, "Elements of Quantum Theory", Second Edition; Addison-Wesley Publishing Company, Massachusetts, USA, 1976.

[45] E. G. Lewars, "Computational Chemistry: Introduction to the Theory and Applications of Molecular and Quantum Mechanics." Second edition; Springer Science, New York, 2011.

[46] J. Sauer, "Molecular Models in ab Initio Studies of Solids and Surfaces: From Ionic Crystals and Semiconductors to Catalysts", *Chem. Rev.*, Vol. 89, 1989, pp. 199- 255.

[47] S. Bell, T. Dines, B. Chowdhry, R. Withnall, "Computational Chemistry Using Modern Electronic Structure Methods", *J. Chem. Educ.*, 84, 2007, pp. 1364- 1370.

[48] E. Clementi, "Ab Initio Computational Chemistry", *J. Phys. Chem*., Vol. 89, 1985, pp. 4426-4436.

[49] D. R. Hartree, "The wave mechanics of an atom with a non-coulomb central field", *Proc. Cambridge Phil. Soc.*, Vol. 24, 1928, pp. 89-132.

[50] D. C. Young, "Computational Chemistry: A Practical Guide for Applying Techniques to Real World Problems", Wiley Interscience: New York, 2001, pp. 19-23.

[51] D. A. McQuairre, "In Quantum Chemistry", 2nd Edition; University Science Books: California, 2008, pp. 690.

[52] J. Foresman, E. Frisch, "Exploring Chemistry with Electronic Structure Methods", 2nd ed., Selecting an Appropriate Theoretical Method, Gaussian, Inc. Pittsburgh, PA, 1995, pp. 111- 125.

[53] F. Rotzinger, "Performance of Molecular Orbital Methods and Density Functional Theory in the Computation of Geometries and Energies of Metal Aqua Ions", *J. Phys. Chem. B*, Vol. 109, 2005, pp. 1510- 1527.

[54] C. Møller, M. S. Plesset, *Phys. Rev.*, Vol. 46, 1934, pp. 618.

[55] J. S. Binkley, J. A. Pople, *Int. J. Quant. Chem.*, Vol. 9, 1975, pp. 229.

[56] M. Mueller, "In Fundamentals of Quantum Chemistry: Molecular Spectroscopy and Modern Electronic Structure Computations", Kluwer Academic/Plenum Publishers: New York, 2001.

[57].P. Hohenberg, W. Kohn, *Phys. Rev. B*, Vol. 136, 1964, pp. 864.

[58] T. Ziegler, "Approximate Density Functional Theory as a Practical Tool in Molecular Energetics and Dynamics", *Chem. Rev.*, Vol. 91, 1991, pp. 651-667.

[59] W. Kohn, A. Becke, R. Parr, "Density Functional Theory of Electronic Structure", *J. Phys. Chem.*, Vol. 100, 1996, pp. 12974-12980.

[60] F. Jensen, "Introduction to Computational Chemistry", Second Edition, Wiley: Hoboken, 2007.

[61] J. C. Slater, *Phys. Rev.*, Vol. 36, 1930, pp. 57-64.

[62] E. Davidson, D. Feller, "Basis Set Selection for Molecular Calculations", Chem. Rev., Vol. 86, 1986, pp. 681-696.

[63]. J.A. Pople and R. K. Nesbet, *J. Chem. Phys.*, Vol. 22, 1954, pp. 571.

[64] M. Dolg, X. Cao, "Relativistic Pseudopotentials: Their Development and Scope of Applications", *Chem. Rev.*, Vol. 112, 403-480.

[65] Gaussian 03, Revision C.02, M. J. Frisch, G. W. Trucks, H. B. Schlegel, G. E. Scuseria, et al., Gaussian, Inc., Wallingford CT, 2004.

[66] ACEnet, Retrieved March 03, 2014 from www.ACEnet.com, 2014.

[67] E. Schrödinger, *Phys Rev.*, Vol. 28, 1926, pp. 1049.

[68] F. Jensen, "Atomic orbital basis sets", *WIREs Comp. Molec. Sci.*, Vol. 3, 2013, pp.273 295.

[69] G. Schaftenaar and J. H. Noordik, "Molden: a pre- and post-processing program for molecular and electronic structures", *J. Comp.-Aided Molec. Design,* Vol. 14, 2000, pp. 123-134.

[70] S. Hofer, B. Rode, "The solvation structure of Pb(II) in dilute aqueous solution: An ab initio quantum mechanical/ mechanical molecular dynamics approach", *J. Chem. Phys.*, Vol. 121, 2004, pp. 6406-6411.

[71] T. J. Swift, W. G. Sayre, *J. Chem. Phys.*, Vol. 44, 1966, pp. 3567.

[72] A. Tongraar and B. M. Rode, " The role of non-additive contributions on the hydration shell structure of Mg^{2+} studied by Born-Oppenheimer ab initio quantum mechanical/ molecular mechanical molecular dynamics simulation", *Chem. Phys. Letters*, Vol. 346, 2001, pp. 485-491.

[73] F. C. Lightstone, E. Schwegler, M. Allesh, F. Gygi, and G. Galli, "A first-principles molecular dynamics study of calcium in water, *Chem. Phys. Chem.*, Vol. 6, 2005, pp. 1745-1749.

[74] H. Ohtaki, T. Radnai, "Structure and dynamics of hydrated ions", *Chem. Rev.*, Vol. 93, 1157-1204, 1993.

[75] T. S. Hofer, B. Randolf, M. Rode, "The dynamics of the solvation of Pb (II) in aqueous solution obtained by an ab initio QM/MM MD approach", *Chem. Phys.*, Vol. 323, 2006, pp. 473-478.

[76] W. Juan, X. Shuwei, Y. Liangmin, "Hydration Structure of Pb (II) from Density Functional theory Studies and First-Principles Molecular Dynamics", *Acta. Chim. Sinica*, Vol. 71, 2013, pp. 1307- 1312.

[77] M. Devereux, M., M. Van Severen, O. Parisel, J. Piquemal, N. Gresh, "Role of Cation Polarization in holo- and hemi-Directed $[Pb(H_2O)_n]^{2+}$ Complexes and Development of a Pb^{2+} Polarizable Force Field", *J. Chem, Theor. Comput.*, Vol. 7, 2011, pp. 138-147.

[78] T. Shi, G. Orlova, J. Guo, D. Bohme, A. Hopkinson, M. Siu, Existence of Doubly Charged Lead Monohydrate: Experimental Evidence and Theoretical Examination", *J. Am. Chem. Soc.*, Vol. 126, 2004, 7975-7980.

[79] S. D. Price, "Investigating the gas-phase chemical reactions of molecular dications", *Phys. Chem. Chem. Phys.*, Vol. 5, 2003, pp. 1717-1729.

[80] T. Shi, J. Zhao, A. Hopkinson, M. Siu, "Formation of Abundant $[Pb(H_2O)]^{2+}$ by Ligand-Exchange Reaction between $[Pb(N_2)_n]^{2+}$ (n=1-3) and H_2O", *J. Phys. Chem. B*, Vol. 109, 2005, pp. 10590-10593.

[81] C. Gourlaouen, J. Piquemal, O. Parisel, "$[Pb(H_2O)]^{2+}$ and $[Pb(OH)]^{+}$: Four-component density functional theory calculations, correlated scalar relativistic constrained-space orbital variation energy decompositions, and topological analysis", *J. Chem. Phys.*, Vol. 124, 2006, pp. 14311–14313.

[82] Y. Luo, F. J. Millero, "Stability constants for the formation of lead chloride complexes as a function of temperature and ionic strength", *Geochim. Cosmochim. Acta*, Vol. 71, 2007, 326-334.

[83] W. Xiao, L. Chao, Q. Chunxiang, H. Hao, L. Xiaoqing, C. Liang, S. Mingyu, S. Fashui, "Influence of lead (II) chloride on the nitrogen metabolism of spinach", *Biol. Trace Elem. Res*, Vol. 121, 2008, pp. 258-265.

[84] H. Braekken, *Zeitschrift für Kristallographie -New Crystal Structures*,Vol. 83**,** 1932, pp. 222–282.

[85] R. L. Sass, E. B. Brackett, T. E. Brackett, "The crystal structure of lead chloride", *J. Phys. Chem.*, Vol. 67, 1963, pp. 2863-2864.

[86] F. H. Allen, The Cambridge Structural Database: a quarter of a million crystal structures and rising, *Acta Cryst.*, B58, 380-388, 2002.

[87] Y. Luo, F. J. Millero, "Stability constants for the formation of lead chloride complexes as a function of temperature and ionic strength". *Geochim. Cosmochim. Acta*, Vol. 71, 2007, pp. 326-334.

[88] L. Saghatforoush, F. Marandi, I. Pantenburg, G. Meyer, "Three Lead (II) Complexes in One Coordination Polymer, [Pb (TpyCl)Cl] [Pb (TpyCl)Cl_2] [Pb Cl_3] (CH_3OH)", *Z. Anorg. Allg. Chem.*, Vol. 635, 2009, 1523- 1526.

[89] S. Freza, M. Kabir, I. Anusiewcz, P. Skurski, J. Blazejowski, "Ab initio of the structure, physiochemical properties and behavior of lead chlorides and chloroplumbate anions in gaseous and aqueous phases", *Comp. Theor. Chem.*,Vol. 1004, 2013, pp. 61-68.

[90] E. V. Stefanovich, A. I. Boldyrev, T. N. Troung, J. Simons, "Ab initio study of the stabilization of multiply charged anions in water" *J. Phys. Chem. B*, Vol. 102, 1998, pp. 4205-4208.

[91] W. E. Boxford and C. E. H. Dessent, "On the stability of $IrCl_6^{3-}$ and other triply charged anions: solvent stabilization versus ionic fragmentation and electron detachment for the $IrCl_6^{3-}$ $(H_2O)_n$ n=0-10 microsolvated clusters" *J. Phys. Chem. A*, Vol. 109, 2005, 5836-5845.

[92] T. R. E. Southwood, "Lead in the Environment", Ninth Report, Royal Commission of Environmental pollution", London, 1983.

[93] W. Perera, G. Hefter, P. Sipos, "An Investigation of the Lead (II)-Hydroxide System", *Inorg. Chem.*, Vol. 40, 2001, 3974-3978.

[94] M. Breza, S. Biskupič, "On the structure of tetralead (II) complexes with OH bridges", *Collect. Czech. Chem. Commun.*, Vol. 69, 2004, pp. 2045-2054.

[95] C. F. Baes, R. E. Mesmer, "The Hydrolysis of cations", Wiley. New York, 1976.

[96] T. Spiro, D. Templeton, A. Zalkin, "The crystal Structure of a Hexanuclear Basic Lead (II) Perchlorate Hydrate: $Pb_6O(OH)_6(ClO_4)_4.H_2O$", *Inorg. Chem.*,Vol. 8, 1968, pp. 856–86.1

[97] G. Johansson, A. Olin, "On the Structures of the Dominating Hydrolysis Products of Lead (II) in Solution" *Acta Chem. Scand.*, 22 (10), 1968, pp. 3197-3201.

[98] A. Olin, R. Soderquist, "The crystal Structure of β-$[Pb_6O(OH)_6](ClO_4)_4.H_2O$", *Acta Chem. Scand.,* Vol. 26, 1972, pp. 3505-3514.

[99] S. Hong, A. Olin, "On the crystal structure of $[Pb_4(OH)_4]_3(CO_3)(ClO_4)_{10}.6H_2O$", *Acta Chem. Scand.*, Vol. 27, 1973, pp. 2309-2320.

[100] S. Hong, A. Olin, "The crystal structure of $[Pb_4(OH)_4](ClO_4)_4.2H_2O$", *Acta Chem. Scand. A*, Vol. 28, 1974, pp. 233-238.

[101] K. Faegri and L. Visscher, "Relativistic calculations on thallium hydroxide", *Theoret. Chem. Acc.*, Vol.105, 2001, pp. 252.

[102] T. Jensen, L. Saue. et al., "DIRAC, a relativistic ab initio electronic structure program", See URL: http://dirac.chem.sdu.dk, 2004.

[103] L. Visscher, T. Saue, "Approximate relativistic electronic structure methods based on the quternion modified Dirac equation", *J. Chem. Phys.* Vol. 113, 2000, pp. 3996.